Influence of surface-modified South African coal fly ash on the mechanical properties of cis-1,4-polyisoprene rubber vulcanizates

By

Dennis S. Moyo

Submitted in partial fulfilment of the requirements for the degree Master of Science (MSc)

In the Faculty of Natural and Agricultural Science,

Department of Chemistry,

University of Pretoria.

(September 2018)

Supervisor: Dr Elizabet van der Merwe

(Department of Chemistry, University of Pretoria)

Co-supervisors:

Dr F.J. Doucet

(Council for Geoscience)

Dr C.D. Woolard

(Centre for Materials Engineering, University of Cape Town)

Dr S.P. Hlangothi

(Department of Chemistry, Nelson Mandela University)

This work is based on the research supported in part by the National Research Foundation of South Africa for the Grant No. 93641. Any opinion, finding and conclusion or recommendation expressed in this material is that of the author(s) and the NRF does not accept any liability in this regard.

Declaration of originality

I, **Dennis Simbarashe Moyo** declare that the thesis/dissertation, which I hereby submit for the degree of **Master of Science (MSc)** at the University of Pretoria, is my own work and has not previously been submitted by me for a degree at this or any other tertiary institution.

1. I understand what plagiarism is and am aware of the University's policy in this regard.

2. I declare that this **thesis** (e.g. essay, report, assignment, dissertation, thesis, etc.) is my own original work. Where other people's work has been used (either from a printed source, Internet or any other source), this has been properly acknowledged and referenced in accordance with departmental requirements.

3. I have not used work previously produced by another student or any other person to hand in as my own.

4. I have not allowed, and will not allow, anyone to copy my work with the intention of passing it off as his or her own work.

Signature: ……..

Date: ……..

Acknowledgements

First and foremost, I would like to thank my supervisor, Dr E.M. van der Merwe, for the patient guidance and encouragement that she has provided me during my time as her student. I have been extremely lucky to have a supervisor who cares so much for my well-being and my work, and who always promptly availed herself to provide insight and direction into my thesis topics and research. Without her support and constant feedback this MSc would not have been achievable.

I greatly appreciate the support received through the collaborative work undertaken with the Centre for Rubber Science and Technology (CRST) at Nelson Mandela University during the rubber application phase of my research. Thanks to Dr S.P. Hlangothi for his supervisory role and valuable input. I'm also grateful to the staff and the postgraduate group at CRST for making those few weeks of rubber research all the more interesting.

Many thanks to Dr Frédéric Doucet of the Council for Geoscience (CGS) for giving me access to their laboratories and facilities in order to complete my experimental research, as well as his guidance in zeta potential and particle sizing analysis. I would especially like to extend my gratitude to Sameera Mohamed, a PhD student working for CGS, who became my main contact and continuously answered my questions and provided me valuable information whenever I needed it.

My thanks go to Dr C.D. Woolard for his expertise and invaluable input during this study.

Special thanks to Richard Kruger who provided guidance and prompt feedback throughout the study.

Continental Tyre for supplying the synthetic cis-1,4-polisoprene rubber used for this study.

S&N rubber for supplying stearic acid, zinc oxide, sulphur, Si-69, carbon black (N330, N660, N770 and N990) and N-tert-butyl-2-benzothiazyl sulfenamide (TBBS).

Eskom for financial support and for supplying fly ash produced at its thermal power stations.

To my parents, Mr and Mrs Moyo, I thank you for the continuous prayer, support and patience, and for asking "how far with the thesis" every second week for 6 months.

Abstract

This study evaluated the capability of ultrafine fly ash (untreated and physico-chemically modified) when utilized as filler in cis-1,4-polyisoprene rubber. Physico-chemical modification of the ultrafine coal fly ash was achieved using two techniques originally intended for aluminium extraction from coal fly ash. These involved (1) thermochemical treatment using ammonium sulphate (TCT-FA), followed by controlled aqueous dissolution (TCT-L) and (2) acid leaching by a sulphuric acid reflux method (SAL). In addition, chemical modification of ultrafine fly ash and physico-chemically modified (TCT-L and SAL) ultrafine fly ash using a silane coupling agent (Si-69) was investigated. The chemical and physical properties of the untreated and modified fly ash were characterized in order to effectively track the changes brought about by the chemical and physical modifications applied. Rubber composites containing fly ash, carbon black and fly ash-carbon black hybrids were prepared and their mechanical properties were studied in order to assess the viability of untreated and modified fly ash as filler in rubber. Several analytical techniques such as XRD, XRF, SEM, TGA, FTIR, BET, zeta potential and PSD analysis were utilised to characterise the fly ash samples and ICP-MS was used to determine the extraction efficiencies of the elements from fly ash during the chemical modification process. As evidenced by contact angle measurements silane treatment was only successful on the untreated coal fly ash (UFA) and not on the TCT and SAL sample.

The thermochemical treatment and aqueous dissolution treatment procedure was successful in increasing the surface area and surface roughness, and decreasing the particle-particle agglomeration of the fly ash sample. Sulphuric acid treatment decreased the particle-particle agglomeration, however, an increase in surface roughness was not observed via FE-SEM measurements. The increase in specific surface of this sample, as recorded by BET, might have been a result of increase in particle porosity instead. The zeta potential of the samples changed from -26.7 mV in untreated fly ash (UFA) to +16.3 mV and -0.5 mV for TCT-L and SAL, respectively. Silane treatment was only successful on the UFA and not on the TCT and SAL sample as evidenced by contact angle measurements.

Incorporation of ultrafine fly ash in cis-1,4-polyisoprene vulcanizates resulted in marginal improvement in the cure and mechanical properties when compared to the neat rubber vulcanizate. The fly ash samples were not significantly reinforcing and the properties they imparted were inferior to the least reinforcing carbon black. Silane treatment of the fly ash improved the mechanical properties of the vulcanizates: in-situ silane treated samples produced better results than the pre-treated samples. TCT-filled vulcanizates performed better than the UFA- and SAL- filled vulcanizates.

Table of Contents

List of tables

List of figures

List of Acronyms and Abbreviations

ASTM	American Society for Testing and Materials
BET	Brunauer–Emmett–Teller analysis
CB	Carbon black
cm^{-1}	Wavenumber
E_b	Elongation at break
FA	Fly ash
FE-SEM	Field Emission Scanning Electron Microscope
FTIR	Fourier Transform Infrared spectroscopy
ICP-OES	Inductively Coupled Plasma Optical Emission Spectroscopy
LOI	loss on ignition
mins	Minutes
NR	Neat rubber
Phr	parts per hundred rubber
PSD	Particle Size Distribution
rpm	Revolutions per minute
SAL	Sulphuric Acid Leached
SEM	Scanning Electron Microscope
SG	Specific Gravity
Si-69	Bis(triethoxysilylpropyl)tetrasulfide
TBBS	N-tert-butyl-2-benzothiazyl sulfenamide

TCT	Thermochemically Treated
TCT-FA	Thermochemically treated coal fly ash before leaching
TCT-L	Thermochemically treated and leached coal fly ah
TGA	Thermogravimetric Analysis
UFA	Untreated coal Fly Ash
UTS	Ultimate tensile strength
v/v	Volume per volume
w/w	Weight per weight
XRD	X-Ray Diffraction
XRF	X-Ray Fluorescence

Chapter One

Introduction

Background of the study, problem statement, aims, objectives and research questions are outlined. Layout of the thesis is summarised.

1.1. Background

South Africa's public electricity utility, Eskom, is the largest producer of electricity in Africa and is among the top utilities globally in terms of annual production (#15) and export (#13) (Central Intelligence Agency, 2014; Sanchez, 2014). In the 2014/15 financial year, Eskom consumed 119.2 million tons of coal, generating 34.4 million tons of ash (Reynolds-Clausen and Singh, 2016). Only 7% (2.4 million tons) of the ash generated is sold for reuse, mostly to cement manufacturers but also for mine backfills and structural fills for roads, the rest is disposed of in ash dams or similar dumps (Kruger and Krueger, 2005; Reynolds-Clausen and Singh, 2016).

When most power stations in South Africa were established, there were large expanses of inexpensive land available at the coal mines which allowed low-cost disposal of fly ash. With the power stations being remotely located, there was minimal public pressure to minimize the environmental and aesthetic consequences of the ash dumps (Kruger and Krueger, 2005). At present, most power stations are running out of storage space for ash and require additional ash storage facilities. The long term maintenance of these storage facilities poses an on-going economic burden (Reynolds-Clausen and Singh, 2016).

Disposal and management of coal fly ash has therefore become a subject of increasing concern because, if not managed effectively, fly ash is a major water, soil and air pollutant and thus detrimental to both the environment and human health (Yao *et al.*, 2014; Tiwari *et al.*, 2016). Coal fly ash contains all the elements with an atomic number less than 92. Its fine particles can reach the pulmonary regions of the lungs and accumulate over long periods to toxic levels of concentration (Tiwari *et al.*, 2016). Trace components of toxic heavy metals

(Chromium, Cadmium, Arsenic, Lead, Nickel, Antimony, etc.) are normally present in coal fly ash. Heavy metals do not biodegrade and improper disposal of coal fly ash might result in heavy metals leaching into the ground, consequently resulting in groundwater pollution (Singla and Chawla, 2010; Yao *et al.*, 2014).

Compared to landfilling, which is environmentally adverse and an unproductive use of land, transformation of the coal fly ash to a product of technical and commercial value will be beneficial from an ecological and economical perspective, (Iyer and Scott, 2001; Kruger and Krueger, 2005). Considerable research on acceptable, socio-economically beneficial utilization of coal fly ash has been done over the past few decades. This includes manufacture of cement and concrete production, adsorbents for waste immobilisation, functional fillers for polymers, road stabilisers, clay bricks, soil ameliorants, mine backfill, zeolites and recovery of valuable metals (Kruger and Krueger, 2005).

1.2. Fly ash as filler in elastomers

The application of synthetic microspheres as fillers in the polymer industry has been on the rise because of the numerous advantages they have over irregularly shaped fillers. Particular interest has been shown in the use of coal fly ash as filler because it has nearly 50% silica (w/w), a spherical morphology and relatively low price (~ 50% cheaper than commercial silica) (Kruger *et al.*, 1999; Sombatsompop *et al.*, 2007).

Carbon black and precipitated amorphous silica are the main reinforcing-fillers used in industry to improve rubber properties. Rubber composites reinforced with carbon black show a higher modulus (a measure of rubber stiffness) when compared to silica-reinforced composites. Nevertheless, silica has proven to be as effective in reinforcement as carbon black and imparts a unique combination of aging resistance, tear strength and adhesion properties (Sombatsompop *et al.*, 2007; Rattanasom *et al.*, 2009). Research focused on silica-rubber systems has shown that amorphous silica has acidic silanol and siloxane functional groups on the surface. Interaction of these acidic groups with basic accelerators (compounds that increase the rate of vulcanization and that facilitate vulcanization to occur at lower temperatures and with better efficiency) results in slow cure rates and, as a result, excessively long cure times. Additionally, the polar and hydrophilic surfaces of silica have a high affinity

for moisture which is also detrimental to the properties of cured rubber (Choi, 2002; Ansarifar *et al.*, 2005).

There has been increased interest by rubber technologists in utilising silica from natural resources as alternative filler in rubber in order to reduce costs, improve mechanical properties and dimensional stability, and to alleviate environmental concerns (Sombatsompop *et al.*, 2007).

Only a few researchers have investigated the effects of fly ash on the properties of rubber vulcanizates. Garde et al. (1999) showed that fly ash-filled polyisoprene rubber had inferior properties to those of silica-filled polyisoprene rubber, but incorporation of an appropriate amount of silane coupling agent considerably enhanced the properties of fly ash-filled rubber. Hundiwale *et al.* (2002) indicated that mechanical properties of natural rubber filled with fly ash had better mechanical properties compared to calcium carbonate-filled composites. They attributed this to the spherical shape of fly ash particles, which provided substantial wetting. Alkadasi *et al.*, 2004 compared the mechanical properties of polybutadiene rubber (PBR) composites filled with untreated and silane treated fly ash and found that treated fly ash-PBR composites exhibited superior properties compared to those of untreated composites. Thongsang *et al.* (2008) showed that treatment of fly ash and precipitated silica with a silane coupling agent marginally improved elasticity, viscosity, and the energy absorbing and dispersing properties of the rubber composites but was barely useful in enhancing dispersion of the fillers.

The present study compares the performance of rubber composites loaded with both untreated and silane-treated ultrafine fly ash, as well as with fly ash residues obtained from several distinct aluminium extraction processes, to that of carbon black fillers conventionally used.

1.3. Problem statement

The rubber industry has indicated that improvements in processability without negatively affecting physical properties of rubber composites should significantly reduce the cost of production. If successfully applied in rubber composites; commercially available ultrafine fly ash may, owing to its relatively low cost as a waste product, reduce the cost of rubber

composites. In addition, the physical properties of fly ash e.g. the predominantly spherical morphology, particle size and specific density would improve flowability and reduce the volume cost when used as filler in rubber. In order to succeed it is a requisite to address the incompatibility between the inorganic surface of fly ash particles and the organic matrix of rubber. In addition, hydroxyl functional groups at the surface of fly ash particles cause them to interact and agglomerate with one another, resulting in uneven distribution throughout the non-polar polymer matrix during the compounding process. This causes structural flaws in the rubber composites. Surface treatment and modification of fly ash particles to improve filler-matrix compatibility will therefore be evaluated.

1.4. Aim

The primary aim of this study is to evaluate the suitability of ultrafine fly ash when applied as inorganic filler in natural rubber. Investigations were carried out using untreated fly ash, chemically modified (silane-treated) fly ash as well as physico-chemically modified fly ash (acid etching and thermochemically treated). Carbon blacks were used for comparative purposes.

1.5. Research approach

An integrated research approach was followed which includes an in-depth literature review on the application of coal fly ash as filler in rubber composites. The experimentation was carried out using commercially available ultrafine coal fly ash from the Lethabo power station (Free State, South Africa). This ash was characterised using a variety of analytical techniques. Physico-chemical modification of ultrafine coal fly ash was achieved using two techniques originally intended for aluminium extraction from coal fly ash. These entailed thermochemical treatment using ammonium sulphate, followed by controlled aqueous dissolution as well as acid leaching by a sulphuric acid reflux method. The efficiency of the thermochemical treatment and aqueous dissolution as well as the sulphuric acid leaching processes on aluminium extraction were evaluated using ICP-OES. Surface modification of the untreated and physico-chemically modified fly ash samples by a silane coupling agent was also investigated. Changes in the physicochemical properties of fly ash samples after modification

were followed by X-ray fluorescence (XRF), X-ray diffraction (XRD), Fourier transform infrared (FTIR) spectroscopy, thermogravimetric analysis (TGA) and zeta potential measurements. Particle size analysis (PSD), Brunauer-Emmet-Teller (BET) surface area analysis and scanning electron microscopy (SEM) analysis were used to determine the physical properties of the samples. Contact angle measurements of the fly ash samples were used as a complementary technique.

The untreated and modified fly ash samples were applied as filler and processing aid in cis-1,4-polyisoprene rubber composites, and various grades of carbon black were used as reference for comparison. Physical properties of the rubber vulcanizates e.g. tensile strength, elongation at break, rebound resilience, and hardness were used to assess the viability of untreated and modified fly ash application in rubber.

1.6. Specific objectives:

- Chemical modification of ultrafine fly ash using a silane coupling agent (Si-69).
- Physico-chemical (thermochemical and sulphuric acid treatment) modification of ultrafine fly ash by acid etching and thermochemical treatment with ammonium sulphate followed by aqueous dissolution.
- Chemical modification of the physico-chemically (thermochemical and sulphuric acid treatment) modified ultrafine coal fly ash samples using a silane coupling agent Si-69.
- Chemical and physical characterization of the untreated and modified fly ash samples in order to assess changes induced about by the chemical (Si-69 treatment) and physico-chemical (thermochemical and sulphuric acid treatment) modifications applied.
- Preparation and analysis of the mechanical properties of the rubber composites in order to assess the viability of untreated and modified fly ash application in rubber.

1.7. Research Hypothesis

- Sulphuric acid treatment, and thermochemical treatment followed by aqueous dissolution of ultrafine coal fly ash will increase the fly ash specific surface area and

reduce agglomeration between its particles. An increase in specific surface area implies an increase in the area available for interaction between the filler and rubber.

- Since fly ash contains 50% of silica (w/w), it is expected to present the same problems in curing as precipitated silica, thus silane treatment of untreated and modified coal fly ash samples will change the surfaces of the fly ash particles from hydrophilic to hydrophobic and subsequently improve compatibility of fly ash with the rubber matrix.
- Untreated and physico-chemically (thermochemical and sulphuric acid treatment) modified ultrafine coal fly ash can be used as replacement filler for carbon black in rubber composites.
- Untreated and physico-chemically (thermochemical and sulphuric acid treatment) modified fly ash can be applied as a processing aid in rubber vulcanization and enhance the mechanical properties of the composites.

1.8. Structure of the thesis

Chapter one: Introduction – the chapter provides a brief background on the proposed research, problem statement, overall objectives and research hypothesis.

Chapter two: Literature review – the chapter gives comprehensive literature review on the origin and uses of coal fly ash. It also includes a brief description of the mechanism of silane grafting and general information on carbon blacks and natural rubber.

Chapter three: Theoretical background of the analytical techniques applicable to the study – This chapter gives brief descriptions of the analytical instruments and techniques to be applied to achieve certain objectives of the study.

Chapter four: Research methodology – This chapter gives a description of the materials and experimental procedures used for the study.

Chapter five: Characterisation of untreated coal fly ash – This chapter is a characterisation of the untreated fly ash used in the study, providing useful information on the chemical, mineralogical and morphological properties.

Chapter six: Characterisation of surface modified coal fly ash – This chapter compares the chemical, mineralogical and morphological properties of the acid treated, thermochemically activated and silane-treated fly ashes with that of untreated fly ash.

Chapter seven: Rubber compounding and testing **–** This chapter presents and discusses the results obtained from the rubber composites.

Chapter eight: Conclusions and recommendations – This chapter concludes the dissertation with a summary of the findings and recommendations for further studies.

Chapter Two

Literature Review

This chapter focuses on the origin of coal fly ash, classification, properties and a discussion of its different applications. Brief discussions on natural rubber and its processing as well as filler properties and classification of carbon black is presented. An in-depth discussion of silane coupling agents and their mechanism of reacting is also given.

2.1. Coal-based power generation

Coal is the predominant commercial fuel in South Africa, where 81% of the electricity produced by Eskom is generated by the combustion of pulverised coal. South Africa produced 260 mega tons (Mt) of coal in 2014, accounting for approximately 3.3% of the world's annual total production. South Africa is ranked sixth amongst the coal exporting nations globally, exporting 69.6 Mt of the coal produced. The remainder of the country's coal production was sold to numerous local industries. More than 50% of it was utilised in the generation of electricity, of which over 90 million tons per annum is used by Eskom (Chamber of Mines of South Africa, 2017; Eskom, 2017).

In order to generate electricity, coal is first pulverised (milled to a fine powder, <75 μm) before it is blown into boilers where it ignites. The heat produced is used to convert water into steam under high pressure which is used to turn turbine blades that are part of the generator that produces an electric current (American Coal Ash Association, 2013; Eskom, 2017). Combustion exhaust gases called flue gases are produced from burning coal. They usually consist of nitrogen, carbon dioxide, water vapour, excess oxygen as well as small amounts of sulphur oxides, carbon monoxides and nitrogen oxides. Loss of heat from the boilers results in the cooling of the flue gases which causes the aggregation of non-combustible mineral residues to form ash. Bottom ash accumulates to form fused coarse ash particles that settle to the bottom of the combustion chamber. However, fly ash remains suspended in the flue gases and is removed by particle filtration equipment such as electrostatic precipitators or

filter fabric collectors (Kalyoncu, 1996; Querol *et al.*, 2002; American Coal Ash Association, 2013).

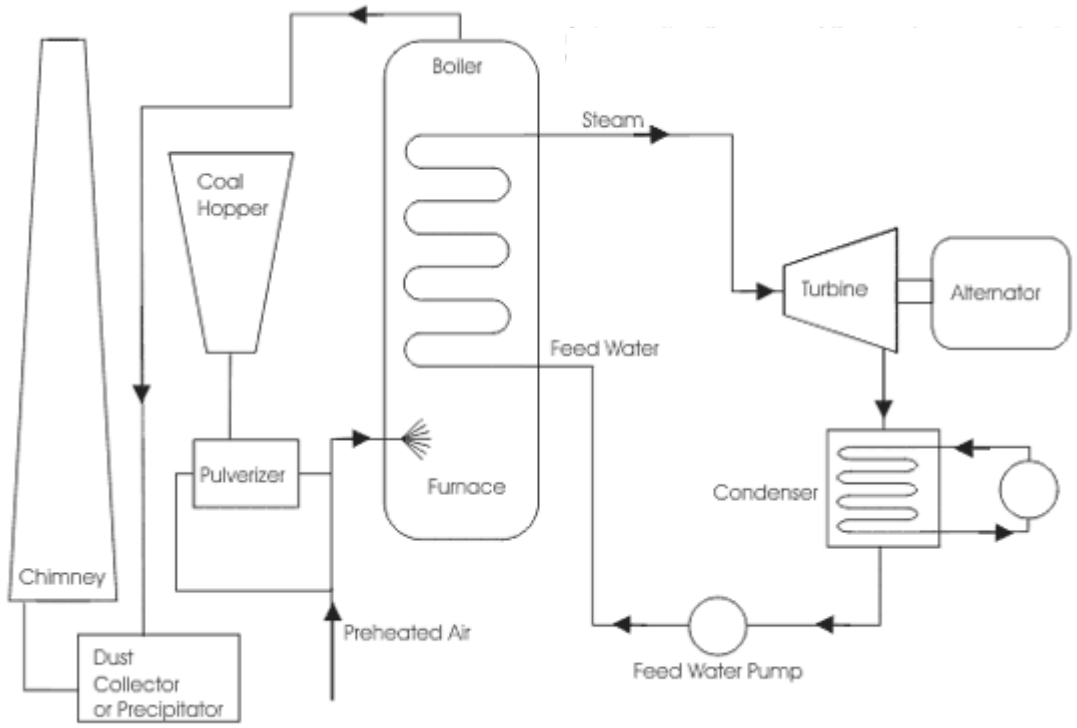

Figure 2.1: Schematic diagram of a thermal power station (Electrical4u, 2011).

Fly ash is typically grey in colour but can be tan to dark grey subject to its mineral and chemical constituents. Tan to light coloured fly ash shows high lime content, brownish ash has high iron content while dark grey to black ash is associated with high unburned carbon content (American Coal Ash Association, 2013). Coal fly ash is made up of silt-sized, predominantly spherical shaped particles that are either hollow or solid (however, many tiny voids are present throughout the structure) and range from 10 to over 200 microns in size. It is a heterogeneous mixture containing two main components: an inorganic constituent, an organic constituent. The inorganic constituent outweighs the other organic and consists of an amorphous (non-crystalline) glass phase and crystalline phases. The organic phase consists of remaining organic minerals and char materials (Openshaw, 1992; Vassilev and Vassileva, 2007; Kruse *et al.*, 2012).

The physical and chemical properties of fly ash vary depending on the parent coal (anthracite, bituminous, sub-bituminous or lignite), the burning conditions within a power plant, the rate

of cooling and efficiency of particulate removal (Thomas, 2007; Valentim *et al.*, 2009). The primary components of fly ash are oxides of silicon (SiO_2), aluminium (Al_2O_3), iron (Fe_2O_3) and calcium (CaO) with varying amounts of magnesium (Mg), potassium (K), carbon (C), sodium (Na), titanium (Ti), phosphorus (P), manganese (Mn) and sulphur (sulphates or sulphides). Most of these major and minor elements exist in the relatively stable inner core of the fly ash where they are not volatilised by the combustion process. Trace and minor elements such as arsenic (As), selenium (Se), cadmium (Cd) and lead (Pb) are concentrated on the surface of the fly ash particles. They volatilise during combustion and condense on the surface of the fly ash spheres as the flue gases cool (Openshaw, 1992; Kruse *et al.*, 2012).

Coal fly ash is broadly classified into two main groups based on the chemical composition and its source of origin, namely siliceous and calcareous (previously known as class F and class C respectively). Siliceous ashes are commonly produced from anthracite and bituminous coal and have ≥ 70% of $SiO_2 + Fe_2O_3 + Al_2O_3$ (Vassilev and Vassileva, 2007; Ahmaruzzaman, 2010). This class has pozzolanic properties being primarily made up of alumino-silicate glass with minor inclusions of mullite, quartz and magnetite (American Coal Ash Association, 2013). On the other hand, calcareous ashes are commonly derived from the burning of sub-bituminous and lignite coal and the sum of SiO_2, Fe_2O_3 and Al_2O_3 is in the range 50 – 70%. This class of ashes is referred to as the higher calcium ashes because it typically has calcium oxide (lime) content greater than 20% (Thomas, 2007; American Coal Ash Association, 2013). Calcareous ashes possess both pozzolanic and cementitious (self-hardening when reacted with water) properties (Thomas, 2007; Ahmaruzzaman, 2010).

2.2. Utilization of Coal Fly Ash

The increasing amount of fly ash generated over the decades has resulted in growing concerns over the cost of management of disposal sites and intensified research efforts in finding economically viable and innovative applications of fly ash other than incorporation in construction materials (Iyer and Scott, 2001; Swanepoel and Strydom, 2002). These applications include, but are not limited to, fills and embankments, addition to concrete and cement products, backfill in mines, lightweight aggregates, soil amendment, water treatment, a mineral resource, filler for metal and polymer matrix composites. A brief description and discussion of the above mentioned applications is given in the following sections.

2.2.1 Cement and concrete products

Siliceous fly ash is a pozzolanic material; the particles react with water and calcium hydroxide (lime) to form cementitious products at ambient temperatures. This feature has made fly ash use in blended cement and concrete the most extensively utilised form of fly ash recycling (Fraay *et al.*, 1989; Openshaw, 1992). Fly ash has two primary applications in concrete, which are as a replacement for cement in Portland cement concrete and a pozzolanic material in the production of pozzolanic cements (Ahmaruzzaman, 2010).

The small size and spherical shape of fly ash particles, when used as cement replacement in cementitious applications, gives rise to enhanced flowability and a decrease in air entrapment. This improves the workability of the cement and at the same time reduces the water requirement to achieve the flow properties of the mix. The subsequent concrete product will have a lower rate and volume of bleeding, will be more densely packed and hence possess a more durable surface (Openshaw, 1992; Earle and Scheetz, 1998; Ahmaruzzaman, 2010). Fly ash also reacts with calcium hydroxide in cement to form calcium silicate hydrate which is a stable and cementitious compound that is resistant to corrosion and makes concrete less accessible to corrosive liquids. The calcium silicate hydrate in fly ash concrete is less soluble than calcium hydroxide and this therefore reduces the incidence of calcium hydroxide leaching from the concrete. Furthermore, the resulting compound tends to fill up capillary voids in the concrete and decrease the permeability of concrete (Ahmaruzzaman, 2010).

The other beneficial effects of fly ash in cement and concrete blends are; reduction of unit cost, reduction of heat of hydration, better control of expansion and shrinkage. Apart from the technical benefits, there are also ecological advantages to the replacement of Portland cement by fly ash such as reduction in greenhouse gases. Carbon dioxide emissions generated during clinker production are reduced if clinker is replaced by fly ash in Portland cement. With less clinker present in the cementitious binder the carbon footprint of the binder is lower. Moreover, the high energy required for the process is also reduced. (Cao *et al.*, 2008; Ahmaruzzaman, 2010).

2.2.2 Synthesis of zeolite

A promising area in the utilization of coal fly ash has been in the synthesis of low grade zeolites. Amorphous alumino-silicate glass, the main component of fly ash, has great compositional similarity with some volcanic materials which are precursors of natural zeolites (Murayama *et al.*, 2002; Querol *et al.*, 2002; Molina and Poole, 2004). Zeolites are crystalline, three-dimensional micro-porous solids made up of mainly aluminium, silicon and oxygen arranged in a framework of interlinked tetraheda of $[SiO_4]^{4-}$ and $[AlO_4]^{5-}$.

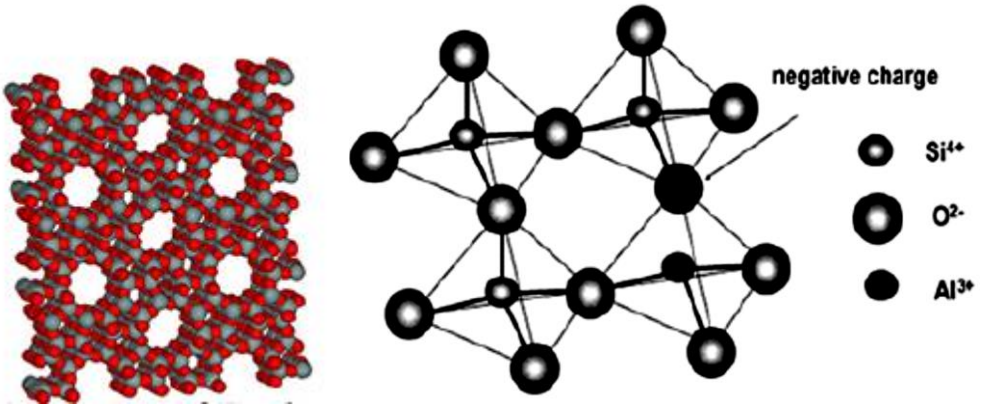

Figure 2.2: Idealised structure of zeolite framework of tetrahedral $[SiO_4]^{4-}$ and $[AlO_4]^{5-}$ (Querol et al., 2002).

The pores contain water and alkali or alkali-earth metals (group I or II elements) that act as exchangeable cations. The atypical structural properties of zeolites give them the ability to exchange ions on the basis of selectivity, to reversibly adsorb liquids and gases, and to act as a catalyst. They have thus found a wide variety of industrial applications such as petrol refining, radioactive waste management, pollution control, purification of gases, and soil improvement (Murayama *et al.*, 2002; Querol *et al.*, 2002; Molina and Poole, 2004; Ahmaruzzaman, 2010).

Most methods used for the synthesis of zeolites are centred on the disintegration of Al-Si-bearing fly ash phases with alkaline chemical reagents (mainly KOH and NaOH solutions) and the subsequent precipitation of zeolitic material (Querol *et al.*, 2002).

2.2.3 Synthesis of hydrotalcite

Recently attempts have also been made to use co-precipitation methods to synthesize Mg- Al hydrotalcite adsorbent materials with bi-functional properties from fly ash and fly ash–based zeolite (Volli and Purkait, 2016). Hydrotalcites (HT) are brucite-like layered double hydroxides (LDHs) that occur naturally. They can be described by the general formula $[M^{2+}_{1-x}M^{3+}_{x}(OH)_2]^{x+}A^{m-}_{x/m}.nH_2O$, where M^{2+} and M^{3+} are divalent and trivalent metal cations, A^{m-} is an intercalated anion (Kuwahara *et al.*, 2010; Volli and Purkait, 2016; Yang *et al.*, 2016). Water molecules, anions and other neutral moieties occupy the interlayer space of hydrotalcite. The basicity of the compounds resulting from their surface hydroxyls, easy accommodation of metal cations in the brucite-like layers and the anion exchange capability in the interlayer has seen HT's being applied as catalysts, ion exchangers, sorbents for CO_2 capture and as antacids (Kuwahara *et al.*, 2010; Muriithi *et al.*, 2017).

Volli and Purkait (2016) synthesized HT from fly ash and fly ash-based zeolites for use as an alternative catalyst for transesterification. They managed to synthesize HT's with an Mg/Al ratio ranging from 1.3 to 2.3. Muriithi *et al.* (2017) successfully developed and optimized a novel procedure to manufacture HT's from South African siliceous coal fly ash by adapting an existing acid-leaching and precipitation technique used for the transformation of blast furnace slag to HT's and zeolites. Except for presence of calcite, the product was structurally similar to HT produced from analytical grade chemicals.

2.2.4 Adsorbents for cleaning of toxic wastewater

A lot of research has been conducted on the use of fly ash as a cost-effective alternative adsorbent for the treatment of industrial wastewater contaminated with heavy metals (Bailey *et al.*, 1999; Babel and Kurniawan, 2003; Gupta *et al.*, 2003; Gupta and Ali, 2004; Mohan and Gandhimathi, 2009), inorganic compounds (Öztürk and Kavak, 2005; Lu *et al.*, 2009; Xu *et al.*, 2011), organic compounds (Nollet *et al.*, 2003; Ahmaruzzaman, 2010) and dyes (Janos *et al.*, 2003; Wang *et al.*, 2005; Dizge *et al.*, 2008).

Heavy metals such as cadmium, lead, nickel, chromium, zinc, copper and mercury present in industrial and municipal wastewater are of great concern because they are generally non-degradable and are toxic and/or carcinogenic in nature. Some metals tend to accumulate in the tissues of organisms inducing adverse health effects associated mostly with the liver,

respiratory organs and kidneys (Weng, 1995; Gupta *et al.*, 2003; Gupta and Ali, 2004). Ferric oxide, amorphous silica, alumina, and carbon black are frequently used to remove numerous metal ions from wastewater because of their high metal adsorption capacity. However, these adsorbents are costly and hard to remove from the wastewater once treatment is finished. Fly ash can therefore be used as an inexpensive adsorbent because its major components are calcium oxide, ferric oxide, alumina and silica. Moreover, fly ash acts as a good neutralising agent because of its alkaline nature (Weng, 1995).

2.2.5 Filler for polymer and metallic composites

Fillers are defined as relatively inert additives that change the mechanical, thermal, physical, and electrical properties or reduce the cost of composite materials. They are generally classified as either functional or non-functional fillers. Functional fillers improve certain parameters in the final composites, for example glass milled fibres and mica for reinforcement, alumina trihydrate for flame retardancy and glass cenospheres for lower weight. Non-functional fillers are used to reduce cost (Landman, 2003; Gangarao *et al.*, 2007). The sphericity and lower density of coal fly ash make it potentially an ideal filler and reinforcement material for the manufacture of polymer-matrix composites (PMC's) and metal-matrix composites (MMC's). Another reason fly ash could be preferentially utilised as a replacement filler or reinforcement in composite materials is because it is produced in abundance as a by-product (millions of tonnes per year) of coal combustion for electricity generation and therefore will reduce production costs of composite materials (Tarun R. Naik, 1993; Matsunaga *et al.*, 2002).

Research has been carried out on the use of fly ash as a replacement for silicon carbide in aluminium-silicon-carbide composites which are extensively used in automatic and electronic packaging (Rohatgi, 2006). Guo, Rohatgi and Nath (1997) incorporated fly ash in aluminium alloys using stir casting and it was noted that green and sintered density of the compacts decreased with increasing weight percentage of fly ash. Increasing the fly ash content resulted in an increase in the strength of the sintered composites. In another study, uncoated fly ash and nickel-coated fly ash were used to synthesise aluminium-fly ash particulate composites using the pressure infiltration technique. The study showed that the effective contact angle between uncoated fly ash and aluminium (111°) was close to that of commercially applied

oxide ceramics. Furthermore, the reported values of threshold pressure for infiltration of the fly ash (≈ 27.58 kPa) were lower than commercial ceramics at similar test conditions (Rohatgi *et al.*, 1998).

Fly ash has also been successfully incorporated in organic polymers in order to achieve; (1) property enhancement or modification, (2) overall cost reduction and (3) better control and improvement of the processing characteristics (Xanthos, 2010).

Fly ash has been used as filler in various polymers such as;

- **Epoxy** (Srivastava *et al.*, 1988; Chaowasakoo and Sombatsompop, 2007; Singla and Chawla, 2010). Chaowasakoo and Sombatsompop (2007) made fly ash/epoxy composites using conventional thermal and microwave curing procedures then evaluated the morphological and mechanical properties of the composites.
- **Polypropylene** (Nath *et al.*, 2009; Karahan and Atiş, 2011). Nath *et al.* (2009) prepared fly ash-isotactic polypropylene composites and investigated the thermal and mechanical properties of their PP-FA composites.
- **PVC** (van der Merwe, Mathebula, *et al.*, 2014). The authors modified the surface of fly ash with sodium lauryl sulphate and used it in PVC composites
- **Rubber** (Garde *et al.*, 1999; Alkadasi *et al.*, 2004; Thongsang *et al.*, 2012a) Thongsang *et al.* 2012 used fly ash-derived silica and precipitated silica as filler in natural rubber and then determined the mechanical and tribological properties of the composites.

Due to its high silica content and fine particle size (which may translate to a high-specific surface area) attempts have been made to use coal fly ash as alternative filler in natural rubber. Experiments have shown that fly ash when untreated does not significantly improve the mechanical properties of rubber composites. This is mainly because the smooth surfaces and the highly hydrophilic surface of fly ash inhibit interaction with organic polymers, resulting in poor compatibility.

The interaction between fly ash and elastomers is most commonly improved by using coupling agents. These compounds contain functional groups that bond with both organic and inorganic compounds and thus can act as an intermediary which bonds fly ash to elastomers. Titanate and silane coupling agents are the frequently used coupling agents in natural rubber

(Ohm, 1990). These have been shown to improve filler dispersion and consequently mechanical properties of polymers (Luo *et al.*, 2013; Sciences, 2013).

2.3. Natural Rubber

Natural rubber (NR) originates from the latex of various tropical trees. The commercial rubber tree, Hevea *brasiliensis*, grows in high humidity (ca. 80%) and warm (25°C to 35°C) climate of South-east Asia, West and Central Africa and South America (Ohm, 1990).

Natural rubber has long, linear macromolecules that have relative molar masses usually ranging between 300 000 and 500 000. The polymer in natural rubber originating from Hevea *brasiliensis* is essentially pure poly-cis-1.4-isoprene (>99.9%). Non-isoprene structural units such as phospholipids, proteins and amino acids may be bonded at the ends of the NR macromolecules (Ohm, 1990; Nicholson, 1997).

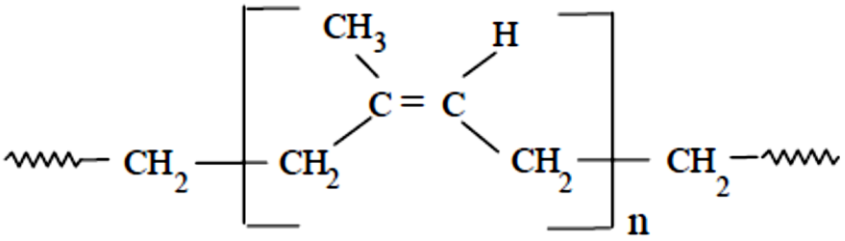

Figure 2.3: Cis-1.4-polyisoprene repeating unit (Ohm, 1990).

Natural rubber is sticky and deforms easily in heat, and is brittle in cold weather. This is a problem for a material from which elasticity is vital. The solution for this was discovered by Thomas Hancock and Charles Goodyear who came up with mastication (1820) and vulcanization (1839), respectively (Sowry, 1980).

Mastication is a process through which rubber is made workable by applying a shearing force to it. The shear force breaks down the molecular chains within the macromolecules and the energy holding the linkages is released in the form of heat. During this process the molecular weight and viscosity of the rubber decreases and the rubber becomes more plastic. In this state, it is easier to treat the rubber, usually done by adding various chemicals in powder form

e.g. sulphur and ZnO. The process is carried out in the presence of peptizers (acting as electron or hydrogen donors) either on mills at low temperatures or in closed mixers at higher temperatures. During the process oxidation degradation occurs simultaneously with macromolecular degradation, and its rate increases with increase in mastication temperature. Mastication of natural rubber is more effective at temperatures below 60 – 70°C and above 120 – 130°C, its effectiveness is minimal in-between these temperatures (Ohm, 1990).

Vulcanisation is a process that involves the bridging of polymer chains in rubber in order to reduce plasticity and develop elasticity after all the chemical constituents required in the mix have been added. In principle, it is the formation of a three-dimensional network of the rubber matrix resulting from cross-linking of the rubber macromolecules. The other ingredients of the rubber compounding may remain in the original form, change, chemically react, disperse or solubilise in the compound. Vulcanisation agents, such as sulphur, resins, metal oxides and peroxides, are predominantly used to react with appropriate functional groups in the rubber macromolecules and form cross-links between them. Sulphur is most widely used for this purpose and is most effective in the presence of activators and accelerators (Matador Rubber s.r.o, 2007; Nicholson, 1997; Sowry, 1980).

2.4. Fillers

Traditionally, fillers were regarded as cheap diluents which, because of their inconsistent geometric features, chemical constituents or surface area, were only able to slightly improve the modulus of the polymer, while the tensile and flexural strengths either remained the same or decreased. The ability of fillers to improve many properties of polymer composites was soon realised and today they are used for many purposes (Rothon, 2002; Xanthos, 2016).

The term functional filler is frequently designated for materials whose purpose is not limited to reduction of the cost of manufacturing. Examples of functional fillers include magnesium and aluminium hydroxide which function as flame retardants, precipitated silica and carbon black which are reinforcements in tyre treads, and wollastonite and calcined clay reinforcement for certain thermoplastics. Functional fillers are classified according their primary properties which affect the resultant material. The most important being surface

chemical composition, specific gravity, hardness, thermal properties, optical properties, morphology (particle size and shape), and processability (Rothon, 2002; Xanthos, 2016).

2.4.1 Surface chemical composition

When selecting a filler, the principal concerns are that the filler should not cause degradation of the polymer, and that the filler is insoluble and inert to the environments encountered when it is in use (Rothon, 2002). An estimate of the interaction between filler and polymer can be derived from the extent of uniformity of the particles and the adhesion of the polymer to their surface. Most mineral fillers have a polar surface therefore there is a lack of intensive interaction with the hydrophobic organic polymer matrices. The difference in polarity between the filler and polymer results in formation of aggregates and poor wettability. Hydrophobization of the filler might be necessary by applying an organic surface modifier which reduces the tendency of the particles to aggregate and improve compatibility between the hydrophilic filler and the hydrophobic polymer matrix (Semakina *et al.*, 2015).

High purity is generally desirable, but not always crucial, in many filler uses. Some impurities can have unfavourable effects on the desired properties of the polymer. Potential impurity issues may include: increased abrasiveness, increased water adsorption, reduction in electrical properties, heat and light stability of the polymer matrix, and health hazards (Rothon, 2002).

2.4.2 Specific gravity

Generally, particulate fillers have specific gravities that range from 2.3 – 2.8 while polymers have considerably lower specific gravities; in the range 0.9 – 1.4. The specific gravity of the composite can substantially increase by incorporation of particulate fillers at usual loadings. This often presents a drawback in polymer composites, however, there are some circumstances where fillers are applied specifically for density control. Examples include lightweight fillers in buoyancy aides and high density fillers in sound deadening composition (Rothon, 2002).

2.4.3 Morphology

The particle size, shape and the specific surface area are fundamental elements that determine particulate filler performance in all composites. Despite appearing to be easy concepts, the suitable measurement and interpretation of the parameters are challenging. The main reason is that particulate fillers have a complex distribution of both shape and size (Rothon, 2002; Wypych, 2010).

Particle size is the most extensively used parameter for filler morphology. The determination of particle size is made difficult by size distribution, shape of particles and the existence of particle aggregates or agglomerates. However, most characteristics of fillers and their successful application are dependent on particle size. Many properties of compounded materials are influenced by filler particle size, for example chemical reactivity, mechanical performance and morphology (Rothon, 2002; Wypych, 2010).

Particle shape is also an important factor in filler use as it affects processing and properties of the composites. Typical shapes of filler particles include; spherical, cubic, tabular, dendritic, flake, elongated and irregular. Each shape contributes certain advantages to the composites. Spherical particles offer the highest packing density, a uniform stress distribution, increased powder and melt flow as well as a decrease in viscosity. Elongated particles decrease shrinkage and thermal expansion, impart exceptional reinforcement and promote thixotropic properties. Cubic and tabular shapes provide good packing density and reinforcement. However, comprehensive descriptions of particle shape in the literature and specifications are rare because it is difficult to perform meaningful measurements (Rothon, 2002; Wypych, 2010).

Specific surface area (SSA), like particle size, is an important parameter useful in explaining how fillers influence the properties of compounded materials. SSA is defined as the area of surface per unit weight of the filler and is commonly determined by techniques such as gas or dye adsorption. The BET technique, which uses nitrogen as the adsorption molecule, is the most precise method. Nitrogen, being a very small molecule, can easily reach surfaces in tiny pores and crevices that larger molecules cannot access. The specific surface is measured before compounding, however, it must be kept in mind that particle breakdown may occur during processing, producing additional surface (Rothon, 2002; Wypych, 2010).

2.5. Carbon black

Carbon black is a generic term that refers to a family of industrial products that are predominantly used for elastomer reinforcement, as pigments and numerous application in the electrical industry because of its electrically conductive properties (IARC Working Group on the Evaluation of Carcinogenic Risks to Humans, 2010b). They are formed by the incomplete combustion of organic substances using several diverse manufacturing methods, for example thermal, furnace, channel and lamp processes (Leblanc, 2010; Rothon, 2002).

Furnace blacks are prepared by partial combustion of hydrocarbons (aromatic oils, natural gas) in a furnace. Channel blacks are made by impingement of natural gas flames on channel irons. Thermal blacks are manufactured by the thermal decomposition of a mixture of natural (hydrocarbons) and inert (N_2) gas. Acetylene black, a special type of thermal black, is produced by pyrolysing acetylene at high temperatures. Lamp black is manufactured by purposely burning hydrocarbons in an atmosphere deficient in oxygen to produce smoke which is cooled down and filtered to recover carbon black particles (Donnet and Voet, 1976; Leblanc, 2010).

Carbon blacks are essentially made up of elemental carbon in the form of near-spherical particles of colloidal sizes, combined primarily into particle aggregates (Donnet *et al.*, 1993). The most significant application of carbon blacks have been in elastomers because of their very fine particle size, relatively low cost, ease of manufacturing fine sizes and shapes, and chemical inertness. Most notably, the surface of carbon blacks naturally form reasonably strong attachments with elastomer molecules, with no need of expensive coupling agents (Rothon, 2002).

2.5.1 Classification

ASTM International (formerly known as the American Society for Testing and Materials) proposed a four digit classification system, ASTM D1765, which has been widely accepted for the classification of rubber. In this system, the first letter designates the curing rate (either N or S). N for normal-curing neutral and basic blacks that do not interfere (too much) with process of vulcanization; S for the slow-curing acidic channel blacks that leave chemical residues which affect the progression of vulcanisation. The first digit (between 0 and 9) indicates the elementary particle size in relation to specific area, as determined by N_2

adsorption (shown in Table 2.1). The last two digits are not standardized, and are randomly chosen and assigned by the manufacturer with reference to the aggregate structure (Donnet and Voet, 1976; Leblanc, 2010).

Table 2.1: ASTM Designation and Surface Area (SA) Limits for Commercial Carbon Blacks (Donnet and Voet, 1976).

ASTM Designation	Particle size (nm)	SA limits (m^2/g)	ASTM Designation	Particle size (nm)	SA limits (m^2/g)
N 110	11 – 19	125 – 155	S 301	26 – 30	105 – 125
N 219	20 – 25	105 – 135	N 440	31 – 39	43 – 69
N 220	20 – 25	110 – 140	N 550	40 – 48	36 – 52
N 242	20 – 25	110 – 140	N 601	49 – 60	26 – 42
N 285	20 – 25	100 – 130	N 660	49 – 60	26 – 42
N 326	26 – 30	75 – 105	N 770	61 – 100	17 – 33
N 330	26 – 30	70 – 90	N 774	61 – 100	17 – 33
N 347	26 – 30	80 – 100	N 880	101 – 200	13 – 17
N 300	26 – 30	95 – 115	N 990	201 – 500	6 – 9
N 339	26 – 30	90 – 105			

2.5.2 Application

Most of the carbon black produced is used for reinforcement of elastomers, mostly in automotive tyres. The carbon black with the highest potential for reinforcement (N 110) is rarely used in tyre applications owing to issues with processing and dispersion. Its application is limited to speciality rubbers. N 220 and N 330 blacks have the high structure form favoured for reinforcement in tyre treads and therefore they are the primary blacks applied in tyre treads. The "structure" refers to the empty space (void volume) found between the three-dimensional chain-like aggregates of carbon black particles (Al-Hartomy *et al.*, 2011). The intermediate N 285 black is sometimes used (Donnet and Voet, 1976).

Semi-reinforcing carbon blacks, such as N 770, are mostly used in tyre carcasses because they allow easy processing and have a high loading capacity. These blacks are ideal for belts, mechanical goods, cable jackets and hoses because they impart good resilience and exceptional flexing resistance to rubber. N 660 carbon blacks are classified under general

purpose blacks and these are used in rubber applications where high reinforcement is not a requirement such as hoses, cable jackets, tyre carcasses and sidewalls (Donnet and Voet, 1976).

N 880 and N 990 have the lowest reinforcing capabilities amongst all the blacks and are classified as thermal blacks. They impart high resilience, low modulus and have a very high loading capacity in rubber. Rubber composites loaded with thermal blacks has very low electrical conductivity therefore they are widely utilised in cable and wire applications, mainly as insulation jackets. These are the cheapest carbon blacks available (Donnet and Voet, 1976).

2.6. Silane coupling agents

Silane coupling agents are silicon-based chemicals that are predominantly used as cross-linkers, adhesion promoters and reactive intermediates between organic and inorganic phases in composite materials (Dow Corning, 2009; Frickel *et al.*, 2010). They have bi-functional groups (organic and inorganic) which react to form stable, chemical- and water-resistant "molecular bridges" between two phases that would otherwise be weakly bonded (Xanthos, 2010; Xie *et al.*, 2010).

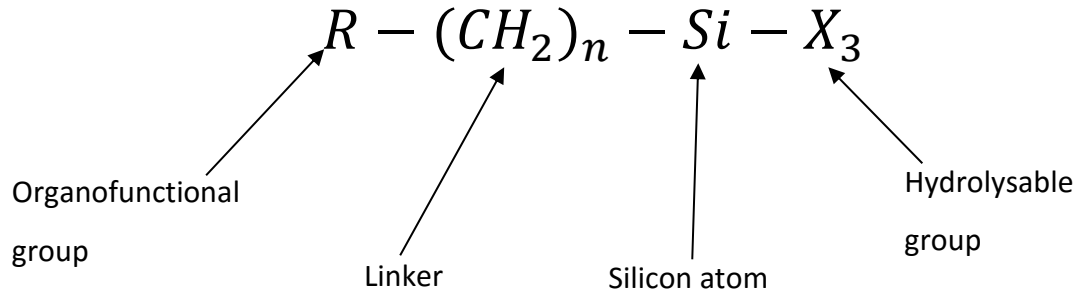

Figure 2.4: General structure of a silane coupling agent (Rosyadah Ahmad et al., 2016).

Silanes have the general chemical formula $R-(CH_2)_2SiX_3$. X is a hydrolysable group, typically ethoxy, methoxy, actetoxy, chlorine and so on. These are directly attached to the silicon and readily react with water to yield a reactive silanol (-Si-OH) which forms bonds with inorganic material. R is the organofunctional group, usually epoxy, amine and methacryloxy. It is tightly bound to the silicon by an alkyl bridge and can interact with organic material (Pardo *et al.*, 2010; Xanthos, 2010).

Two mechanisms can be used for the surface treatment applications of silanes, i.e. hydrolytic deposition and anhydrous deposition of silanes. Figures 2.5 and 2.6 illustrate the two reaction mechanisms.

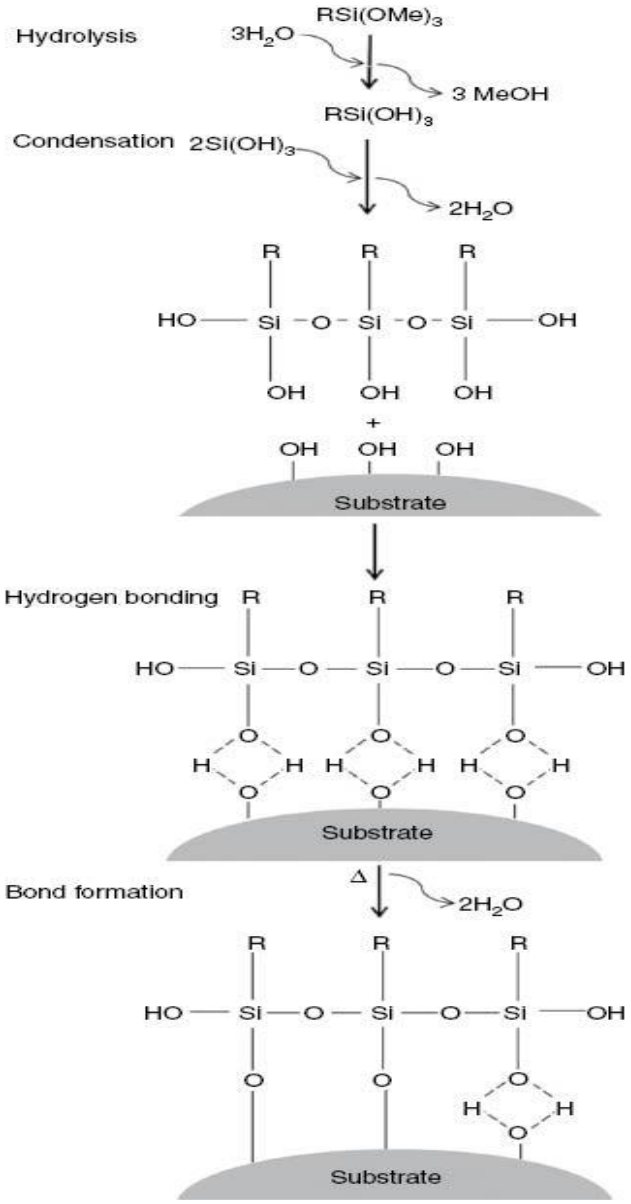

Figure 2.5: Mechanism steps for the hydrolytic deposition of silane on the substrate (Rosyadah Ahmad *et al.*, 2016).

Hydrolytic deposition of silanes involves four main steps; (1) hydrolysis, (2) condensation, (3) hydrogen bonding and (4) bond formation (Rosyadah Ahmad *et al.*, 2016). The first step is the formation of reactive silanol groups by hydrolysis of the inorganic groups. The water of hydrolysis may either be added, come from the atmosphere or may be present on the surface

of the substrate. When the silanol groups are present in solution condensation follows, forming a rigid polysiloxane $(-Si-O-Si-)$ network in the solution. The organic substituent and the amount of water available determine the degree of polymerization. Low solubility silanes favour a high degree of polymerization while the presence of multiple organic substituents (e.g. tertiary butyl or phenyl groups) will favour the formation of monomeric silanols. The monomers or oligomers then adsorb onto the hydroxyl groups of the substrate by hydrogen bonding. Lastly, a covalent bond is formed between the substrate and the monomers/oligomers, which is accompanied by the liberation of water during drying or curing (Xanthos, 2010; Xie *et al.*, 2010; Rosyadah Ahmad *et al.*, 2016).

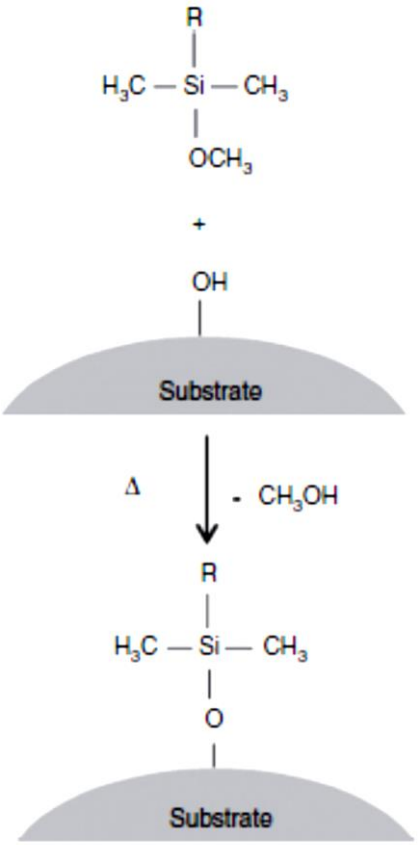

Figure 2.6: Mechanism of anhydrous deposition of silane on the substrate (Rosyadah Ahmad et al., 2016).

Anhydrous silane deposition occurs in a single step, in which covalent bond formation binds directly the silane to the hydroxyl groups on the substrate. The reaction is typically carried

out at elevated temperatures (50˚ - 120˚C) for extended reaction times (4 – 12 hours) (Arkles, 2006; Rosyadah Ahmad *et al.*, 2016).

2.6.1 Reactivity of silanes towards filler

Silane coupling agents are activated through hydrolysis, therefore their reactivity with natural fibres and polymer matrices depends on both the silane structure and on the hydrolytic conditions during the hydrolysis of the silane (Xie *et al.*, 2010; Rosyadah Ahmad *et al.*, 2016). The hydrolysis rate is significantly influenced by the type of silicon functional/alkoxy groups. The reactivity under the same hydrolytic condition is as follows: propoxy ≪ ethoxy < methoxy. Hydrolysis of methoxy groups in trimethoxysilane is faster than the hydrolysis of ethoxy groups in triethoxysilane.

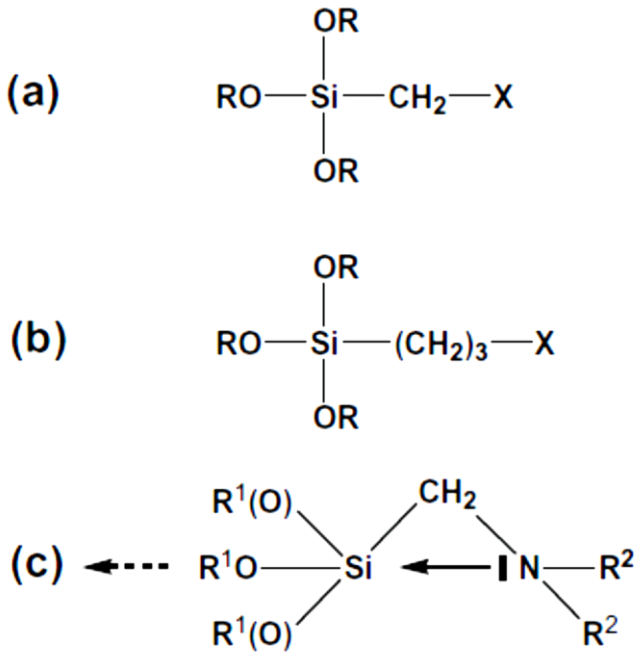

Figure 2.7: Different lengths of the bridge connecting the silicon atom and functionalities: α-silane having a methylene spacer (a), γ-silane bearing a propylene spacer (b), and a schematic diagram of the "α-effect" in the aminomethylene silane (c) (Xie *et al.*, 2010).

The hydrolysis rate of silane is also influenced by the length of the alkyl spacer by what is termed the "α effect" of silanes. Shorter alkyl groups induce greater electron interaction

between the silicon atom and the organofunctional group *(R)* and thus make the alkoxy groups more reactive. An illustration of this effect was seen by the faster hydrolysis rate of α-methacryloxymethyltrimethoxy silane (MMS, α-silane) compared to γ-methacryloxymethyltrimethoxy silane (MPS, γ-silane) in an acetone/water mixture at pH 4. This was explained by back-bonding of the free electron pair of nitrogen in α-aminoalkysilanes to the silicon atom which weakens the Si – O bonds thereby increasing the reactivity of the alkoxy group (Fig. 2.7) (Xanthos, 2010; Xie *et al.*, 2010; Rosyadah Ahmad *et al.*, 2016).

2.7. Aluminium extraction from coal fly ash

Considering the high relative abundance of aluminium content, coal fly ash has been identified as a viable option as an alternative source or supplement of aluminium in countries with scarce/without bauxite resources (Iyer, 2002; Sibanda *et al.*, 2016). Professor Grzymek of Poland pioneered alumina recovery from coal fly ash driven by diminishing bauxite resources as well as an increase in alumina demand during the Cold War in the 1950's (Yao *et al.*, 2015).

A lot of research has been conducted to develop new aluminium recovery technologies. The recent technologies of aluminium recovery can be grouped into three main categories: the acid leaching process, the soda-lime sintering process and the HiChlor process (Yao *et al.*, 2014, 2015). This study will be utilizing the acid leaching process for surface fly ash modification therefore emphasis will only be placed on that aluminium recovery technology.

Aluminium in coal fly ash occurs in both the mullite and amorphous phases. Aluminium in the amorphous phase is acid soluble, while the crystalline mullite phase is chemically stable and not directly soluble in acidic medium (Matjie *et al.*, 2005; Nayak and Panda, 2010; Sedres, 2016). Aluminium leaching processes by inorganic acids such as sulphuric acid are brought about by proton attack. The metal ion is displaced from the ash particle matrix by the hydronium ion, promoting discharge of metal ions into solution (Shemi *et al.*, 2012):

$$CaO + Al_2O_3(s) + 8H^+(aq) + SO_4^{2-}(aq) \rightarrow 2Al^{3+}(aq) + CaSO_4(s) + 4H_2O(l)$$

The extracted aluminium, in the form of an aluminium sulphate leach supernatant, is recovered by techniques such as precipitation, solvent extraction and crystallization (Shemi *et al.*, 2012).

Doucet *et al.* (2015) used a novel process that utilises ammonium sulphate ($(NH_4)_2SO_4$) as a chemical activator under thermal conditions to aid the extraction of aluminium from the amorphous phase of coal fly ash. The thermal treatment is combined with an aqueous dissolution step during which the formed, water-soluble aluminium-based salts are solubilized for further purification. Aluminium recovery of up to 95% from the amorphous phase was reported.

It has been noted that both the sulphuric acid leaching and the ammonium sulphate thermal activation processes generate large quantities of solid residues with fly ash particles retaining the desired spherical morphology but with alterations in the surface chemistry (Doucet *et al.*, 2015; Li *et al.*, 2017).

Chapter Three

Theoretical background of the analytical techniques applicable to this study

This chapter gives brief descriptions of the analytical instruments and techniques to be applied to achieve certain objectives of the study.

3.1. X-Ray Fluorescence (XRF)

X-ray fluorescence (XRF) is an analytical technique that is broadly used in the qualitative and quantitative determination of both the elemental and chemical composition of all kinds of materials. It is suitable for analysis of solids, liquids and powders, and has the added advantages of being fast and requiring minimal sample preparation (Brouwer, 2010).

The basic principle behind XRF spectrometry is that a sample is irradiated by a stream of high energy X-rays from a controlled primary X-ray source. If an electron in any of the atoms in the sample absorbs a light wave (photon) with energy (hν) greater than the shell binding energy it will be ejected from the atom. The void left behind by the emitted electron makes the electronic structure of the atom unstable. To stabilise the atom, an electron from a higher energy orbital shell in the atom drops to the lower energy vacant orbital by emitting fluorescence X-ray with energy that is equivalent to the energy difference between the final and initial orbital (Atkins and De Paula, 2010). Planck's Law can be used to calculate the wavelength of the fluorescent radiation

$$\lambda = \frac{hc}{E}$$

where λ is the wavelength, h is Planck's constant, c is the speed of light and E is the energy of the fluorescent radiation (Atkins and De Paula, 2010). The identity of a particular element can be deduced by determining the energy (wavelength) of the photon emitted since the energy difference between two orbital shells in any given element will always be the same and is characteristic of that element (Atkins and De Paula, 2010; Brouwer, 2010).

3.2. X-Ray Diffraction (XRD)

X-ray diffraction (XRD) analysis is a unique technique used to identify unknown crystalline compounds, determine atomic arrangement, structural properties and identity of polymorphic forms as well as distinguish between crystalline and amorphous phases in solids (Lin and Barron, 2014).

Analysis is carried out by an X-ray diffractometer which is made up of three main components; an X-ray tube, a sample holder and an X-ray detector. The X-ray tube produces an X-ray beam which is filtered to form a monochromatic beam and focused onto the sample. The collision of the incident ray with the electrons of the atoms in the sample scatters (diffracts) the X-ray waves to produce constructive interference as well as a diffracted ray. The detector rotates around the plane of the diffraction rays and monitors the positions and intensities of the diffraction rays when the diffraction angle satisfies Braggs Law:

$$n\lambda = 2d \sin\theta$$

where λ is the wavelength of the X-ray, θ is the incidence angle; n is any integer and d is the distance between atomic layers in crystal.

X-ray diffraction patterns are unique to each substance and can be considered a fingerprint of the substance (Willard *et al.*, 1974; Lin and Barron, 2014).

3.3. Scanning Electron Microscopy (SEM)

Scanning Electron Microscopy (SEM) is a powerful technique used to obtain morphological and topographical information from high magnification images, and to obtain elemental composition from energy dispersive signals (EDS). SEM utilizes a high-energy electron beam, rather than light photons used in optic microscopy, to generate a high resolution SEM image (Hawkes and Spence, 2007; Goldstein *et al.*, 2012).

The scanning electron microscope has the following main components; an electron source, focusing lenses, vacuum chamber, sample chamber and stage, detectors and a display system. The electron gun, typically fitted with a tungsten filament cathode, generates a beam of electrons that are accelerated down the column. The electrons are focused into a thin beam and directed onto the sample by electromagnetic lenses. When the beam of electrons reaches

the sample, electron-sample interactions produce signals which contain information about the sample shape, size, texture and composition. The signals are in the form of secondary electrons, backscattered electrons, diffracted backscattered electrons, photons, visible light and heat. Secondary electrons provide SEM images; X-rays provide mineral and elemental information while backscattered electrons provide information about the crystal structure and orientation of the specimen. These signals are picked up by a variety of detectors and are sent to the display (Hawkes and Spence, 2007; Goldstein *et al.*, 2012).

SEM imaging is done under vacuum so that the electron beam only interacts with the sample and not the air therefore the sample must be able to withstand the vacuum. The sample also needs to be conductive and electrically grounded to inhibit surface charging which may cause scanning faults like image distortion, leading to misinterpretation of results. Non-conductive material can be coated with a thin layer of conductive material (e.g. gold, platinum or graphite) using low-vacuum spattering (Hawkes and Spence, 2007; Sim *et al.*, 2010; Goldstein *et al.*, 2012).

3.4. Thermogravimetric analysis (TGA)

Thermal analysis is a technique that is used to monitor a specific parameter, under controlled heating or cooling, as a function of time and temperature. Thermogravimetric analysis (TGA) is a branch of thermal analysis which quantitatively measures any weight changes associated with a transition, whether due to oxidation, thermal degradation, dehydration or other heterogeneous reactions. TGA is used for determination of thermal stabilities, material purity and moisture content as well as to examine kinetic processes, gasification processes and corrosion (e.g. oxidation).

Three types of thermogravimetry exist; (1) Dynamic TGA, (2) Isothermal or Static TGA, and (3) Quasistatic TGA. Dynamic TGA follows a change in a specific physical property while the sample subjected to an increase/ decrease in temperature. Isothermal TGA records the change in mass over time while the sample is maintained at constant temperature. Quasistatic TGA heats the sample to a constant mass at each of a series of increasing temperatures.

A Thermobalance is the instrument used for thermogravimetry and has three major parts; an electrobalance, furnace, and a display. Results are presented in the form of thermogravimetric curves, which are a plot of mass change versus temperature or time. Thermogravimetric curves are distinctive for each compound or system because its molecular structure determines the unique order of physico-chemical changes and its associated reaction rates taking place over certain temperature ranges. The formation of heavier reaction products or evolution of volatile products that is accompanied by formation and breakage of various chemical and physical bonds at elevated temperatures causes the measured change in mass. The reaction mechanisms, thermodynamics and kinetics of the different chemical reactions, and final and intermediate products can be obtained from the data of thermogravimetric curves (Dodd and Tonge, 1987; Haines, 1995).

3.5. Infrared Spectroscopy

Infrared (IR) spectroscopy is the study of interaction between matter and electromagnetic fields in the IR region. It is used to provide qualitative and quantitative information about inorganic and organic materials. The technique utilises the interaction between infrared light and matter to produce spectra that can be analysed to deduce the types of molecules present and the concentration thereof.

The infrared absorption region of the electromagnetic spectrum starts at the edge of the red visible spectrum and extends to the microwave region, which includes radiation at wavelengths between 600 and 4000 cm^{-1}.

The total internal energy of atoms or atomic groups in molecules in a first approximation can be resolved into the sum of rotational, vibrational and electronic energy levels. In the infrared region, the electromagnetic waves couple with the molecular vibrations. Absorption of infrared radiation will increase the natural vibration of a molecule and emission of infrared radiation by a molecule is accompanied by a decrease in vibrational motion. For infrared absorption to occur, the energy of the radiation must correspond to the energy difference between the excited and the ground states of the molecule, i.e., the following relationship must be satisfied:

$$E = h\nu$$

where E is the energy of the infrared radiation, h is Planck's constant and v is the frequency of the radiation. In a conventional dispersive type spectrophotometer, a grating or prism is used to disperse light into individual frequencies, and a slit placed in front of the detector determines which frequency reaches the detector. However, a Fourier Transform Infrared Spectrometer uses an interferometer which includes two plane mirrors at right angles to each other and a beam splitter at 45° to the mirrors. FTIR is based on constructive interference of two beams to yield an interferogram. The spectrum is then obtained using a mathematical principle called Fourier Transform which is expressed as

$$F(\omega) = \int_{-\infty}^{+\infty} f(x) e^{i\omega x} dx$$

And the reverse Fourier transform is

$$f(x) = \frac{1}{2\pi} \int_{-\infty}^{+\infty} F(\omega)\, e^{-i\omega t} d\omega$$

Where ω is angular frequency and x is optical path difference, $F(\omega)$ is the spectrum and $f(x)$ is called the interferogram (Bates, 1976; Jaggi and Vij, 2006; Siesler *et al.*, 2008).

3.6. Inductively Coupled Plasma Mass Spectroscopy (ICP-MS)

A mass spectrometer is a device which breaks up gaseous molecules by bombarding them with an electron beam to produce positively charged particles consisting of the parent ion and ionic fragments of the original molecule. The charged particles are accelerated through an electric field and consequently separated in a magnetic field according to their mass/charge ratios. The relative abundance of each charged species is then plotted against the mass to charge ratio in what is termed a mass spectrum (Montaser, 1998; Barshick *et al.*, 2000).

The technique can also be applied to solids and liquids, however, the material must be vaporizable at the temperature and pressure present in the ion source. Qualitatively, mass spectrometry is useful in the determination of structure, molecular weight, elemental composition and isotopic distribution. Quantitatively, it is useful for the analysis of mixtures of liquids or gases (Barshick *et al.*, 2000).

The components of mass spectrometers vary considerably according to application; however, they all possess four basic units; (1) a sample inlet system; (2) the ion source; (3) an electrostatic accelerating system; and (4) the detector and readout system. Additionally, a high vacuum should be maintained from the inlet to the detector (Montaser, 1998).

The Inductively Coupled Plasma Mass Spectrometer (ICP-MS) is used for the determination of most elements in the periodic table. It is mostly used for quantitative analysis, however, it can also function as an excellent semi-quantitative tool. An ICP-MS is made up of the following components; (1) a sample inlet system; (2) ICP torch and RF coil; (3) interface; (4) vacuum system; (5) collision/reaction cell (6) ion optics; (7) mass spectrometer (8) detector; and (9) data handling and system controller (Montaser, 1998; Barshick *et al.*, 2000).

3.7. Brunauer-Emmet-Teller analysis (BET)

The Brunauer-Emmet-Teller (BET) theory was developed and named after Stephen Brunauer, Paul Emmet and Edward Teller in 1983. The theory intends to explain the physical adsorption of gaseous molecules onto solid surfaces and is used for the direct measurement of surface area and pore size distribution. The BET theory builds upon the Langmuir theorem, which explains the monolayer adsorption of gaseous molecules, to infinite multilayer adsorption of gaseous molecules.

Nitrogen is usually used in BET surface area analysis because it is available in high purity and it strongly interacts with most solids. Due to the weak interaction between gaseous and solid phases, liquid nitrogen is used to cool down the surface in order to obtain detectable amounts of adsorption. Stepwise addition of known amounts of gaseous nitrogen is then performed at vacuum induced pressures which are relatively lower than atmospheric pressure. Changes in pressure resulting from the adsorption process are monitored by highly precise and accurate pressure transducers. After formation of the adsorption layers, the sample is removed from the nitrogen atmosphere and heated to release the adsorbed nitrogen from material and quantify it. A BET isotherm, which is a plot of amount of gas adsorbed against the relative pressure, is displayed.

Information obtained from the isotherm is used in the BET equation to determine the surface are of the sample;

$$\frac{1}{X[(P_0/P)-1]} = \frac{1}{X_m C} + \frac{C-1}{X_m C}\left(\frac{P}{P_0}\right)$$

where X is the weight of the nitrogen adsorbed at a given relative pressure (P/P_0), X_m is monolayer capacity, which is the volume adsorbed at standard temperature and pressure (STP), and C is the BET constant. STP is defined as 273 K and 1 atm. The BET constant (C), is expressed by;

$$C = \exp\left(\frac{E_1 - E_L}{RT}\right)$$

E_1 is the heat of adsorption for the first layer, and E_L is that of the second and higher layers and is equal to the heat of liquification (Hwang and Barron, 2011; Lowell *et al.*, 2012).

The specific surface area is calculated from X_m and the cross sectional area (δ).

$$S_{BET} = \frac{X_m}{22414}.6.02 \times 10^{23}.\delta.10^{-18}$$

3.8. Zeta potential

A difference in potential develops at the interface between two phases when they are placed in contact with each other. For example if one phase is water, the dipolar molecules of water are likely to orient themselves in a specific direction at the interface thereby producing a potential difference. Normally, there is a distinctive separation in electric charge in the region where two phases come in contact in such a way that there is an excess of charge of one sign near to or on the surface of phase I and the balancing charge is spread over the adjacent surface areas of phase II.

Zeta potential (ζ) is a parameter that measures the magnitude of average electrostatic potential in the surface of shear. The surface of shear is an imaginary surface which is considered to lie near the surface of the solid phase and within which the fluid is stationary. The measurement of ζ-potential brings understanding to processes like dispersion and aggregation, and can be useful in improving the formulation of dispersions, suspensions and emulsions. The higher the zeta potential, the stronger the repulsion, the more stable the system becomes preventing particle aggregation (Clogston and Patri, 2011; Hunter, 2013).

3.9. Particle-Size Distribution

Compaction and flow properties of particulate materials (e.g. aerosols, emulsions, suspensions and powders) are influenced by the size and shape of the particles, which are useful indicators of quality and performance. Particles which are large and more spherical will usually flow much easier when compared to smaller or high aspect ratio particles. For soluble substances, smaller particles dissolve quicker than larger ones and result in higher suspension viscosities. These and many other reasons make measurement and control of particle size distribution important.

Particle size distribution (PSD) is an index that expresses the sizes and proportions of particles of varying sizes that are present in the measured sample particle group. The standard dimensions for particle amount are quantity, area, length and volume.

Laser light scattering is the most widely used technique for PSD determination. The technique uses the forward diffraction of a laser beam by particles to determine their size distribution. The angle of diffraction is inversely proportional to particle size, and the intensity of the diffracted beam at any angle is a measure of the number of particles with a specific cross-sectional area in the beam's path. Two variations of the technique exist; Fraunhofer diffraction (FD) and dynamic light scattering (DLS). The size range of particles to be investigated determines the choice of technique (Allen, 1996; Eshel *et al.*, 2004).

3.10 Rubber Process Analyser (RPA)

Rubber process analysers are used to measure the viscoelastic properties of elastomeric compounds and polymers before, during and after cure. The data obtained provides precise information about the cure speed, the cure characteristics, and the processability along with the behaviour of the compound after cure. The following parameters can be determined: torque (S' and S"), complex torque (S*), shear modulus (G' and G"), complex shear modulus (G*), dynamic real viscosity (n'), among others (Mark *et al.*, 2013).

3.11 Moving Die Rheometer (MDR)

The moving die rheometer examines the vulcanization characteristics of rubber mixtures, elastomers and India rubber. The following parameters can be determined using an MDR; lowest torque (M_L), time to vulcanization start (scorch time) t_s, torque steady-state value (M_{HF}), highest determined torque (M_H), among others. A MDR has a sealed, heated, rotorless, mobile test chamber system (MonTech Werkstoffprufmaschinen).

Chapter Four

Research Methodology

This chapter gives a description of all the experimental work that was undertaken in order to successfully complete this study. This includes sulphuric acid treatment of the ultrafine coal fly ash, thermochemical treatment of the ultrafine coal fly ash with ammonium sulphate, grafting of the silane coupling agent onto treated and untreated coal fly ash and application of all the samples as filler in natural rubber. A description of the characterisation techniques applied on treated and untreated fly ash samples as well as physical tests performed on the rubber composites are also included in the discussion.

4.1. Materials used in the study

Plasfill 5, a commercially available ultra-fine air-classified coal fly ash, with a mean particle size between 3.9 and 5.0 µm and volume distribution of more than 90% of its particles having a diameter < 11 µm, was used in this study. The fly ash sample was acquired from Ash Resources (Pty) Ltd, and originated from the Lethabo Thermal Power station in the Free State, South Africa.

The reagents used for fly ash modification were Bis[3-(triethoxysilyl)propyl]tetrasulfide (Si-69) ($S_4[C_3H_6Si(OC_2H_5)_3]_2$; reagent grade, ≥ 90%) and sulphuric acid (H_2SO_4; reagent grade, 95-98%) purchased from Sigma-Aldrich (South Africa). Ammonium sulphate $(NH_4)_2SO_4$; reagent grade, ≥99%) was purchased from Merck (South Africa). Distilled water was used in all experiments unless specified otherwise.

The rubber compounding ingredients such as stearic acid, zinc oxide, sulphur, Bis[3-(triethoxysilyl)propyl]tetrasulfide (Si-69), carbon black (N330, N660, N770 and N990) and N-tert-butyl-2-benzothiazyl sulfenamide (TBBS) were obtained from S&N Rubber (Pty) Ltd, Port Elizabeth, South Africa. Synthetic cis-1,4 polyisoprene was rubber obtained from Continental Tyre, Port Elizabeth, South Africa. Polyethylene glycol (PEG) was obtained from Sigma Aldrich, South Africa.

4.2. Physico-chemical modification of coal fly ash – preliminary study

All experiments were initially carried out on small scale to test feasibility of the treatments before upscaling. The procedures followed and the results thereof are presented in Appendix A.

4.3. Physico-chemical modification of coal fly ash for rubber compounding

This section reports on the procedures followed during upscaling of the coal fly ash modification experiments described in section 4.2 and appendix A. The samples prepared using this methodology were applied in rubber compounding.

4.3.1 Thermochemical treatment of coal fly ash using ammonium sulphate, $(NH_4)_2SO_4$

300 g of coal fly ash and 450 g of $(NH_4)_2SO_4$ (2:3 ratio) were thoroughly mixed in a 1 L ceramic container that could withstand heat up to 1000°C. The resulting mixture was placed in a static muffle furnace for 24 hours at 500°C. The reaction vessel was left to cool down for 5 hours after which the resulting solid was weighed. The same procedure was carried out 12 times to produce a sufficient amount of thermochemically treated coal fly ash. These samples were combined and milled to a fine powder in a laboratory ball mill using an alumina pot and alumina milling balls.

Water-soluble phases formed during thermochemical treatment were leached using distilled water. 1 kg of the thermochemically treated coal fly ash was added to 10 L of distilled water and stirred with an overhead stirrer at 1000 rpm at room temperature for 48 hours to ensure optimal dissolution of the water-soluble phases. The pH and conductivity of the solution was recorded at regular intervals during the first dissolution experiments in order to determine the time required to reach a plateau, i.e. maximum dissolution has been attained for the leaching conditions employed. Optimization of dissolution conditions were not investigated and falls outside the scope of this study. After the 48 hour dissolution period, the solid residue was left to settle from solution for 12 hours. The supernatant was siphoned out using a vacuum pump while ensuring that none of the solid residue was sucked out. This was filtered and stored at 4°C until analysis by ICP-MS in order to determine the extraction efficiency of aluminium from the coal fly ash. The solid residue was then washed 3 times using 1 L of

distilled water before being dried in an oven at 80°C for 24 hours. The product was milled in a laboratory ball mill to ensure homogenisation and characterised by means of FE-SEM, FTIR, PSD, TGA, XRD and XRF.

4.3.2 Sulphuric acid treatment of coal fly ash

100 g of coal fly ash was added to 400 mL of 5 M H_2SO_4 in a 500 mL Duran glass bottle with polypropylene screw cap. The slurry was placed in a reciprocal shaker set at 80°C and 200 rpm and left to react for 9 hours. Thereafter, the reaction slurry was left to cool down for 10 hours. Solid-liquid separation was performed by centrifugation at 3000 rpm for 2 minutes. The solid residue was washed 3 times using 250 mL deionised water then dried at 100°C for 24 hours. This procedure was repeated to obtain 4 kg of treated product. These products were combined and milled in a laboratory ball mill to ensure homogenisation then characterised by means of FE-SEM, FTIR, PSD, TGA, XRD and XRF.

4.3.3 Silane grafting on to coal fly ash

Silane grafting treatment on untreated, thermochemically treated (by $(NH_4)_2SO_4$) and sulphuric acid treated fly ash samples was done at room temperature. 40 mL of Si-69 (2% v/v Si-69: ethanol) and 20 mL of distilled water was added to 2 L of ethanol and stirred at 1000 rpm for 15 minutes using an overhead stirrer. 2 kg of the relevant fly ash sample was added to the ethanol solution which was then stirred for 1 hour to achieve uniform distribution of the coupling agent. The resulting slurry was oven-dried for 12 hours at 120 °C to ensure completion of the dehydration and bond formation steps (Section 2.6). The product was milled in a laboratory ball mill to ensure homogenisation then characterised by means of FE-SEM, FTIR, PSD, TGA, XRD and XRF.

4.4. Chemical and physical characterization of solid and liquid samples

The untreated fly ash, thermochemically treated fly ash, thermochemically treated and leached fly ash, sulphuric acid treated fly ash and their respective leachates, as well as the respective silane-treated samples were analysed using the analytical techniques described in the previous chapter. The methodology followed is discussed in more detail below.

4.4.1 X-ray Fluorescence (XRF) analysis

X-ray fluorescence analysis was used to determine the chemical/elemental composition of the fly ash samples. A Thermo Fisher ARL Perform'X Sequential fluorescence spectrometer with OXSAS software was used. The samples were prepared as pressed powders. Blank and certified reference materials are analysed with each batch of samples. The analysis was performed in duplicate. The values were not normalised as no LOI was done.

Fused bead analysis presented inaccurate results for SO_3 and for this reason XRF analysis was performed on a pressed powder on which the loss on ignition (LOI) cannot be measured. A discussion on the LOI will be included in the discussion of the TGA data. Accuracy of SO_3 data determined by XRF was validated using LECO SC-632 Carbon and Sulphur Determinator (LECO Corporation, Australia).

4.4.2 X-ray Diffraction (XRD) analysis

XRD was used to determine the mineralogical composition of the fly ash samples. A PANalytical X'Pert Pro powder diffractometer with an X'Celerator detector and variable divergence with Fe filtered Co-Kα radiation was used. The phases were identified using X'Pert Highscore plus software, and 20% Si (Aldrich 99% pure) was added to the coal fly ash to determine the amorphous (glass) content. The relative phase amounts were estimated by the Rietveld method (Autoquan Program).

4.4.3 Field Emission Scanning Electron Microscopy (FE-SEM)

FE-SEM was used to examine the morphology of the untreated and treated fly ash samples. The samples were mounted onto an adhesive, double-sided carbon tape before coating with carbon using an Emitech K550X sputter coater (Ashford, England). Carbon paint was applied to the edges of the samples to improve conductivity of the samples. The images were viewed under high vacuum conditions using a Zeiss Ultra SS (Germany) Field Emission Scanning Electron Microscope operated at an acceleration voltage of 1kV.

4.4.4 Thermogravimetric Analysis (TGA)

Thermogravimetric analysis was done using a Thermogravimetric Analyser (TA Instruments SDT Q600), Fig. 4.1. A multipoint temperature calibration was performed using indium, zinc

and gold calibration standards. Weight calibration was carried out using the manufacturer supplied calibration weights. Approximately 20 mg of the sample was weighed out into a 150µL alumina pan and heated in the TGA furnace under dynamic conditions from 25°C to 1200°C at a constant heating rate of 10°C per minute. All TGA experiments were conducted in high purity Afrox nitrogen gas (N_2; 99.997%) with constant flow rate of 100 mL/min.

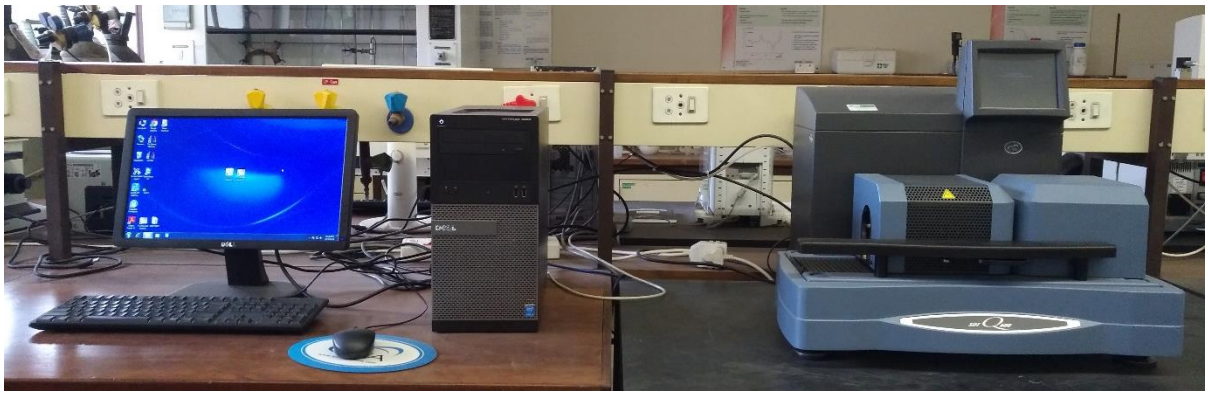

Figure 4.1: TA Instruments SDT Q600 TGA/DSC analyser

4.4.5 Fourier Transform Infrared (FTIR) Spectroscopy

FTIR analysis was carried out in order to gain insight into the bulk characteristics of the untreated and treated samples. FTIR spectra were recorded using a Bruker Alpha Platinum ATR (attenuated total reflection), Fig. 4.2, by placing the finely ground samples on a diamond ATR sample holder.

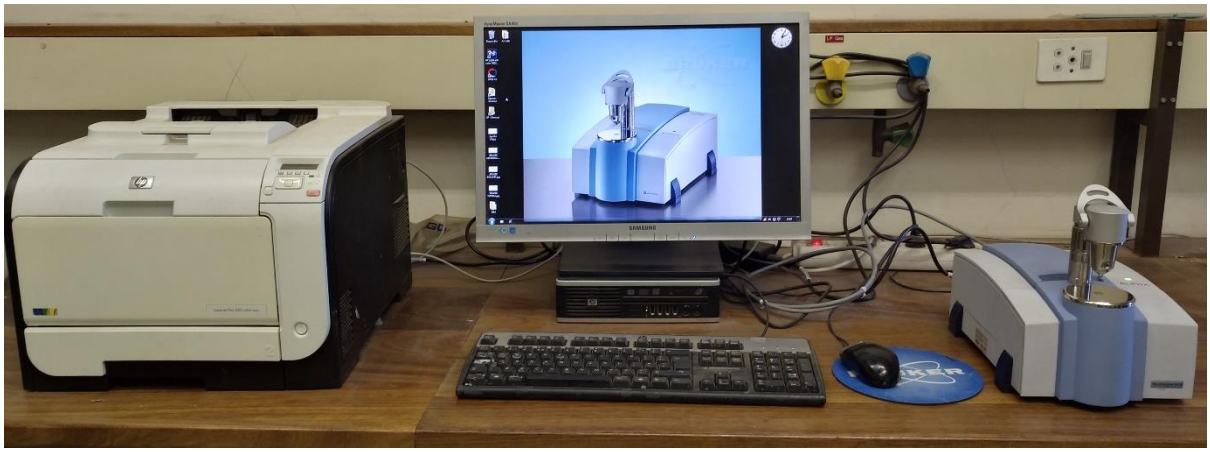

Figure 4.2: Bruker Alpha Platinum ATR

The FTIR spectra of the fly ash samples were recorded under atmospheric conditions in the range 400 to 4000 cm^{-1} at a resolution of 2 cm^{-1} and 64 scans were signal-averaged in each interferogram.

4.4.6 Inductively Coupled Plasma Mass Spectroscopy (ICP-MS)

The major, minor and trace elements in the leachates were quantitatively analysed using a NexIon 300D ICP-MS (Perkin Elmer, USA). Analysis was performed by an accredited laboratory (Waterlab (Pty) Ltd, Pretoria, South Africa). A 1 ppm multi-element stock solution was used to perform the calibration for all trace elements as well as 100-500 ppm standards for Al, Ca, Fe, Mg, K and Na. The measurements were done in triplicate.

The elemental extraction efficiencies following dissolution of water-soluble species from thermochemically treated coal fly ash were calculated.

4.4.7 Brunauer-Emmet-Teller analysis (BET)

The surface area of the fly ash samples was determined using a TriStar II surface area and porosity analyser (Micromeritics, USA), Fig. 4.3, by the Brunauer-Emmet-Teller theory. Nitrogen gas was used as adsorbent.

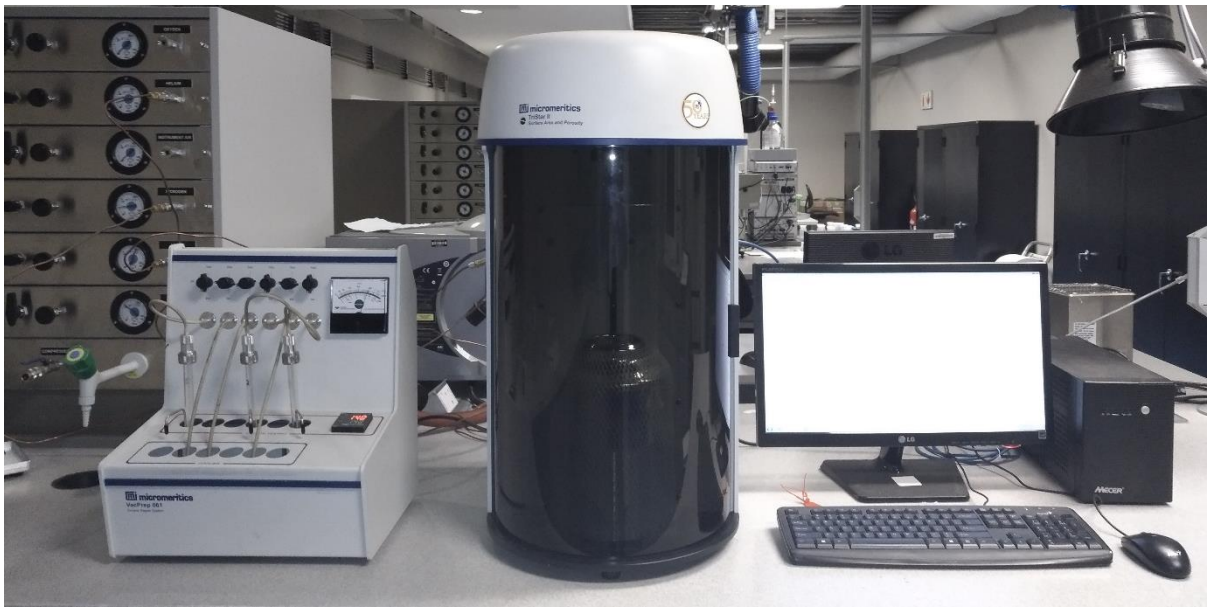

Figure 4.3: TriStar II Surface Area and Porosity Analyser

The coal fly ash samples were degassed at 140°C for 2 hours before the gas adsorption tests were performed. The measurements were performed in duplicate.

4.4.8 Zeta potential

The zeta potential of the fly ash particles was measured using a Malvern Nano ZS Zetasizer Nano particle analyser (Malvern Instrument Ltd., Worcester, UK). 0.1 g of the fly ash particles were hydrolysed in 25 mL ultra-pure water for 30 minutes before measurement. The initial pH was measured on 10 mL of the suspension and recorded while the suspension was being stirred at 25°C. Auto-titration was performed to determine the iso-electric points of the powders, during which the pH of the ash suspension was adjusted by HCl (0.25 M) or NaOH (0.10 M) to cover a pH range from 2.5 to 10 in approximately 1.0 pH unit increments. The zeta potential was measured in triplicate at each pH value.

4.4.9 Particle-Size Distribution (PSD) Analysis

PSD for the treated and untreated fly ash samples were obtained by laser diffraction using a Malvern Mastersizer 2000 (Figure 4.4) fitted with a Hydro 2000G dispersion unit (Malvern Instruments Ltd., Worcester, UK.).

Figure 4.4: Malvern Mastersizer 2000

The samples were dispersed in water at ambient temperature and the analysis was conducted under the following set of variables: constant obscuration between 10 – 20%, stirring speed of 650 rpm, pump speed of 1650 rpm, and ultrasonic power of 10%. The samples were run in duplicate with three runs per duplicate. The results were logged as particles per volume

percent and an average obtained to produce the particle size distribution. The particle sizing analysis was done in order to determine the effect of the surface modification treatments on the particle size of the coal fly ash samples.

4.5. Formulations and mixing procedures followed for the preparation of the rubber-fly ash composites

This section reports on the formulations and mixing procedures followed for the preparation of the rubber-fly ash/carbon black composites.

Table 4.1 gives a brief description of the instruments used and their respective functions in preparation of fly ash/carbon black composites.

Table 4.1: Instruments used in the preparation of rubber-fly ash/carbon black composites

Instrument	Function
Brabender internal mixer with 330 mL volume capacity	Mixing of cis-1,4-polyisoprene and vulcanization agents with fly ash, carbon black or fly ash/carbon black hybrid fillers.
Two roll mill	Blending and cooling of fly ash/carbon black mixture composites.
MonTech rubber process analyser (RPA)	Determination of viscoelastic properties of rubber composites.
MonTech moving die rheometer (MDR)	Determination of optimum cure time at a specific temperature
Hydraulic heat press	Curing fly ash/carbon black composites under pressure to form cross-linked flat sheets.

4.5.1 Formulation and mixing procedure followed for the neat rubber.

Table 4.2: Formulation used for cis-1,4-polyisoprene rubber (no filler)

Material	phr[a]	SG[b] (g/mL)	Volume (mL)	Mass (g)
Cis-Polyisoprene	100	0.97	103.09	224.54
ZnO	5	5.40	0.93	11.23
Stearic acid	2	0.92	2.17	4.49
Sulphur	1	2.07	0.48	2.25
TBBS	2	1.29	1.55	4.49
Polyethylene glycol (PEG)	2	1.00	2.00	4.49
Total	112	1.02	110.23	251.48

[a] parts per hundred rubber

[b] Specific gravity

Cis-1,4-polyisoprene rubber (no filler) composites were prepared using the compounding formulation in Table 4.2.

I. Pieces of the weighed out cis-polyisoprene were added to the internal mixer for mastication for 45 ± 15 seconds at 80 rpm.
II. Polyethylene glycol (PEG) was added to the mixture and left to mix for 120 seconds.
III. ZnO and Stearic acid were added followed by mixing for another 120 seconds.
IV. The mixture was removed from the internal mixer and run 3 times through a two roll C mill (1 mm nip) set to a circulation temperature of 25°C, cut into strips and allowed to cool down. The mix was turned at 90° after each pass.
V. The strips were fed back into the internal mixer at 80rpm and masticated for 45 ± 15 seconds before sulphur and TBBS were added. This was followed by 120 seconds of mixing.
VI. The compounded elastomer was taken out from the internal mixer and run 3 times through the two roll mill (1 mm nip).

4.5.2 Formulation and mixing procedure followed for the rubber-carbon black-fly ash composites.

Table 4.3: Formulation used for fly ash-filled cis-1,4-polyisoprene rubber (Fill factor = 0.75)

Material	phr[a]	SG [b] (g/mL)	Volume (mL)	Mass (g)
Cis-Polyisoprene	100	0.97	103.00	203.98
Fly Ash	25	2.25	11.10	50.99
ZnO	5	5.40	0.93	10.20
Stearic acid	2	0.92	2.17	4.08
Sulphur	1	2.07	0.48	2.04
TBBS	2	1.29	1.55	4.08
PEG	2	1.00	2.00	4.08
Total	137	1.13	121.34	279.45

[a] parts per hundred rubber

[b] specific gravity

Table 4.4: Formulation used for carbon black-filled cis-1,4-polyisoprene rubber (Fill factor = 0.75)

Material	phr[a]	SG[b] (g/mL)	Volume (mL)	Mass (g)
Cis-Polyisoprene	100	0.97	103.09	199.41
Carbon Black	25	1.80	13.89	49.85
ZnO	5	5.40	0.93	9.97
Stearic acid	2	0.92	2.17	3.99
Sulphur	1	2.07	0.48	1.99
TBBS	2	1.29	1.55	3.99
PEG	2	1.00	2.00	3.99
Total	137	1.10	124.12	273.19

[a] parts per hundred

[b] specific gravity

Table 4.5: Formulation for cis-1,4-polyisoprene rubber partially filled with carbon black and fly ash (Fill factor = 0.75)

Material	phr[a]	SG[b] (g/mL)	Volume (mL)	Mass (g)
Cis-Polyisoprene	100	0.97	103.09	199.41
Fly Ash	12.5	2.25	5.56	25.21
Carbon Black	12.5	1.80	6.94	25.21
ZnO	5	5.40	0.93	10.08
Stearic acid	2	0.92	2.17	4.03
Sulphur	1	2.07	0.48	2.01
TBBS	2	1.29	1.55	4.03
PEG	2	1.00	2.00	4.03
Total	137	1.12	122.73	273.29

[a] parts per hundred

[b] specific gravity

Carbon black and fly ash filled cis-1,4-polyisoprene rubber composites were prepared using the compounding formulation in Tables 4.3 – 4.5.

I. Pieces of the weighed out cis-polyisoprene were added to the internal mixer for mastication for 45 ± 15 seconds at 80 rpm.
II. Fly ash/Carbon black was added to the mixer and the plunger was lowered. Mixing was continued for 120 seconds at 80 rpm.
III. PEG was added to the mixture and left to mix at 80 rpm for 120 seconds.
IV. ZnO and Stearic acid were added followed by mixing for another 120 seconds.
V. The mixture was removed from the internal mixer and run 3 times through a two roll mill (1 mm nip) set to a circulation temperature of 25°C, cut into strips and allowed to cool down. The mix was turned at 90° after each pass.
VI. The strips were fed back into the internal mixer at 80rpm and masticated for 45 ± 15 seconds before sulphur and TBBS were added. This was followed by 120 seconds of mixing.
VII. The compounded elastomer was taken out from the internal mixer and run 3 times through the two roll mill (1 mm nip).

4.5.3 Formulation and mixing procedure followed for in-situ addition of Si-69 to rubber-fly ash composites.

Table 4.6: Formulation used for in-situ addition of Si-69 to fly ash-filled cis-1,4-polyisoprene rubber (Fill factor = 0.85)

Material	phr[a]	SG[b] (g/mL)	Volume (mL)	Mass (g)
Cis-Polyisoprene	100	0.97	103.09	231.14
Fly Ash	25	2.25	11.11	57.78
Si69	0.8	1.10	0.73	1.85
ZnO	5	5.40	0.93	11.56
Stearic acid	2	0.92	2.18	4.62
Sulphur	1	2.07	0.48	2.31
TBBS	2	1.29	1.55	4.62
PEG	2	1.00	2.00	4.62
Total	137.8	1.13	122.06	318.51

[a] parts per hundred

[b] specific gravity

In-situ Si69 addition to fly ash filled cis-1,4-polyisoprene rubber composites was done using the compounding formulation in Table 4.6. A higher fill factor (0.85) was used in order to increase the temperature of the mixture during compounding.

I. Pieces of the weighed out cis-1,4-polyisoprene were added to the internal mixer for mastication for 45 ± 15seconds at 80 rpm.
II. Fly ash was added to the mixer and the plunger was lowered. Mixing was continued for 120 seconds at 80 rpm.
III. Si-69 was added to the mixture and left to mix at 80 rpm for 120 seconds.
IV. PEG was added to the mixture and the mixer rate was increased to 100 rpm. Mixing continued until the temperature increased to 140°C after which mixing was timed for 120 seconds.
V. ZnO and Stearic acid were added followed by mixing for another 120 seconds.

VI. The mixture was removed from the internal mixer and run 3 times through a two roll mill (1 mm nip) set to a circulation temperature of 25°C, cut into strips and allowed to cool down. The mix was turned at 90° after each pass.

VII. The strips were fed back into the internal mixer at 80rpm and masticated for 45 ± 15 seconds before sulphur and TBBS were added. This was followed by 120 seconds of mixing.

VIII. The compounded elastomer was taken out from the internal mixer and run 3 times through the two roll mill (1 mm nip).

4.6. Vulcanization/ curing of the rubber composites

The curing characteristics of a rubber composite determine the behaviour of the composite during processing and therefore influence the physical properties indirectly. Hence they are regarded as one of the most important features (Kruger *et al.*, 1999; Mark *et al.*, 2013).

The curing characteristics of the prepared rubber composites were determined at 150°C using a Moving Die Rheometer (MDR 3000 Basic, MonTech; Figure 4.1) under a constant frequency of 1.67 Hz and an angle of 0.5°.

Figure 4.5: MonTech MDR 3000 Basic Moving Die Rheometer

The optimum cure time (t_{90}) values were derived from the vulcanization curves. 50 – 60 g of the compounded elastomers were pressed in a flat sheet mould and vulcanized to optimum cure (t_{90}) at 150°C. After t_{90}, the sheets were quenched in water to prevent over-curing. 40 – 50 g of the compounded elastomers were also pressed in block moulds and vulcanized until t_{90} at 150°C. The blocks were used for hardness and rebound tests.

4.7. Mechanical property measurements of the rubber vulcanizates

The neat cis-1,4-polyisoprene rubber, fly ash- and carbon black filled rubber composites were tested for their physical properties. A durometer was used to determine the hardness of the neat rubber (NR), fly ash filled rubber (FAR) and carbon black filled rubber (CBR) in accordance with the ASTM D2240 standard. The hardness was determined at three different positions and the median value indicated.

Samples were tested using a method that was as close to ASTM D412 as possible. An Instron 3360 tensile test machine with a knurled, self-tightening grip, crosshead speed of 500 mm/min and 1-kN load cell was used to determine the tensile properties. The sheets from which the dumbbells were cut were left overnight to condition before being subjected to the tensile test machine. Since a Die C (ASTM D412) dumbbell cutter was not available at the rubber testing centre, a special cutter was used to produce smaller non-standard dumbbell shaped specimens. The sample dimensions were 25 mm by 4 mm instead of 33 mm by 6 mm in die C. The specimens were symmetrically placed at the grips of the testing machine to achieve uniform tension distribution over the cross section.

Chapter Five

Characterization of untreated coal fly ash

This chapter provides detailed characterization of the untreated coal fly ash (UFA) sample in order to effectively assess changes induced by the chemical (Si-69 treatment) and physico-chemical (thermochemical and sulphuric acid treatment) modifications applied; as well as to better understand the interaction between fly ash samples and cis-1,4-polyisoprene rubber.

5.1. Chemical and mineralogical composition

The concentrations of major and minor elements in UFA were determined by XRF analysis. Table 5.1 reports the composition of the minor and major elements found in untreated fly ash (UFA). The samples were prepared as pressed powders. Blank and certified reference materials are analysed with each batch of samples. The analysis was performed in duplicate. The values were not normalised as no LOI was done. The major constituents of the fly ash sample were SiO_2 (52.6%), Al_2O_3 (37.1%), CaO (4.3%), Fe_2O_3 (2.9%), MgO (1.4%) and TiO_2 (1.6%). Trace amounts of elements such as ZrO_2, MnO, V_2O_5, Cr_2O_3, NiO, Na_2O and CuO were also present in wt. % concentrations < 0.1%.

Table 5.1: The elemental composition of untreated coal fly ash (UFA) *(n = 3)*

	Concentration (wt. %)[a]									
	SiO_2	Al_2O_3	CaO	Fe_2O_3	TiO_2	MgO	K_2O	P_2O_5	SO_3	Total
UFA	52.6	37.1	4.3	2.9	1.6	1.4	0.8	0.9	0.2	102.7

[a] Other elements present in small amounts (<0.1%): ZrO_2, MnO, V_2O_5, Cr_2O_3, NiO, Na_2O, CuO.

The combined aluminium and silica content in untreated fly ash (UFA) was more than 85%, and the average SiO_2/Al_2O_3 ratio was 1.4. According to the American Society of Testing

Materials (ASTM C618), a low lime ash containing more than 70% Al_2O_3 + SiO_2 + Fe_2O_3 is classified as siliceous (ASTM International, 2010). The total alkaline earth metals (CaO + MgO) content was about 6%, while the total alkaline (Na_2O + K_2O) concentration was less than 1%. These findings are consistent with results obtained from a similar study (van der Merwe, Prinsloo, *et al.*, 2014).

XRD analysis was used for mineral identification and the quantification of the crystalline and amorphous phases present in untreated fly ash. The background corrected X-ray diffraction pattern of the untreated fly ash sample is shown in Figure 5.1.

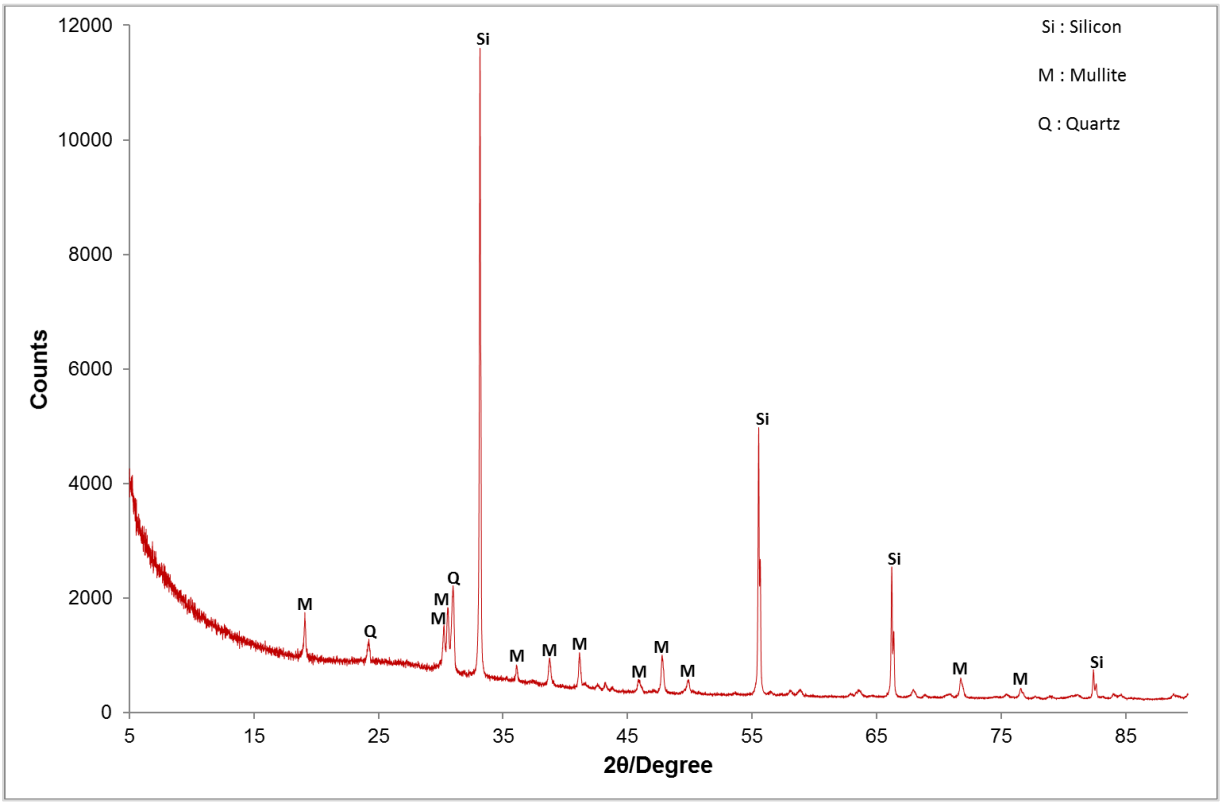

Figure 5.1: Background corrected X-Ray Diffraction pattern of untreated coal fly ash (UFA).

Table 5.2 presents the quantitative XRD results of the untreated coal fly ash. The results shown are an average of three measurements *(n = 3)*. These indicate that the coal fly ash sample consisted of an amorphous alumina-silicate glass phase (69.1 wt. %) and two crystalline phases; mullite (29.1 wt. %) and quartz (5.8 wt. %). These results are consistent with data obtained by van der Merwe *et al.* (2014) for a similar coal fly ash sample.

Table 5.2: Quantitative XRD results of untreated coal fly ash (UFA) *(n = 3)*

Mineral Phase	Chemical formula	Weight%
Amorphous		69.1
Mullite	$Al_6Si_2O_{13}$	29.1
Quartz	SiO_2	5.8

5.2. Spectroscopic analysis

The FTIR spectrum of the untreated fly ash is shown in Figure 5.2. Occurrence of the many phases (both glassy and crystalline) present in fly ash is evident in the broad band appearing between 729 cm^{-1} and 1100 cm^{-1}. This band is attributed to the presence of the Si–O–Si and Al–O–Si networks (van der Merwe *et al.*, 2011; Al Bakri Abdullah *et al.*, 2012). It is difficult to distinctly resolve and identify the position of infrared bands in fly ash due to the overlapping of bands related to Si–O–Si and Al–O–Si networks in the regions between 729 and 1100 cm^{-1} (Nookala, 2006; Rees *et al.*, 2007).

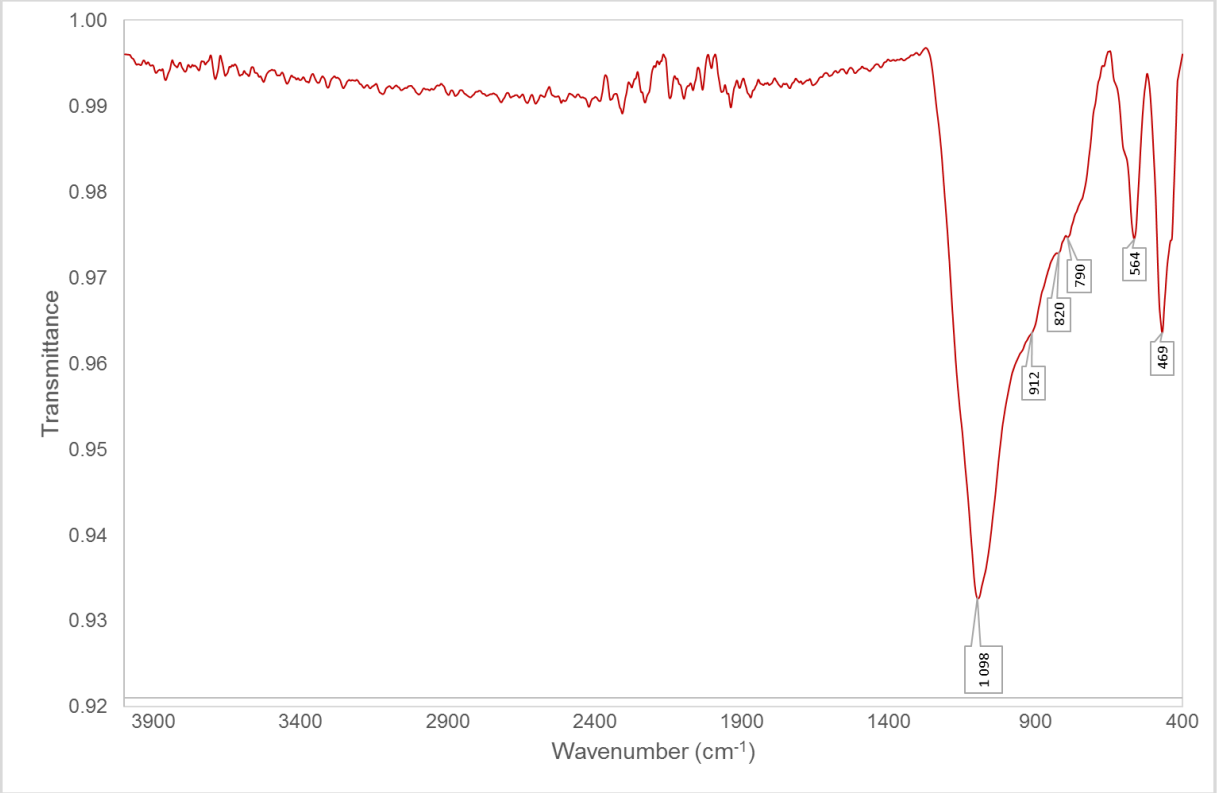

Figure 5.2: FTIR spectrum of untreated coal fly ash (UFA).

The strongest band was observed at 1098 cm^{-1} and is attributed to Si–O–Si asymmetric stretching from quartz, mullite and the glass phases (Numluk and Chaisena, 2012; van der Merwe, Prinsloo, *et al.*, 2014). The band at 911 cm^{-1} is assigned to Al–O symmetrical stretching vibrations from mullite, while the band at 786 cm^{-1} is assigned to Al–O stretching (Numluk and Chaisena, 2012). Al–O stretching vibrations from mullite occur at about 561 cm^{-1} while Si–O–Si and Al–O–Al symmetric bending vibrations present a peak at 470 cm^{-1} (Belver *et al.*, 2002; van der Merwe, Prinsloo, *et al.*, 2014).

5.3. Thermal analysis

The thermal behaviour of the fly ash was investigated using TGA analysis in order to understand the effect of thermal treatment thereon. Figure 5.3 indicates the mass loss curve obtained from TGA analysis.

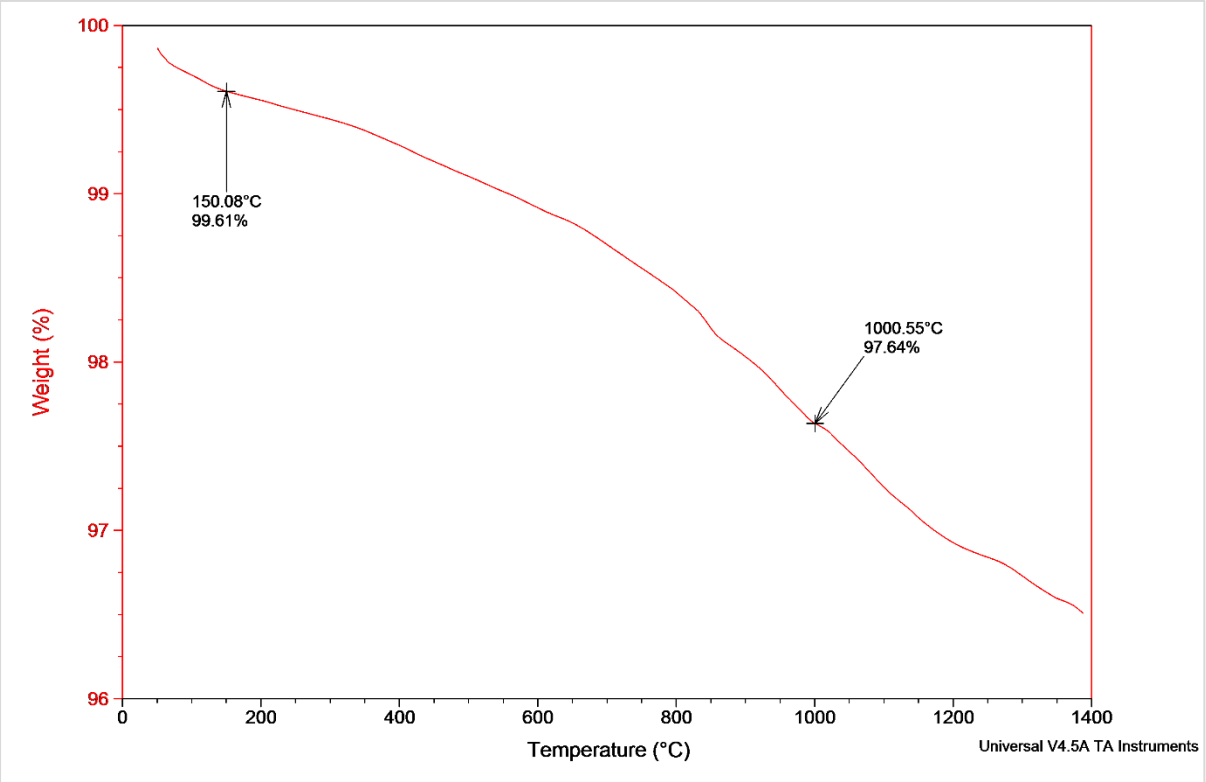

Figure 5.3: Thermogravimetric analysis of untreated coal fly ash (UFA).

The overall mass loss from the sample up to 1400°C was less than 4% and therefore it is difficult to assign mass loss events to specific decomposition and/or oxidation steps. For this

reason a general discussion on the thermal behaviour of untreated fly ash, based on literature, is included.

When coal fly ash is heated in air, the initial mass loss recorded (100 to 400°C) in the TG curves can be assigned to the loss of physically bound and unbound water, and dehydration of silanol present in low percentages in the coal fly ash (Kuusik *et al.*, 1985; van der Merwe *et al.*, 2011). TGA results of the UFA sample (Figure 5.3) indicate a low mass loss (<1%) in this region.

Heating coal fly ash in an oxidizing environment, a mass loss in the temperature range between 500 and 740°C can be attributed to the oxidation of carbon and/or the decomposition of calcium carbonate ($CaCO_3$) (Payá *et al.*, 1998; van der Merwe, Prinsloo, *et al.*, 2014):

$$2C(s) + xO_2 \rightarrow 2CO_x(g) \ \ (x = 1 \ or \ 2) \quad [1]$$

$$CaCO_3(s) \rightarrow CaO(s) + CO_2(g) \quad [2]$$

A very low mass loss (approx. 0.5%) was observed for the UFA sample over this temperature range (Figure 5.3). The TGA runs were performed in an inert nitrogen atmosphere, limiting the oxidation of carbon as described in equation 1. Previous results reported for a similar fly ash sample from the same source indicated a carbon content of 0.3% (van der Merwe, Prinsloo, *et al.*, 2014). No $CaCO_3$ was detected in the sample by any of the other analytical techniques applied (e.g. XRD); however, it is possible that the UFA sample contained $CaCO_3$ in quantities below the detection limit of these techniques.

The literature describes the decomposition of $CaSO_4$ contained in coal fly ash to occur over a wide temperature range, with its onset being approximately 800°C (van der Merwe, Mathebula, *et al.*, 2014; Shimizu, et al.):

$$CaSO_4(s) \rightarrow CaO(s) + SO_3(g) \quad [3]$$

The $CaSO_4$ content of UFA would have been in an amount lower than the detection limit of the XRD (Table 5.2), but sulphur analysis by the LECO SC-632 Carbon and Sulphur Determinator quantified the SO_3 content to be approximately 0.15%. Considering the mass loss from UFA between 800 and 1200°C (approx. 1.2%), the contribution from the loss of SO_3 is minimal.

The loss on ignition (LOI) is a parameter that is generally used to describe the suitability of fly ash use in concrete. The oxidation of unburnt free carbon, decomposition of carbonates and sulphates, and removal of volatile components as well as combined water present in the ash all contribute to the LOI. Fly ash samples with high carbon content will normally have high LOI values (Payá *et al.*, 1998; Vandenberghe *et al.*, 2010; Wang *et al.*, 2012). The low density of carbon allows it to absorb significant amounts of water, hence the maximum dry density and moisture content of fly ash samples are influenced by the LOI value. Generally, the lower the carbon content of fly ash, the better its prospects of utilization (Cao *et al.*, 2008).

The UFA sample had a low LOI (approx. 2.36%) which was confirmed by TGA analysis as the mass loss up to 1000°C (Figure 5.3). This showed that UFA had a low carbon and moisture content before use, and the volatile content remaining after the coal combustion process was not very high.

There is negligible mass loss recorded for UFA up to 150°C (Figure 5.3), the temperature at which vulcanization was carried out.

5.4. Particle size distribution and BET surface area

The particle size of the untreated fly ash (UFA) sample was found to fit a log-normal size distribution (Figure 5.4).

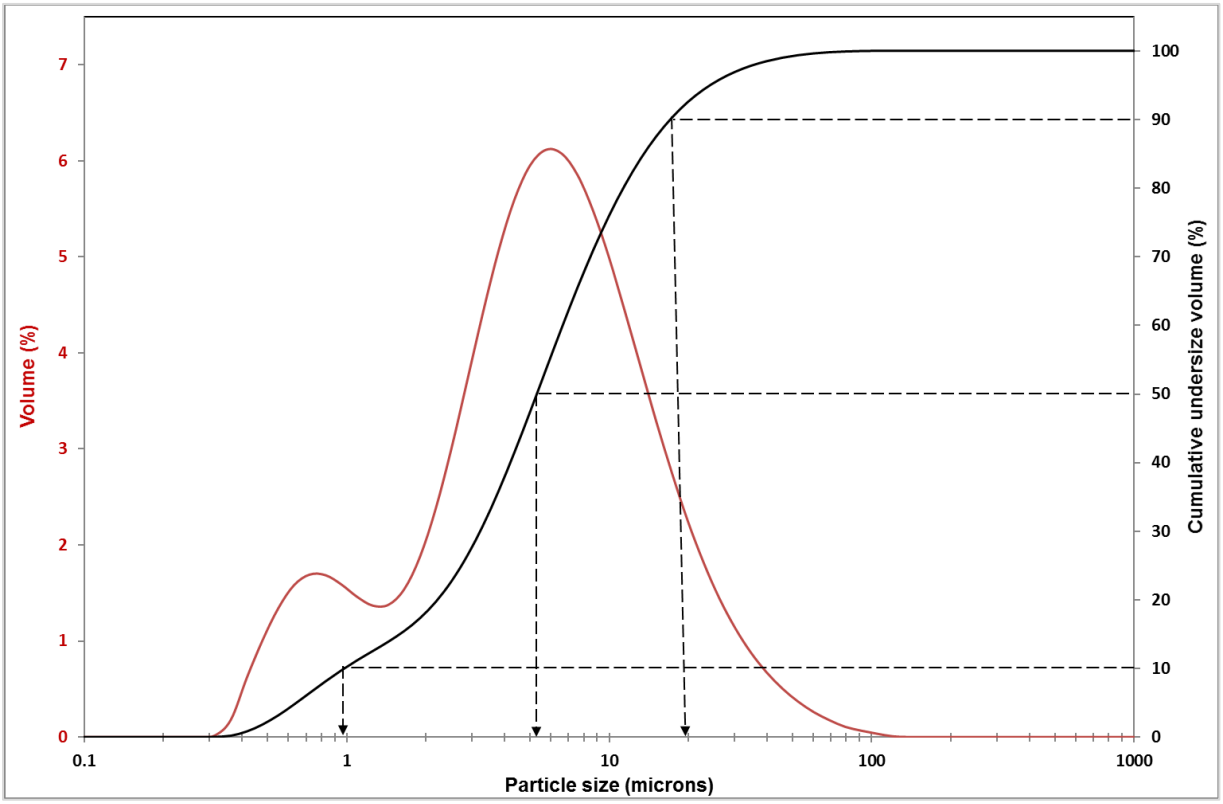

Figure 5.4: Particle size distribution of the untreated coal fly ash (UFA).

The sample presented a bimodal peak ranging widely in particle size (0.3 – 100.0 µm). The mean particle size of the ash was determined to be 5.2 µm with 90% of the volume distribution having particle sizes smaller than 16.0 µm. The particle size distribution appeared to be consistent with the data obtained from the SEM micrographs (Section 5.6). The BET surface area of the untreated coal fly ash was determined to be 0.99 m^2/g. The data obtained for particle size and surface area analyses corresponded with the results obtained for a similar sample by van der Merwe *et al.* (2014).

5.5. Zeta Potential

The change in zeta potential of untreated fly ash in water measured at various pH values are presented in Figure 5.5. Under the conditions tested, the fly ash-water system had an initial

pH of approximately 9 and it was observed that the fly ash particles were positively charged at low pH and negatively charged above pH 3.7. The isoelectric point (IEP) was measured at pH 3.72. The IEP is the pH at which the negative surface charge on the fly ash equals the positive surface charge (Weng and Huang, 2004).

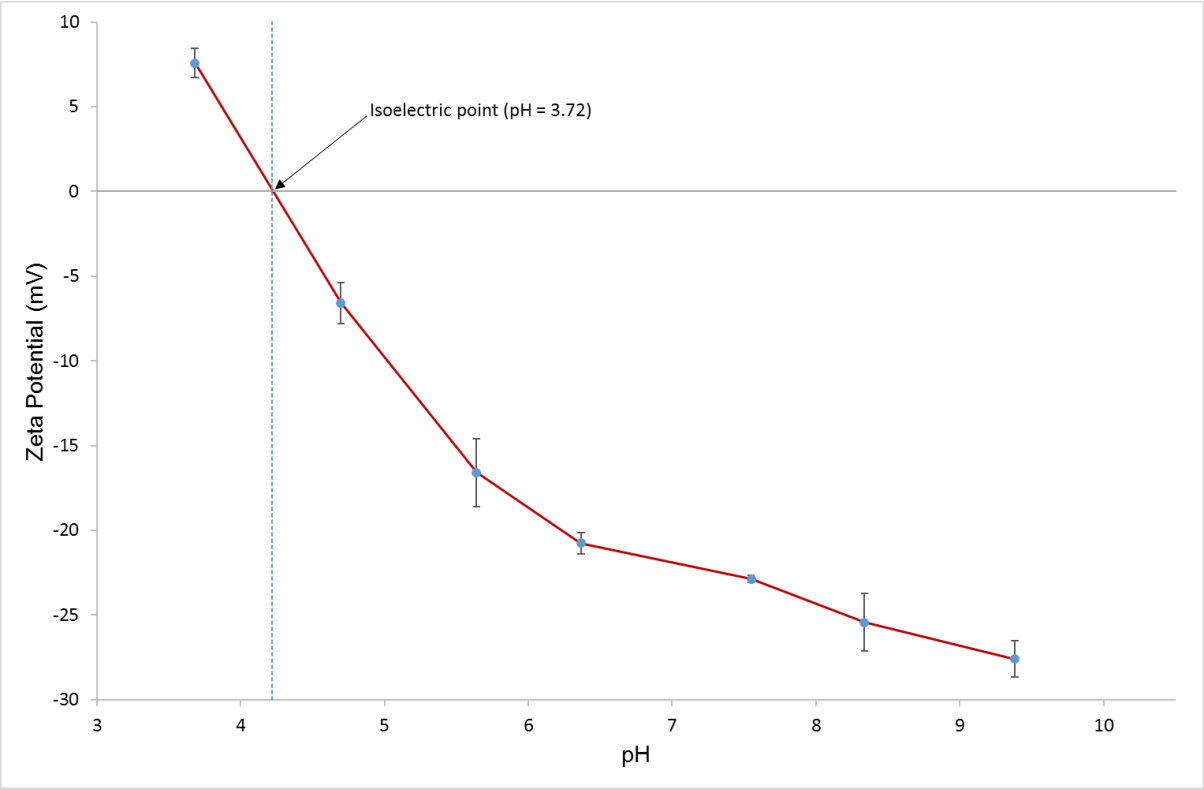

Figure 5.5: Variation of zeta potential of the untreated fly ash (UFA) sample with pH.

The zeta potential of the fly ash was found to be negative (-27 mV) upon dispersion in deionised water (at pH = 9). The surfaces of fly ash particles have a high concentration of silica and alumina functional groups, the most common being silicates (–O –SiO_2^-) and aluminates (–O – AlO^-). The surface silicate groups are likely to be extensively deprotonated owing to the high pH of the fly ash-water system giving rise to the negatively charged surface (Gunasekara *et al.*, 2015). Silanol groups on the fly ash surface may dissociate according to the following reactions (Júnior and Baldo, 2014):

$$SiOH + OH^- \leftrightharpoons SiO^- + H_2O \qquad [4]$$

$$SiOH + H^+ \rightleftharpoons SiOH_2^+ + H_2O \qquad [5]$$

Weng and Huang, (2004) speculated that the low value of the isoelectric point observed for fly ash particles can be attributed to its high silica content, leading to extensive deprotonation under basic conditions.

5.6. Morphological characterization

FE-SEM was used to observe the morphology and surface characteristics of untreated fly ash. The images obtained for the untreated coal fly ash sample are presented in Figure 5.6.

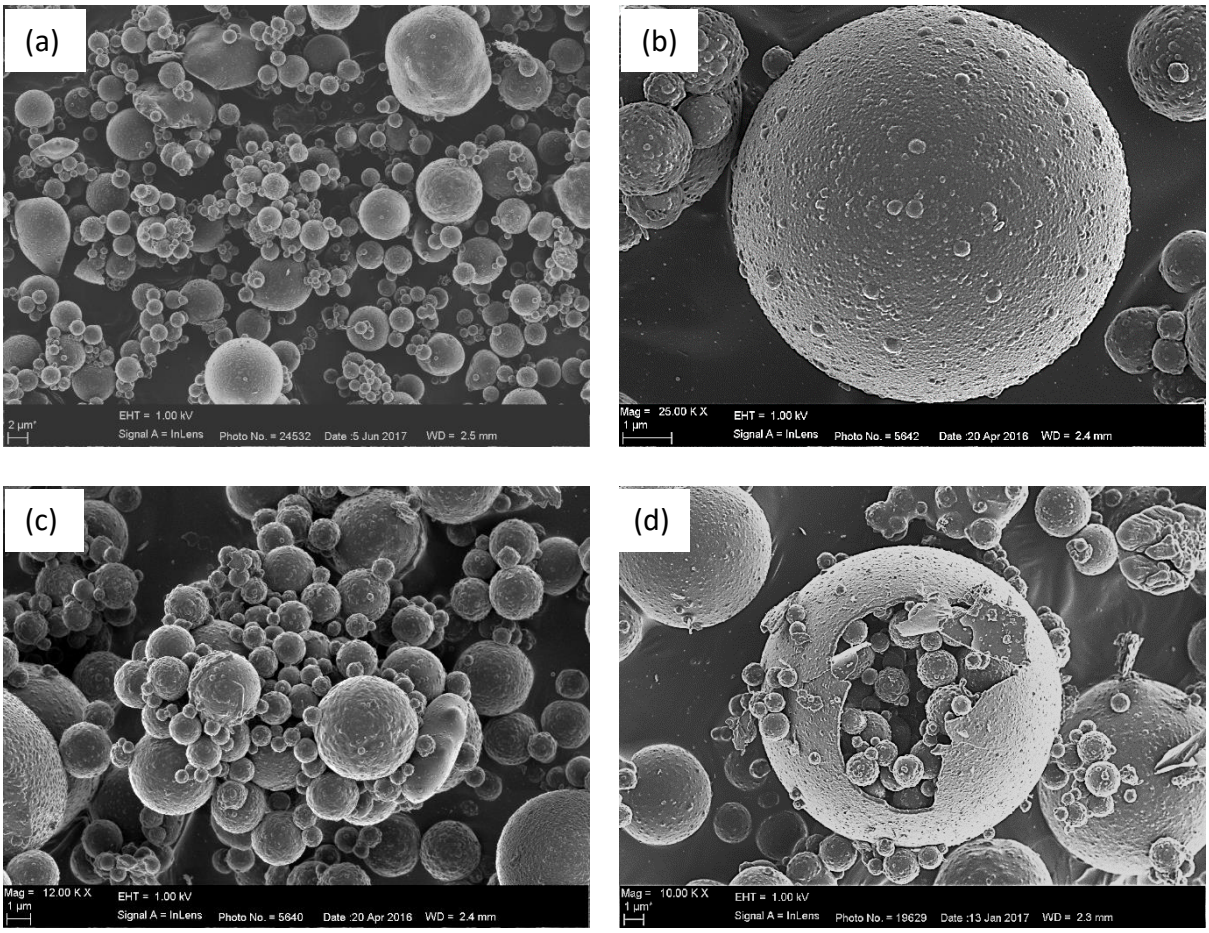

Figure 5.6: FE-SEM micrographs of untreated coal fly ash (UFA).

The combustion temperature and cooling rate during coal combustion determines the shape of the fly ash particles (Kutchko and Kim, 2006). Figure 5.6 (a) shows the characteristic spherical shape of fly ash particles. The particle sizes are highly diversified, ranging from small to very large ones, consistent with the PSD data. Figure 5.6 (b) shows a high magnification FE-SEM image of a fly ash particle from which irregular deposits can be observed on the surfaces

of the particles. Considerable clustering of the different sized particles and inter-particle agglomeration was observed in Figure 5.6 (c). Figure 5.6 (d) shows a hollow fly ash particle containing other smaller fly ash particles within it. These hollow fly ash particles are called cenospheres and are assumed to develop from the expansion of gaseous CO_2 and H_2O evolved from minerals within the coal during combustion (Landman, 2003).

The sphericity and the broad size range of the fly ash particles are desired properties in fillers. Spherical fillers offer a combination of intrinsic superior properties over their irregularly shaped counterparts. The sphericity of fly ash particles provides a low surface area to volume ratio which increases the volume loading capacity. This in turn means decreased shrinkage, reduced Volatile Organic Compounds (VOC's), and reduced cost through lower filler demand in specific applications. Small particles contribute a smooth feel to composites. Spherical fillers roll easily over one another, unlike irregularly shaped fillers, thus, reducing viscosity and improving flow (Kruger *et al.*, 1999; Thomas *et al.*, 2017).

Chapter Six

Characterization of physico-chemically modified coal fly ash

This chapter provides a detailed characterization of the physico-chemically modified coal fly ash samples that were obtained from thermochemical-, sulphuric acid- and silane treatments. The modified samples are compared to the untreated coal fly ash sample in order to track the changes brought about by the physico-chemical treatments and better understand how the modifications affect fly ash-rubber matrix interactions.

6.1. Characterization of the thermochemically treated coal fly ashes.

Thermochemically treated coal fly ash was prepared as described in section 4.3.1. Untreated coal fly ash (UFA) was mixed thoroughly with ammonium sulphate ($(NH_4)_2SO_4$) at a solid-solid mass ratio of 2:3 before being placed in a static muffle furnace at 500°C for 24 hours. The resulting sintered solid (TCT-FA) was milled to a fine powder which was then leached in distilled water for 48 hours to dissolve the water soluble phases. The solid residue was separated from the supernatant, washed with distilled water and then dried in an oven at 80°C for 24 hours (TCT-L). TCT-L is the product to be tested in natural rubber compounds (Chapter 7).

TCT-FA was analysed by XRD and TGA to identify new phases formed during thermochemical treatment of UFA with $(NH_4)_2SO_4$, while TCT-L was thoroughly analysed using all the techniques applied to characterise UFA (Chapter 5). In summary, the samples characterised and compared in Chapter 6.1 and their corresponding sample codes are

- Untreated coal fly ash : UFA
- Coal fly ash thermochemically treated with $(NH_4)_2SO_4$: TCT-FA
- Coal fly ash thermochemically treated with $(NH_4)_2SO_4$ followed by aqueous dissolution to remove water-soluble phases : TCT-L

6.1.1 Chemical and Mineralogical Composition of thermochemically treated coal fly ash.

The chemical composition of untreated (UFA) and thermochemically treated and leached (TCT-L) coal fly ashes are listed in Table 6.1.1. The samples were prepared as pressed powders. Blank and certified reference materials are analysed with each batch of samples. The analysis was performed in duplicate. The values were not normalised as no LOI was done. The major constituents of TCT-L coal fly ash were SiO_2 (63.0%), Al_2O_3 (19.1%), CaO (3.7%), Fe_2O_3 (2.7%), TiO_2 (1.9%) and MgO (1.1%). Trace elements such as ZrO_2, MnO, V_2O_5, Cr_2O_3, NiO, Na_2O and CuO were also present in wt. % concentrations < 0.1%.

Table 6.1.1: Elemental composition of untreated (UFA) and thermochemically treated and leached (TCT-L) coal fly ash as determined by XRF analysis.

	Concentration (wt. %)[a]									
	SiO_2	Al_2O_3	CaO	Fe_2O_3	TiO_2	MgO	K_2O	P_2O_5	SO_3	Total
UFA	52.6	37.1	4.3	2.9	1.6	1.4	0.8	0.9	0.2	102.7
TCT-L	63.0	19.1	3.7	2.7	1.9	1.1	0.4	1.0	3.1	96.3

[a] Other elements present in small amounts (<0.1%): ZrO_2, MnO, V_2O_5, Cr_2O_3, NiO, Na_2O, CuO.

The average SiO_2/Al_2O_3 ratio increased from 1.4 in UFA to 3.3 in TCT-L. This can be ascribed to the extraction of Al with minimal co-extraction of Si resulting in enrichment of the silica in the fly ash product after thermochemical treatment and aqueous dissolution. A study by Doucet *et al.* (2016) on a similar fly ash sample also demonstrated very little silicon (≤0.6%) extraction after $(NH_4)_2SO_4$ treatment, which indicated the lack of reactivity between the Si-O linkages, in the amorphous phase of fly ash, and $(NH_4)_2SO_4$. This is consistent with the results obtained from the ICP-MS analysis of the TCT-L supernatant (Figure 6.1.1).

The elemental extraction efficiencies following dissolution of water-soluble species from thermochemically treated coal fly ash were calculated from ICP analysis of the supernatant and are presented in Figure 6.1.1.

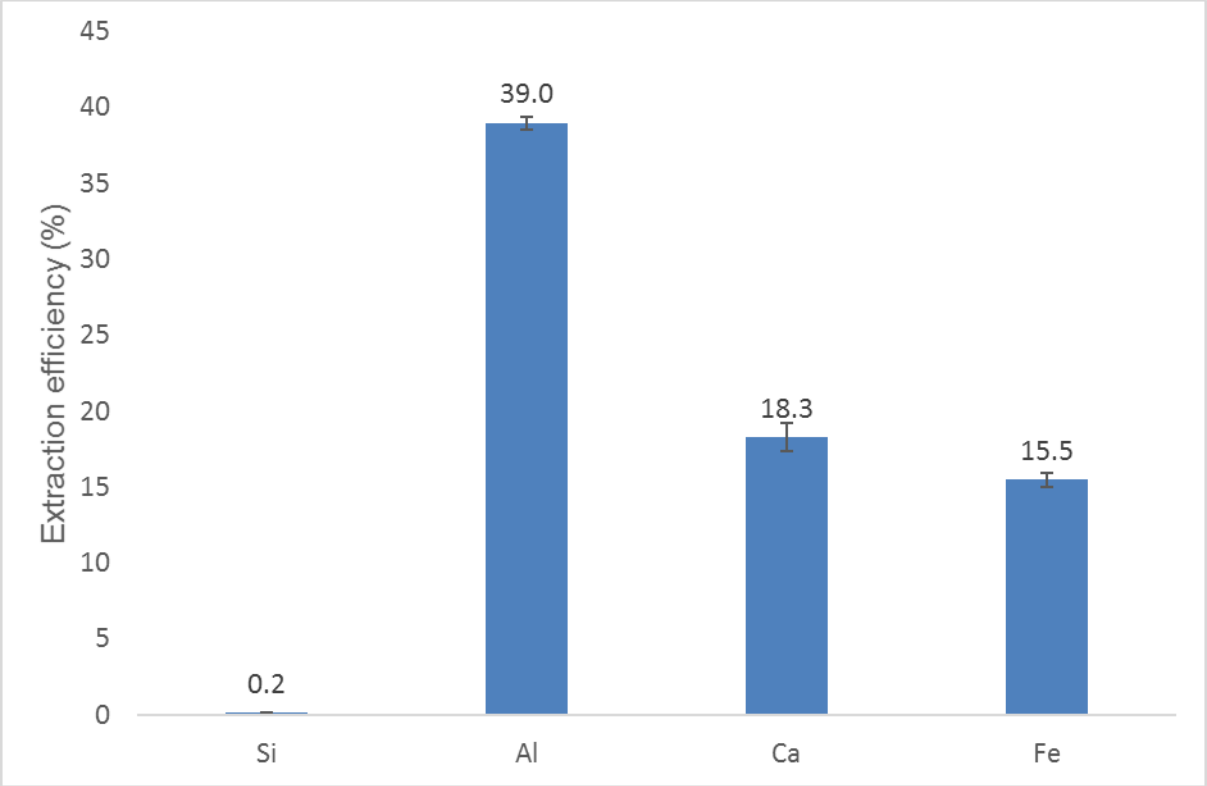

Figure 6.1.1: Elemental extraction efficiency (%) following dissolution of thermochemically treated coal fly ash (TCT-FA) (*n = 3*).

Only extraction data for elemental oxides occurring in quantities exceeding 2 wt. % in UFA (Table 6.1.1) are reported. The major elements extracted were Al (39.0 %), Ca (18.3 %) and Fe (15.5 %) with very little Si (0.2 %) released into solution, which explains the relative increase in SiO_2 content of TCT-L after dissolution of the water-soluble phases from TCT-FA. Extraction of Al, Ca and Fe from UFA after thermochemical treatment and dissolution (TCT-L) resulted in a decrease in these elements with subsequent increase in the Si content (Table 6.1.2).

XRD analysis was performed on all three samples to gain insight into the changes in mineralogy of UFA following both the thermochemical treatment and dissolution stages (Figure 6.1.2)

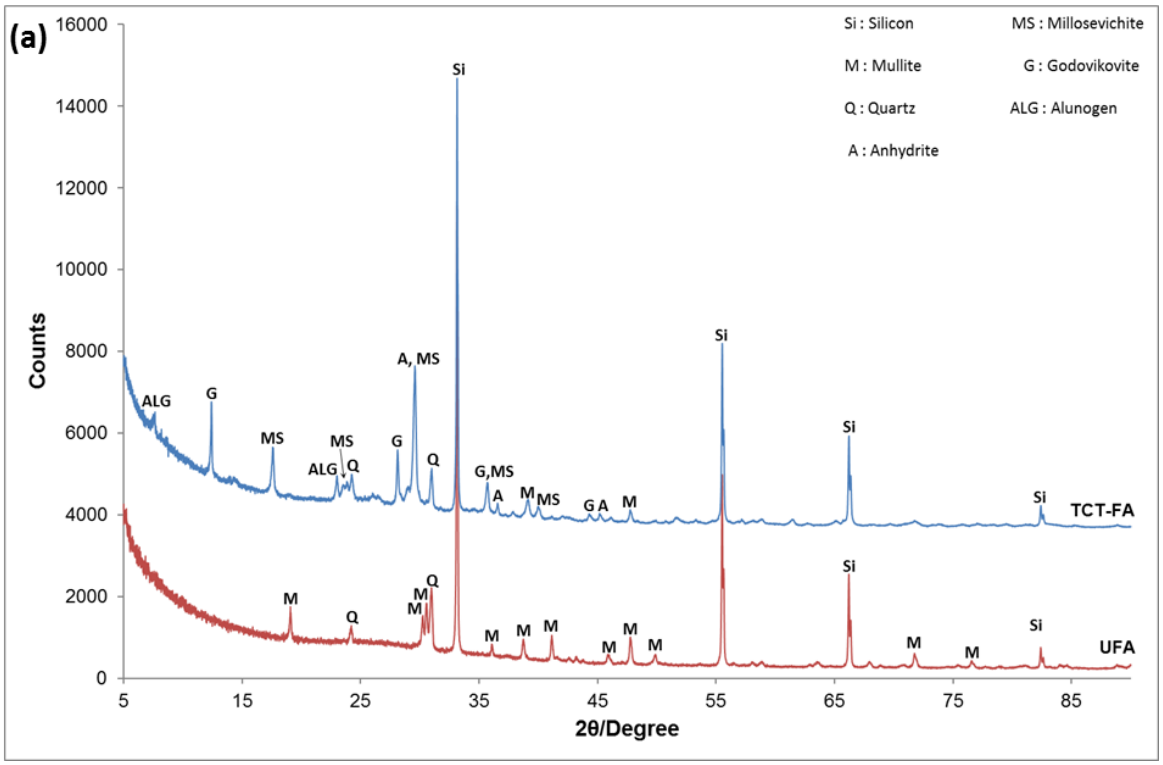

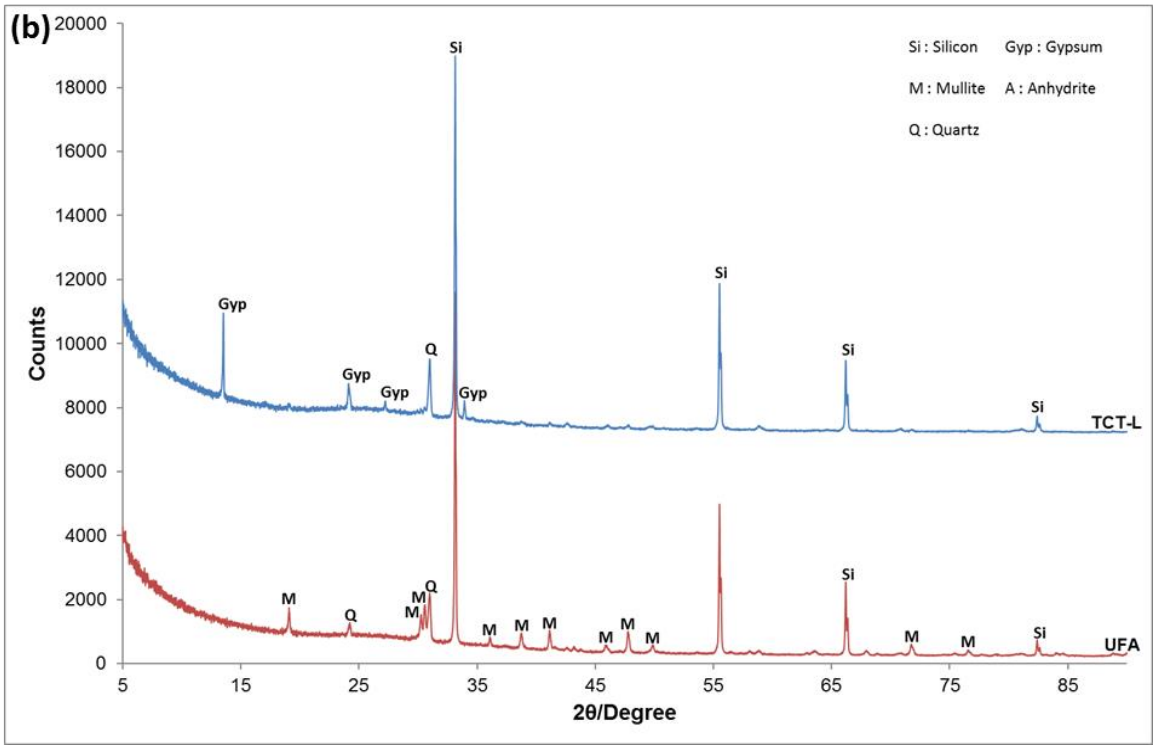

Figure 6.1.2: Comparison of the background-corrected X-Ray Diffraction patterns of untreated (UFA) with (a) thermochemically treated fly ash (TCT-FA) before leaching, and (b) thermochemically treated and leached (TCT-L) coal fly ash.

Table 6.1.2: Quantitative XRD results of untreated (UFA) and thermochemically treated coal fly ashes *(n = 2)*.

Mineral phase	Chemical formula	UFA wt. %	TCT-FA wt.%	TCT-L wt. %
Amorphous		69.1	39.5	86.6
Mullite	$Al_6Si_2O_{13}$	29.1	1.6	3.5
Quartz	SiO_2	5.8	3.8	6.9
Gypsum	$CaSO_4.2H_2O$	n.d.	n.d.	3.0
Anhydrite	$CaSO_4$	n.d.	3.8	n.d.
Hematite	Fe_2O_3	0.7	n.d.	n.d.
Alunogen	$Al_2(SO_4)_3.17H_2O$	n.d.	16.0	n.d.
Godovikovite	$NH_4Al(SO_4)_2$	n.d.	9.8	n.d.
Millosevichite	$Al_2(SO_4)_3$	n.d.	25.6	n.d.

n.d.: not detected.

The two primary crystalline phases (mullite and quartz) and the amorphous phase were present in all the treated and untreated coal fly ash samples. The XRD pattern of TCT-FA (Figure 6.1.2(a)) indicates that four additional crystalline phases were formed during thermochemical treatment of UFA with ammonium sulphate. Three new crystalline phases related to the extraction of aluminium were identified and quantified as water-soluble alunogen $Al_2(SO_4)_3.17H_2O$ (16.0%), godovikovite $NH_4Al(SO_4)_2$ (9.8%), and millosevichite $Al_2(SO_4)_3$ (25.6%) (Table 6.1.2). A fourth crystalline phase present at 3.8% resulted from the extraction of calcium was identified as anhydrous calcium sulphate ($CaSO_4$), also known as anhydrite. These phases were not present in the XRD pattern of UFA and therefore their formation was induced by thermochemical treatment with ammonium sulphate.

After aqueous dissolution of the water-soluble phases from thermochemically treated coal fly ash (TCT-L: Figure 6.1.2(b)), three (alunogen, godovikovite and millosevichite) of the four phases formed after thermochemical treatment were no longer present in the XRD pattern indicating that the aluminium species formed during thermochemical treatment are readily dissolved during the aqueous dissolution process. Calcium which had crystallized in the form

of anhydrite ($CaSO_4$) during thermochemical treatment was transformed to the hydrated form ($CaSO_4.2H_2O$), i.e. gypsum.

Figure 6.1.2(b) and Table 6.1.2 indicates that the mullite peak intensities decreased from 29.1% to 3.5% following the aqueous leaching process. This can be attributed to the fact that ammonium sulphate reacts with the alumina contained in the mullite phase of the coal fly ash, but not with the quartz. The reduction in mullite is accompanied by a slight increase in quartz content (5.8% to 6.9%) because amorphous quartz is produced when mullite decomposes (Xu *et al.*, 2016; Sun *et al.*, 2017). There was a significant increase in the amorphous phase (69.1% to 86.6%) after thermal treatment and dissolution.

The mid-infrared spectra of untreated (UFA) and thermochemically treated and leached (TCT-L) coal fly ash are shown in Figure 6.1.3. FTIR analysis was not carried out on the thermochemically fly ash prior to leaching (TCT-FA) because only TCT-L was applied in the rubber compounds.

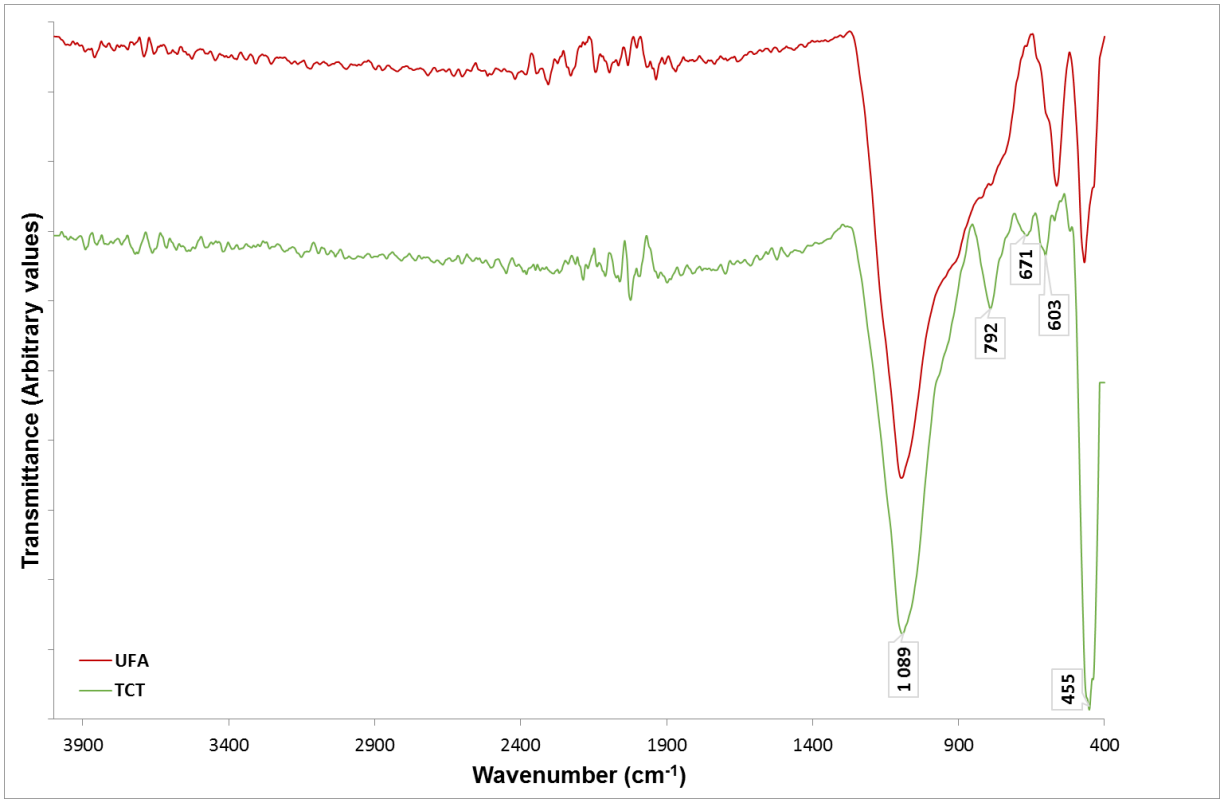

Figure 6.1.3: FTIR spectra of untreated (UFA) and thermochemically treated and leached (TCT-L) coal fly ash.

There is no substantial difference between the spectra of the thermochemically treated and leached sample (TCT-L) and that of untreated coal fly ash (UFA) except that the prominent band in the region 729 to 1100 cm^{-1} is much narrower and more distinct bands can be identified. The narrowing of the band between 729 to 1100 cm^{-1} is due to the decrease in the Al–O–Si asymmetric stretching vibrations as a result of aluminium extraction. Consequently, the overlap in the bands associated with Si–O–Si and Al–O–Si networks also decreases so that distinct bands could be observed. According to Jeyageetha and Kumar (2016) the band now visible at 792 cm^{-1} in TCT-L confirms the presence of quartz and is a result of Si–O symmetrical stretching vibrations. The bands present at 603 cm^{-1} and 671 cm^{-1} correspond to the presence of Al–O–Si structures (Rees *et al.*, 2007).

6.1.2 Thermal analysis of thermochemically treated coal fly ashes

Figure 6.1.4 presents the TGA and DTG curves obtained from the TGA analysis of TCT-FA and TCT-L.

It is necessary to understand the decomposition of pure $(NH_4)_2SO_4$ over the temperature range studied in order to interpret the TGA curve of thermochemically treated fly ash. The decomposition mechanism involves the following main steps (Mohamed *et al.*, 2016):

$$T \approx 300℃: 2(NH_4)_2SO_4(s) \rightarrow (NH_4)_3H(SO_4)_2(s) + NH_3(g) \quad [1]$$

$$T \approx 300℃: (NH_4)_2SO_4(s) \rightarrow NH_4H(SO_4)_2(s) + NH_3(g) \quad [2]$$

$$T \approx 300℃: (NH_4)_2SO_4(s) + NH_4H(SO_4)_2(s) \rightarrow (NH_4)_3H(SO_4)_2(s) \quad [3]$$

$$T \approx 400℃: 3(NH_4)_3H(SO_4)_2(s) \rightarrow 3(NH_4)_2S_2O_7(s) + 3NH_3(g) + 3H_2O(g) \quad [4]$$

$$T \approx 400℃: 3(NH_4)_2S_2O_7(s) \rightarrow 2NH_3(g) + 6SO_2(g) + 9H_2O(g) + 2N_2(g) \quad [5]$$

$$3(NH_4)_2SO_4(s) \rightarrow 4NH_3(g) + 3SO_2(g) + 6H_2O(g) + N_2(g) \quad [6]$$

At temperatures exceeding the melting point of ammonium bisulphate, $NH_4H(SO_4)_2$ (>180°C), $(NH_4)_2SO_4$ decomposes to $NH_4H(SO_4)_2$ and may be immediately converted to ammonium pyrosulphate ($(NH_4)_2S_2O_7$) with an accompanied loss of water. The reaction is reversible, therefore $(NH_4)_2SO_4$ can be formed from the hydration of $(NH_4)_2S_2O_7$ (M Jariwala *et al.*, 2007; Mohamed *et al.*, 2016).

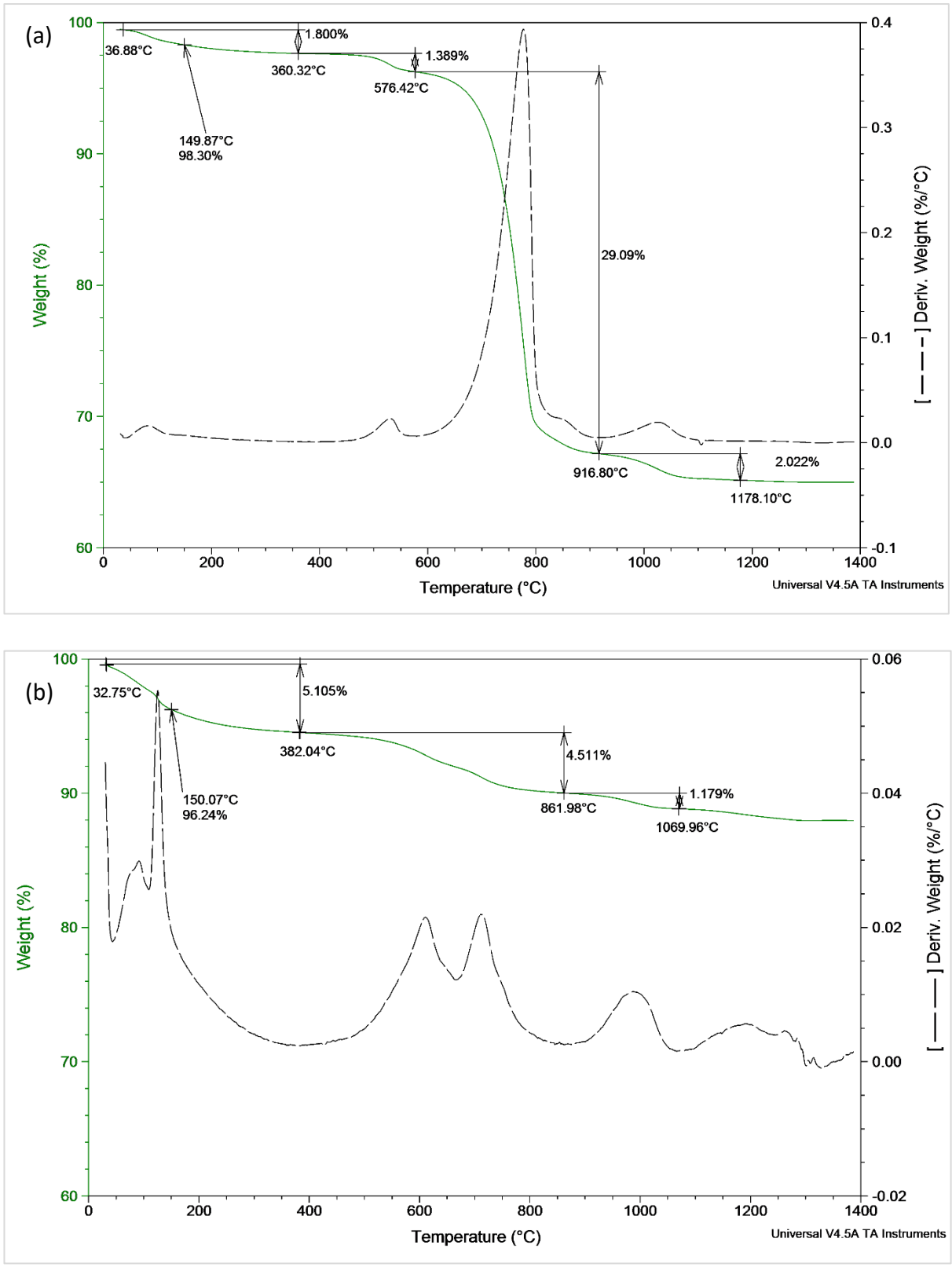

Figure 6.1.4: Thermal analysis of thermochemically treated fly ash (a) before (TCT-FA) and (b) after (TCT-L) aqueous dissolution.

Sulphamic acid (NH_2SO_3H) has been reported as an intermediate during $(NH_4)_2SO_4$ decomposition, followed by a formation of $(NH_4)_2S_2O_7$. The mechanism for the formation of NH_2SO_3H which occurs from 170°C is as follows (R Kiyoura and Urano, 1970; Mohamed *et al.*, 2016):

$$T < 170℃: 2(NH_4)_2SO_4(s) \rightarrow (NH_4)_3H(SO_4)_2(s) + NH_3(g) \quad [7]$$

$$T > 170℃: (NH_4)_2SO_4(s) \rightarrow (NH_4)HSO_4(s) + NH_3(g) \quad [8]$$

$$(NH_4)_2SO_4(s) \leftrightarrow NH_2SO_3H + H_2O(g) \quad [9]$$

NH_2SO_3H melts at around 250°C and subsequently decompose into ammonia, hydrogen and sulphur dioxide. The formation of $(NH_4)_2S_2O_7$ through the decomposition of NH_4HSO_4 and via the reaction between NH_2SO_3H and $(NH_4)_2SO_4$ has also been reported (Raisaku Kiyoura and Urano, 1970; Maheshwari Jariwala *et al.*, 2007; Mohamed *et al.*, 2016):

$$NH_2SO_3H(s) + NH_4HSO_4(s) \rightarrow (NH_4)_2S_2O_7(s) \quad [10]$$

$$2NH_4HSO_4(s) \leftrightarrow (NH_4)_2S_2O_7(s) + H_2O(g) \quad [11]$$

The first mass loss obtained in the TGA and DTG curves of TCT-FA and TCT-L correspond to the loss of physically-bound water, which is complete by 200°C. The mass loss in TCT-L in this region (100 – 400°C; Figure 6.1.5 (b)) cannot be distinctly annotated because there is an overlap between the loss of physically-bound water and the loss of water of crystallization from gypsum, $CaSO_4.2H_2O$ (Clifton, 1972), illustrated by the following two transformations:

$$CaSO_4.2H_2O(s) \overset{150°C}{\longleftrightarrow} \beta - CaSO_4.{}^1/_2\,H_2O(s) + {}^3/_2\,H_2O(v) \quad [12a]$$

$$\beta - CaSO_4.{}^1/_2\,H_2O(s) \overset{197°C}{\longleftrightarrow} \gamma - CaSO_4(s) + {}^1/_2\,H_2O(v) \quad [12b]$$

The mass loss at 150°C (approx. 2% in TCT-L) was recorded because this is the temperature at which rubber compounding was conducted.

The mass loss occurring from 400 to 600°C in TCT-FA (Figure 6.1.4(a)) can be assigned to the de-ammoniation of unreacted $(NH_4)_2SO_4$ intermediates and godovikovite (Nagaishi *et al.*, 1982).

$$(NH_4)_2SO_4 \xrightarrow{230-350°C} NH_4HSO_4 + NH_3 \quad [13]$$

The rate of decomposition of ammonium hydrogen sulphate peaks at 410°C and the process is complete at 450°C:

$$NH_4HSO_4 \xrightarrow{350-450°C} NH_3 + H_2SO_4 \qquad [14]$$

De-ammoniation of godovikovite into $Al_2(SO_4)_3$ occurs at approximately 500°C:

$$6NH_4Al(SO_4)_2 \xrightarrow{\sim 500°C} 3Al_2(SO_4)_3 + gaseous\ products \qquad [15]$$

Aluminium sulphate (originating from alunogen, godovikovite and millosevichite) dissociates in two stages (Pelovski *et al.*, 1992; ÇIlgI and Cetişli, 2009). The first stage is assigned to the loss of water of crystallization from the molecule aluminium sulphate which ends in the region 330-384°C:

$$Al_2(SO_4)_3.17H_2O \rightarrow Al_2(SO_4)_3 + 17H_2O \qquad [16]$$

The second stage is the decomposition of the aluminium sulphate to alumina by desulphuration. The literature (Truex *et al.*, 1977; Nagaishi *et al.*, 1982; Pelovski *et al.*, 1992; ÇIlgI and Cetişli, 2009; Bustanafruz and Fazli, 2013) points out that the decomposition of aluminium sulphate takes place at temperatures from 600 to 990°C according to the following reaction mechanism:

$$6Al_2(SO_4)_3(s) \rightarrow Al_2O_3(s) + 5Al_2(SO_4)_3 + 3SO_3(g) \qquad [17a]$$

$$Al_2O_3(s) + 5Al_2(SO_4)_3(s) \rightarrow 6Al_2O_3(s) + 15SO_3(g) \qquad [17b]$$

$$Al_2(SO_4)_3(s) \rightarrow Al_2O_3(s) + SO_3(g) \qquad [17c]$$

The TGA and DTG peaks in TCT-L (Figure 6.1.4(b)) in the region 400 to 850°C show a loss of mass events which can be an indication that there were small amounts of undissolved alunogen, godovikovite or millosevichite present. If this was the case, the concentrations were below the detection limit of XRD and therefore cannot be confirmed. Doucet *et al.* (2016) observed that godovikovite does not always completely dissolve under the dissolution conditions employed.

The amount of aluminium sulphate contained in TCT-FA can be estimated from TGA and compared with XRD data. For the decomposition of $Al_2(SO_4)_3$:

$$Al_2(SO_4)_3(s) \rightarrow Al_2O_3(s) + SO_3(g) \qquad [18]$$

The theoretical percentage mass loss for this reaction is determined as follows:

$$\frac{M_r(Al_2(SO_4)_3 - Mr(Al_2O_3)}{Mr(Al_2(SO_4)_3} = \frac{(342.5 - 101.96)g/mol}{342.5\ g/mol} \times 100\% = 70.2\%$$

From the TGA result of TCT-FA (Figure 6.1.4(a)), the percentage mass loss for the decomposition of $Al_2(SO_4)_3$ in the range 500 - 900°C is 29.09%. The amount of $Al_2(SO_4)_3$ contained in TCT-FA was calculated as

$$\%\ Al_2(SO_4)_3 = \frac{29.09}{70.2} \times 100\% = 41.4\%$$

Using the quantitative XRD data of aluminium sulphate phases formed during thermochemical treatment of UFA with ammonium sulphate, the total amount of aluminium sulphate contained in TCT-FA can also be estimated via stoichiometric calculations (Table 6.1.3).

Table 6.1.3: Quantitative XRD data of $Al_2(SO_4)_3$ phases formed during thermochemical treatment.

Mineral phase	Chemical formula	TCT-FA wt. %	$Al_2(SO_4)_3$ wt.%
Alunogen	$Al_2(SO_4)_3.17H_2O$	16.0	8.4
Godovikovite	$NH_4Al(SO_4)_2$	9.8	7.1
Millosevichite	$Al_2(SO_4)_3$	25.6	25.6
Total $Al_2(SO_4)_3$			41.1

The result obtained from XRD (41.1%) compares favorably with the $Al_2(SO_4)_3$ content calculated from the TGA (41.4%).

The reaction of decomposition of $CaSO_4$ is illustrated by the following equation:

$$CaSO_4(s) \rightarrow CaO(s) + SO_3(g) \qquad [19]$$

The onset of decomposition of $CaSO_4$ is known to start from temperatures as low as 780°C and the decomposition reaction may continue up to temperatures as high as 1385°C (West and Sutton, 1954; Kuusik *et al.*, 1985). Decomposition of calcium sulphate (in the form of anhydrite) contained in a similar fly ash sample was previously described to occur between 825 and 1000°C (van der Merwe, Prinsloo, *et al.*, 2014). Our result, obtained from the TGA curve of TCT-FA (Figure 6.1.4(a)) indicates that decomposition of $CaSO_4$ from gypsum occurs between 915 and 1180°C. The presence of $CaSO_4$, which did not dissolve during the dissolution experiment, was confirmed by a small mass loss in the region 915 - 1180°C in the TCT-L curve (Figure 6.1.4(b)).

The removal of water-soluble phases during the dissolution step is apparent in the decrease in the total mass loss in the TGA of TCT-L (approx. 8% in Figure 6.1.4(b)) when compared to the mass loss (approx. 34%) in TCT-FA (Figure 6.1.4(a)).

6.1.3 Particle size distribution and BET surface area of thermochemically treated coal fly ash

The frequency curves and the corresponding calculated diameters for untreated (UFA) and thermochemically treated and leached (TCT-L) coal fly ashes are presented in Figure 6.1.5 and Table 6.1.4, respectively.

Table 6.1.4: Particle size distribution of the treated and untreated coal fly ash samples *(n=2)*.

Sample	d_{10}(µm)	d_{50}(µm)	d_{90}(µm)
UFA	0.99 ± 0.01	5.19 ± 0.18	16.04 ± 1.53
TCT-L	1.98 ± 0.07	6.47 ± 0.75	15.08 ± 0.99

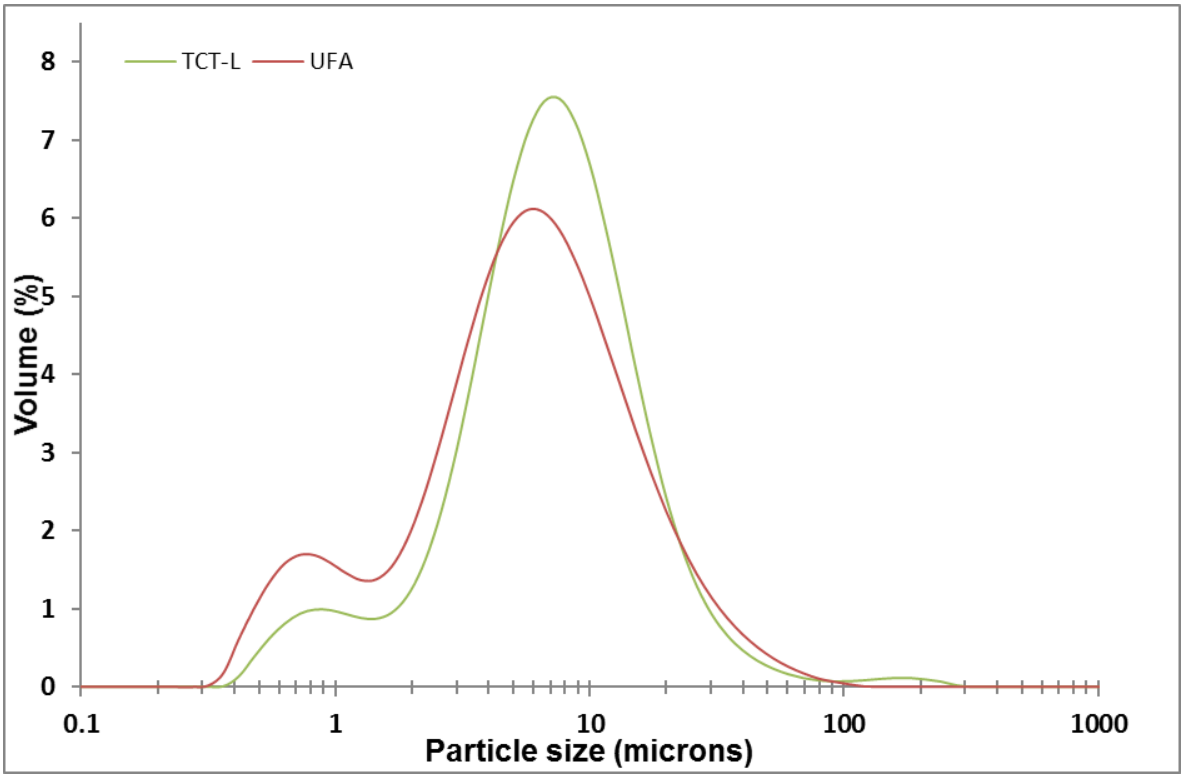

Figure 6.1.5: Particle size distribution of untreated (UFA) and thermochemically treated and leached (TCT-L) coal fly ash.

Following thermochemical treatment and dissolution, the two populations of particles (i.e. ca. 1 and 10 µm) remained the same. However, there was a decrease in the volume percentages of particles with sizes ranging between 0.2 and 1 µm and an increase in particles in the size range between 1.2–11 µm. This was probably a result of particle agglomeration in the thermochemically treated sample, also evident in the small hump above 100 µm in TCT-L. The d_{90} values of UFA and TCT-L were found to be 16.04 µm and 16.73 µm, respectively. The d_{10} and d_{50} values of the TCT-L coal fly ash samples increased slightly from 0.99 to 1.98 µm and from 5.19 to 6.47 µm, respectively, in comparison with the untreated coal fly ash.

There was a substantial increase in the BET surface area of the fly ash sample after thermochemical treatment and dissolution. The surface area of thermochemically treated and leached (TCT-L) coal fly ash was determined to have increased to 7.97 m^2/g from 0.99 m^2/g in untreated fly ash (UFA). This may be explained by the increase in surface roughness observed in the FE-SEM micrographs (section 6.1.5). A larger surface area enables

greater interaction of the fly ash with the rubber matrix and curatives (Da Costa, L L Y Visconte, *et al.*, 2002).

6.1.4 Zeta Potential

When compared to UFA, there was a substantial change in the zeta potential and the iso-electric pH of the fly ash-water system after thermochemical and dissolution treatment of the coal fly ash. The zeta potential of TCT-L measured in water at various pH values is presented in Figure 6.1.6 (a – c). The TCT-L-water system had a pH of approximately 4.0, compared to pH9 in UFA it meant the treatment had made the fly ash acidic. It was observed that the fly ash particles were positively charged at pH values lower than 8.0 and negatively charged at above pH 8.4. The fly ash particles had a positive zeta potential (+16.3 mV) in deionized water. The isoelectric point (IEP) was measured three times and occurred at pH values 7.75, 7.92 and 8.28.

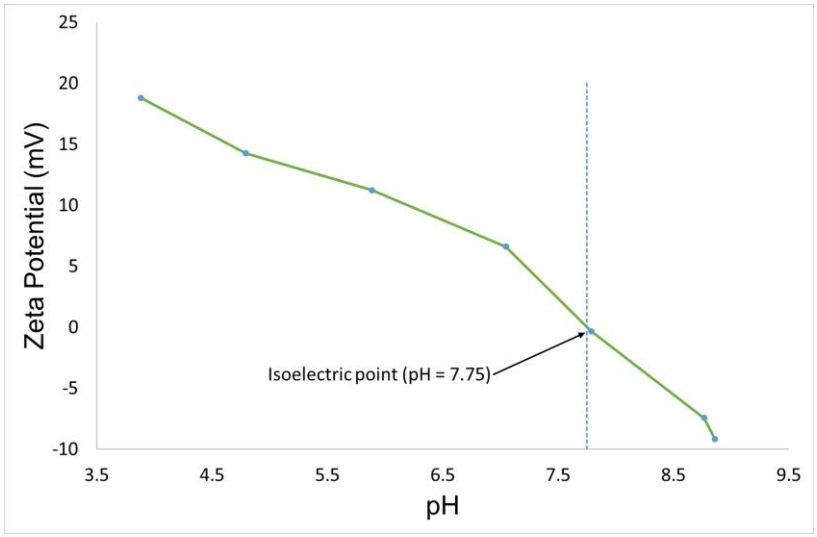

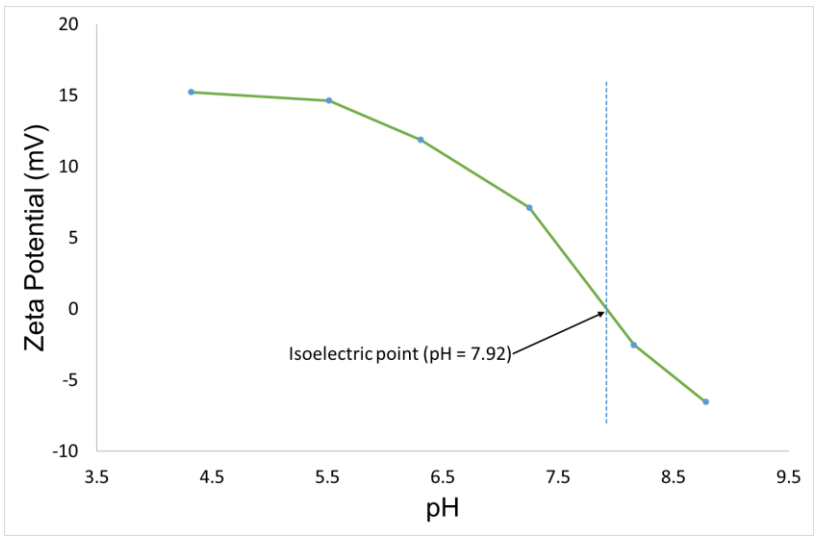

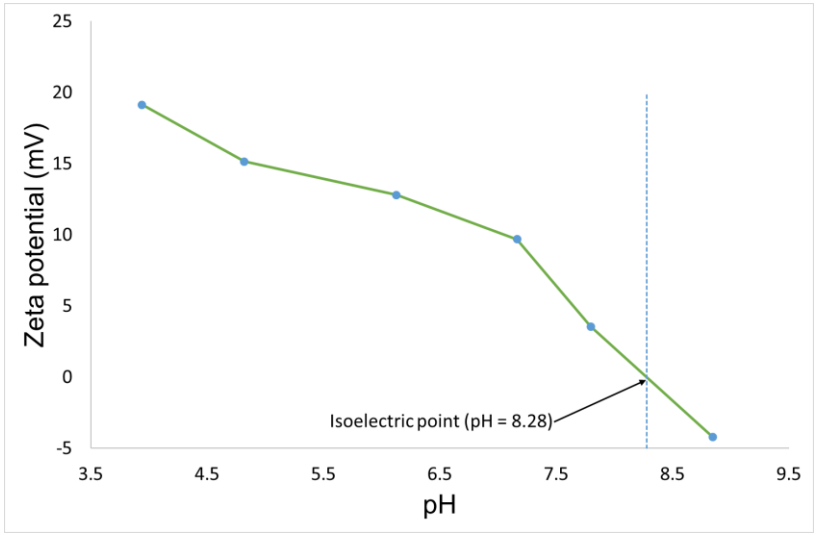

Figure 6.1.6: Zeta potential of thermochemically treated and leached (TCT-L) fly ash at various pH values.

6.1.5 Morphological characterization of thermochemically treated coal fly ash.

The morphology of the thermochemically treated and leached coal fly ashes was observed by FE-SEM and is presented in Figure 6.1.7.

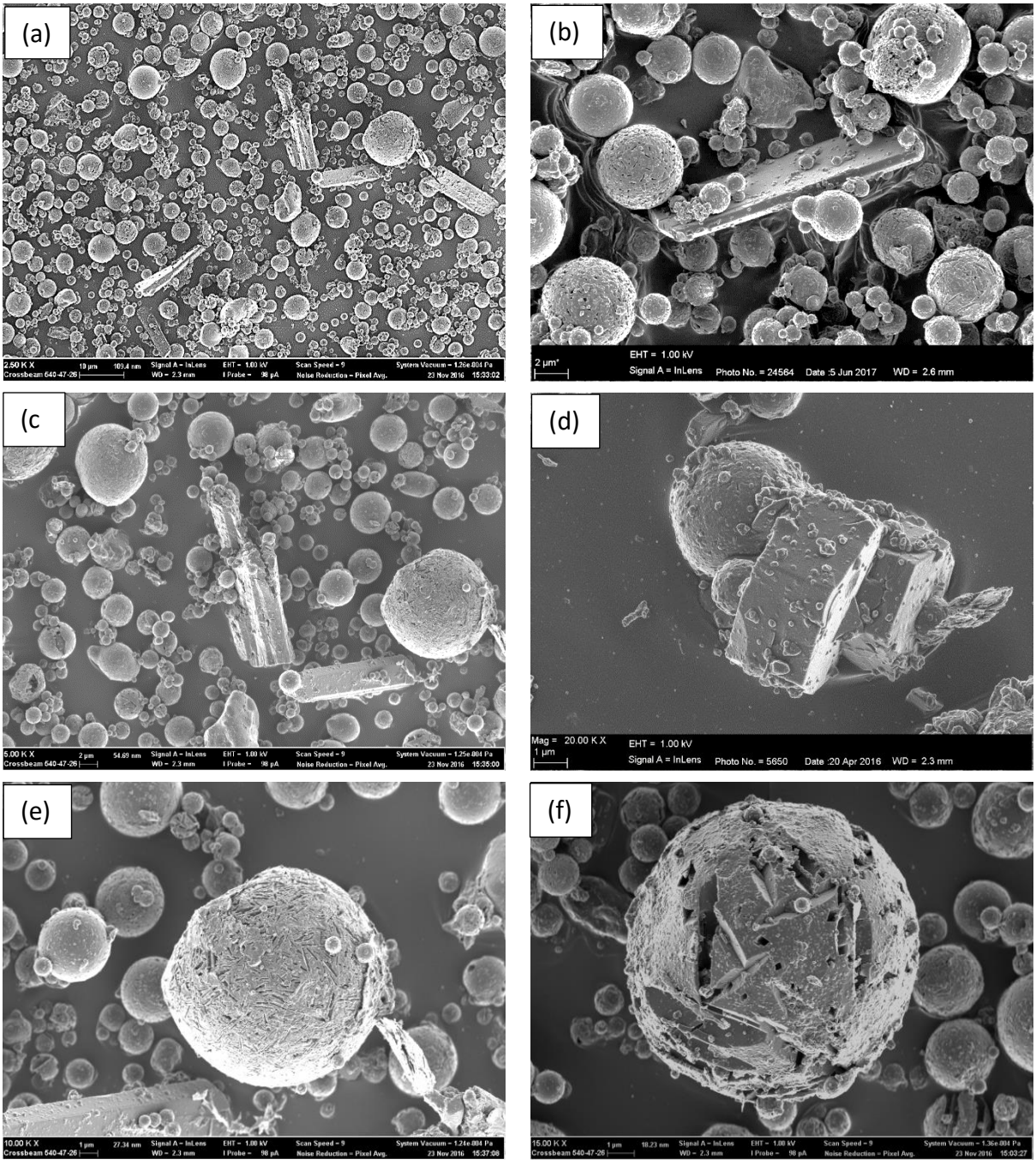

Figure 6.1.7: FE-SEM images of thermochemically treated and leached coal fly ash.

The thermochemically treated coal fly ash contained numerous needle-like structures (Figures 6.1.7(a), (b) and (c)) similar to those observed in the sulphuric acid treated sample (to be discussed later). These structures were identified by XRD as anhydrite ($CaSO_4$). A high-magnification micrograph (Figure 6.1.7(d)) showed the occurrence of hexagonal structures which were interlocked to form clusters of varying sizes. These structures may have been godovikovite ($NH_4Al(SO_4)_2$)) or millosevichite ($Al_2(SO_4)_3$) as identified by XRD, considering that these minerals are crystals with a hexagonal configuration (Doucet *et al.*, 2016).

The FE-SEM images (Figure 6.1.7(e) and (f)) show that the fly ash particles retained their spherical shape, however, surface roughness increased following thermochemical treatment and leaching of UFA. This explains the increase in specific surface area observed in the BET analysis. This surface roughness makes the fly ash surface more accommodating to adhesion with polymer chains and is important in the development of adhesive forces between the fly ash filler and the rubber matrix (Wypych, 2010).

6.2. Characterization of sulphuric acid treated coal fly ash.

Sulphuric acid leached (SAL) coal fly ash was prepared as discussed in section 4.3.2. Untreated coal fly ash (UFA) was added to 5M H_2SO_4 at 1:4 solid to liquid ratio. The slurry was placed in a reciprocal shaker set at 80°C and 200 rpm and left to react for 9 hours. Thereafter, the reaction slurry was left to cool down after which solid-liquid separation was performed by centrifugation at 3000 rpm for 2 minutes. The solid residue was washed using deionised water, dried at 100°C for 24 hours and then milled in a laboratory ball mill to ensure homogenisation.

In summary, the samples characterised and compared in Chapter 6.2 and their corresponding sample codes are

- Untreated coal fly ash : UFA
- Coal fly ash leached in sulphuric acid: SAL

6.2.1 Chemical and mineralogical composition of sulphuric acid treated coal fly ash

The chemical compositions of the minor and major elements found in untreated (UFA) and sulphuric acid treated (SAL) coal fly ashes are listed in Table 6.2.1. The samples were prepared as pressed powders. Blank and certified reference materials are analysed with each batch of samples. The analysis was performed in duplicate. The values were not normalised as no LOI was done. The major constituents of SAL coal fly ash were SiO_2 (55.5%), Al_2O_3 (28.5%), CaO (4.0%), Fe_2O_3 (1.7%), TiO_2 (1.3%) and MgO (0.7%). Trace elements such as ZrO_2, MnO, V_2O_5, Cr_2O_3, NiO, Na_2O and CuO were also present in wt. % concentrations < 0.1%.

Table 6.2.1: Elemental composition of untreated and sulphuric acid leached fly ashes as determined by XRF *(n=2)*.

	Concentration (wt. %)[a]									
	SiO_2	Al_2O_3	CaO	Fe_2O_3	TiO_2	MgO	K_2O	P_2O_5	SO_3	Total
UFA	52.6	37.1	4.3	2.9	1.6	1.4	0.8	0.9	0.2	102.7
SAL	55.5	28.5	4.0	1.7	1.3	0.7	0.7	0.2	4.4	97.1

[a] Other elements present in small amounts (<0.1%): ZrO_2, MnO, V_2O_5, Cr_2O_3, NiO, Na_2O, CuO.

The average SiO_2/Al_2O_3 ratio increased from 1.4 in the UFA to 1.9 in the SAL. Similar to the result obtained for thermochemically treated and leached fly ash, the increase in SiO_2/Al_2O_3 ratio can also be explained by the extraction of Al with minimal co-extraction of Si from UFA. This is consistent with the results obtained from the ICP-MS analysis of the SAL supernatant (Figure 6.2.1), which indicated that 17.9% Al and no Si was extracted from UFA during the sulphuric acid treatment process.

The elemental extraction efficiencies following sulphuric acid treatment of coal fly ash are presented in Figure 6.2.1. Extraction efficiency of the major elements were Fe (28.9%), Al (17.9%), Ca (0.8%) and Mg (44.0%). No detectable Si was released to solution which explains the increase in silica content after dissolution (Table 6.2.1). The extraction efficiencies obtained correspond well with the XRF data obtained (Table 6.2.1).

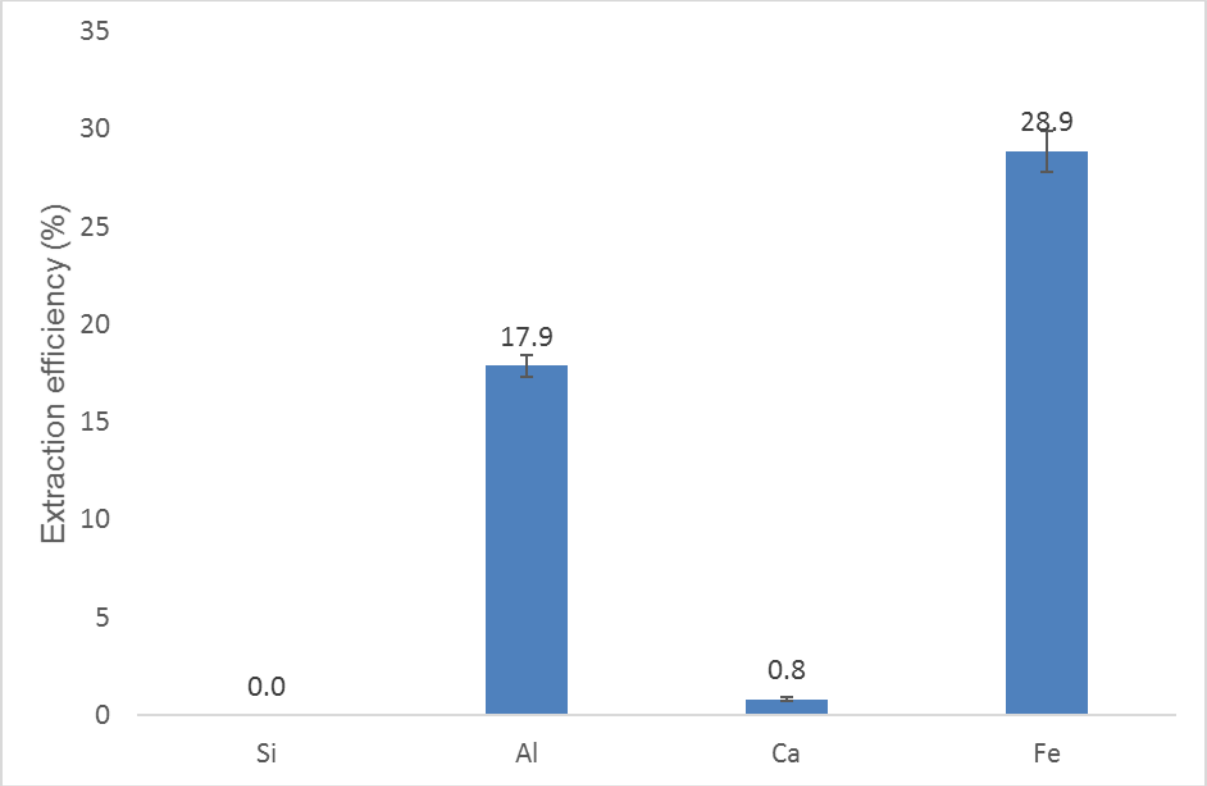

Figure 6.2.1: Elemental extraction efficiency of the sulphuric acid leaching process (*n = 3*).

The X-ray diffraction pattern of untreated (UFA) and sulphuric acid treated (SAL) coal fly ashes are presented in Figure 6.2.2. The XRD pattern of the SAL sample was similar to that of the UFA sample except for the appearance of anhydrite peaks (anhydrous calcium sulphate, $CaSO_4$). The quantitative XRD data given in Table 6.2.2 show a decrease in the amorphous content (69.1% to 57.1%) in the fly ash sample after acid treatment. This is due to extraction of aluminium from the amorphous phase. An appearance of anhydrite (6.4%) and disappearance of hematite are also observed. The mullite content remained constant because mullite is acid-insoluble and therefore the aluminium in this phase cannot be readily recovered by direct acid leaching (Shemi *et al.*, 2015).

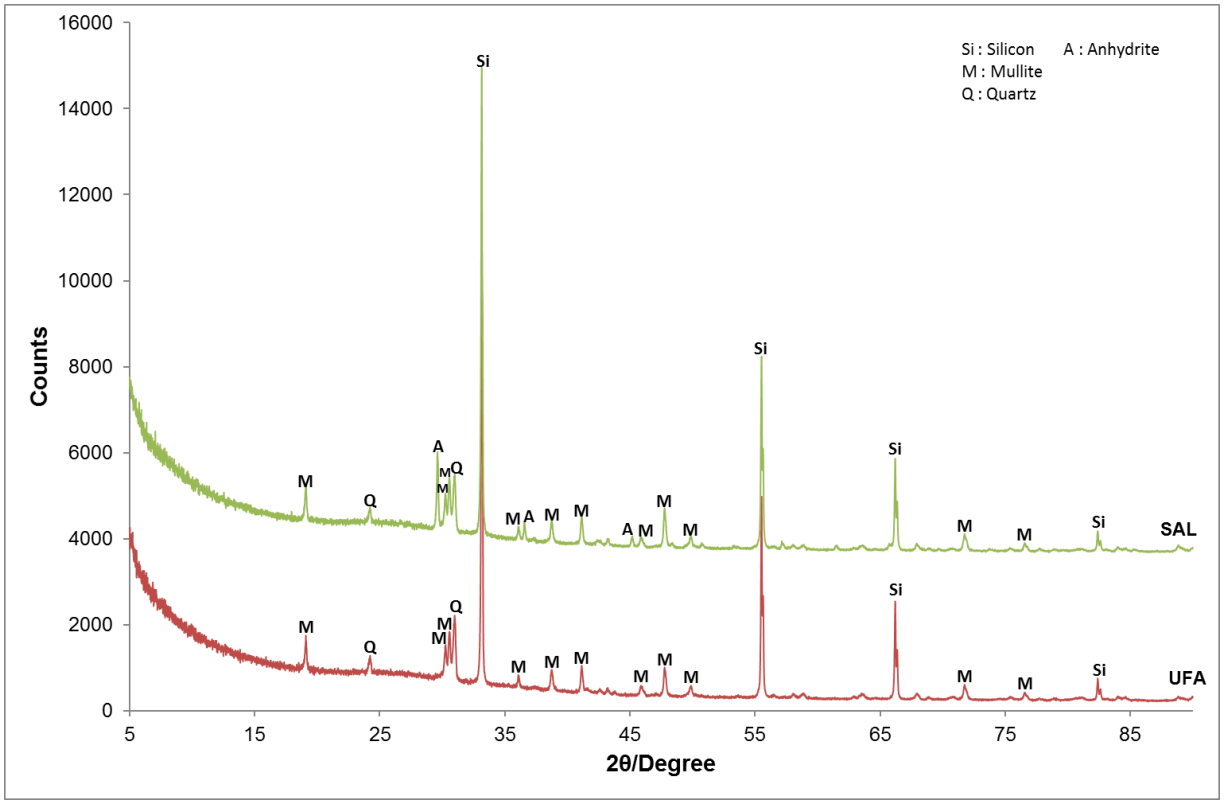

Figure 6.2.2: Background-corrected X-Ray Diffraction pattern of untreated and sulphuric acid leached coal fly ashes.

Table 6.2.2: Quantitative XRD results of untreated and sulphuric acid leached coal fly ashes *(n = 2)*.

Mineral phase	Chemical formula	UFA wt. %	SAL wt. %
Amorphous		69.1	57.1
Mullite	$Al_6Si_2O_{13}$	29.1	29.6
Quartz	SiO_2	5.8	7.0
Anhydrite	$CaSO_4$	n.d.	6.4
Hematite	Fe_2O_3	0.7	n.d.

n.d.: not detected.

6.2.2 Spectroscopic analysis of sulphuric acid treated coal fly ash

The infrared spectra of untreated and sulphuric acid treated coal fly ash are presented in Figure 6.2.3.

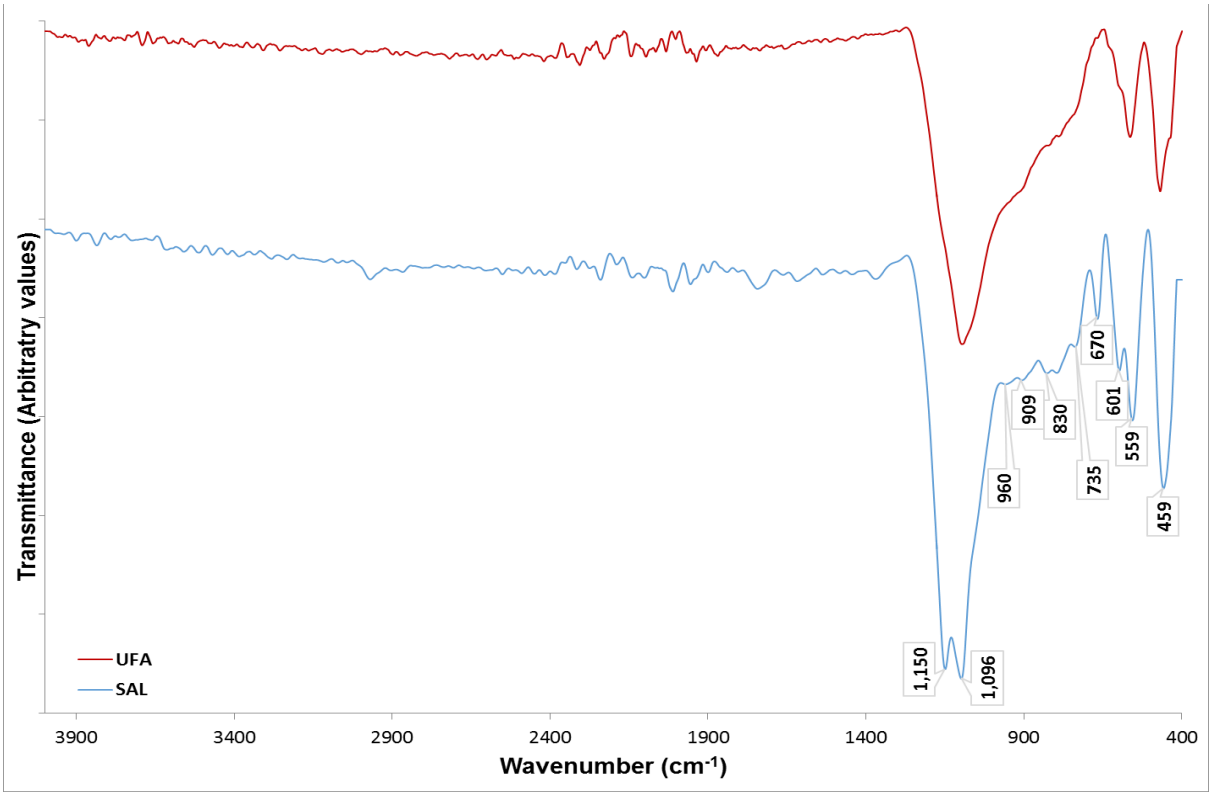

Figure 6.2.3: FTIR spectrum of untreated, sulphuric acid treated coal fly ashes.

The FTIR spectrum showed bands typical of fly ash except for the splitting of the most prominent peak at ca. 1150 cm^{-1}. The peak splitting might be a result of the reduction of the Al–O–Al and Al–O –Si networks due to the extraction of aluminium from the amorphous phase and as a result the bands from the acid-insoluble mullite become visible. The bands at 1150 cm^{-1} and 456 cm^{-1} can be assigned to vibrational mode of the asymmetric stretch of Si–O–Si and bending of Si–O–Si groups of mullite, respectively. The band at 735 cm^{-1} agrees with the bending mode of (Si,Al) –O –(Si,Al) in mullite (Gören *et al.*, 2012).

6.2.3 Thermal analysis of sulphuric acid treated coal fly ash

Figure 6.2.4 presents the DTG and TG curves of sulphuric acid leached (SAL) coal fly ash. The first peak in the DTG and TG curves in the region 100 to 200°C are attributed to the loss of

physically bound water and the water of crystallization in gypsum, $CaSO_4.2H_2O$ (Clifton, 1972), represented by the two reaction mechanisms given in equations 12(a) and (b).

The mass loss in the region 400 to 800°C is assigned to the combined dehydration and decomposition of aluminium sulphate ($Al_2(SO_4)_3$) formed during the acid leaching process (Wahoud *et al.*, 2011).

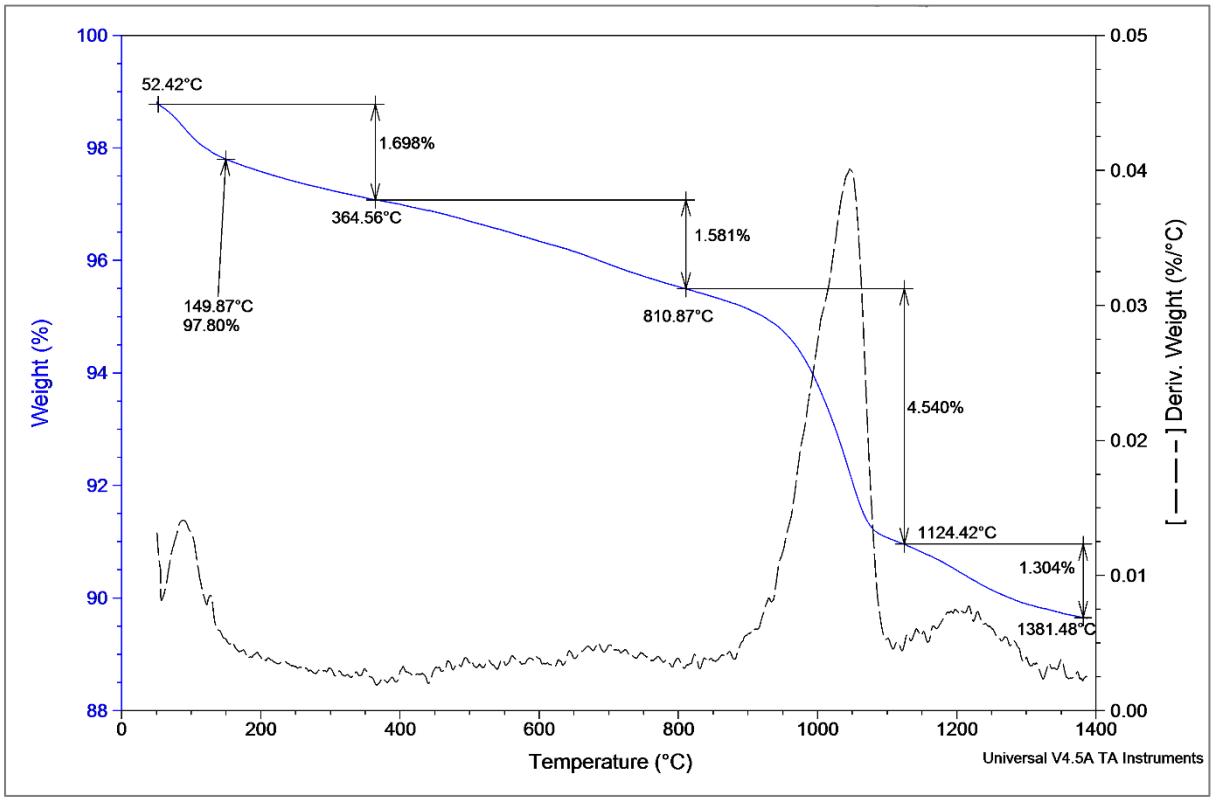

Figure 6.2.4: Thermal analysis of sulphuric acid treated coal fly ash.

Decomposition of aluminium sulphate occurs according to equation 17(c). The decomposition of $CaSO_4$ starts at 780°C, is at its highest at 865°C and is complete at 1385°C (Kuusik *et al.*, 1985; West and Sutton, 2005). The mass loss taking place between 825 and 1000°C can be assigned to the decomposition of anhydrite, $CaSO_4$ (van der Merwe, Prinsloo, *et al.*, 2014), and is illustrated by the following reactions:

$$CaSO_4(s) \rightarrow CaO(s) + SO_3(g) \qquad [1a]$$

$$SO_3(g) \rightarrow SO_2(g) + \frac{1}{2}O_2(g) \qquad [1b]$$

6.2.4 Particle size distribution and BET surface area of sulphuric acid treated coal fly ash

Figure 6.2.5 and Table 6.2.3 represent the particle size distribution of the UFA and the SAL coal fly ashes as determined by the Mastersizer 2000 technique.

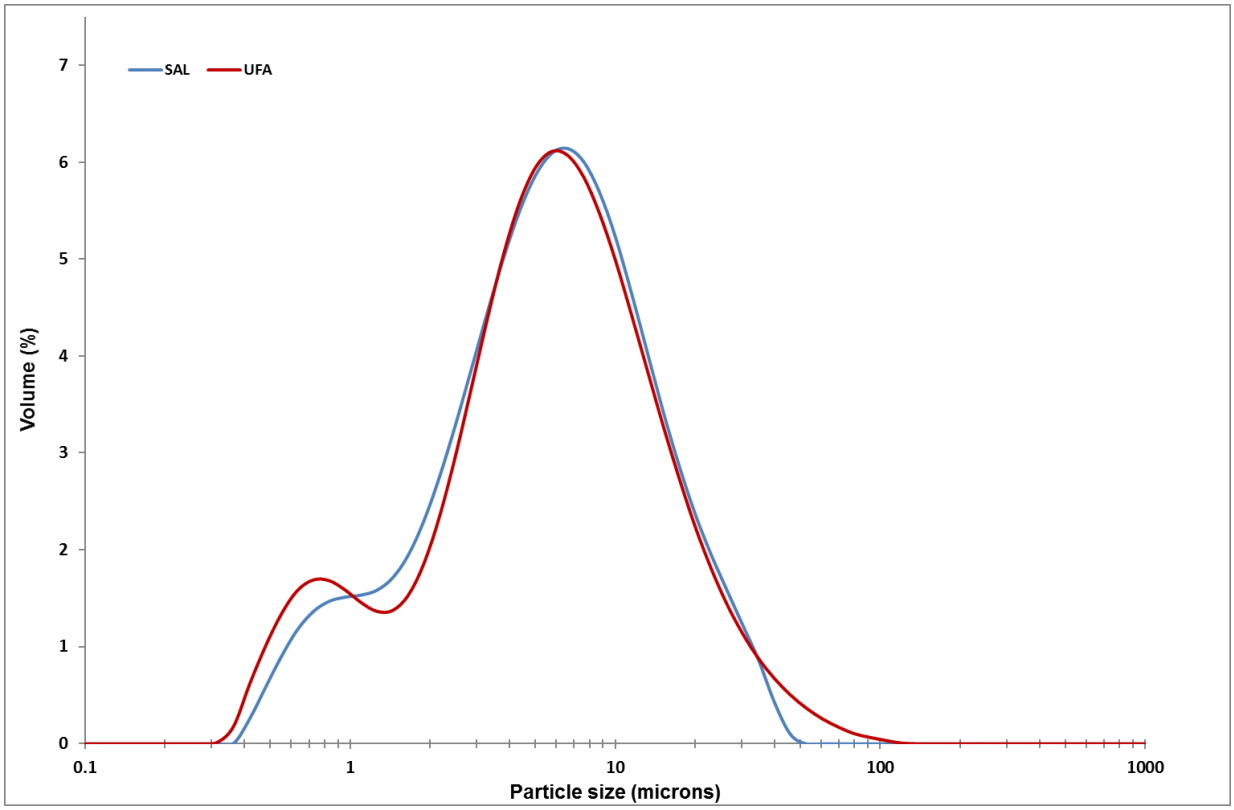

Figure 6.2.5: Particle size distribution of untreated and sulphuric acid treated coal fly ashes.

The size fractions given in Table 6.2.3 show that d_{50} and d_{90} values of the UFA are 5.19 and 16.04 µm respectively, and the d_{50} and d_{90} values of the SAL are 5.42 and 16.40 µm respectively. This shows that the sulphuric acid treatment did not make a significant difference to the particle size distribution of the coal fly ash.

Table 6.2.3: Particle size distribution of the treated and untreated coal fly ash samples (n=2).

Sample	d_{10}(µm)	d_{50}(µm)	d_{90}(µm)
UFA	0.99 ± 0.01	5.19 ± 0.18	16.04 ± 1.53
SAL	1.27 ± 0.08	5.42 ± 0.13	16.40 ± 0.34

There was a significant increase in the BET surface area of the fly ash sample after sulphuric acid (SAL) treatment. The surface area increased from 0.99 m^2/g for untreated fly ash (UFA) to 11.02 m^2/g for the sulphuric acid treated ash (SAL).

6.2.5 Morphological characterization of sulphuric acid treated coal fly ash

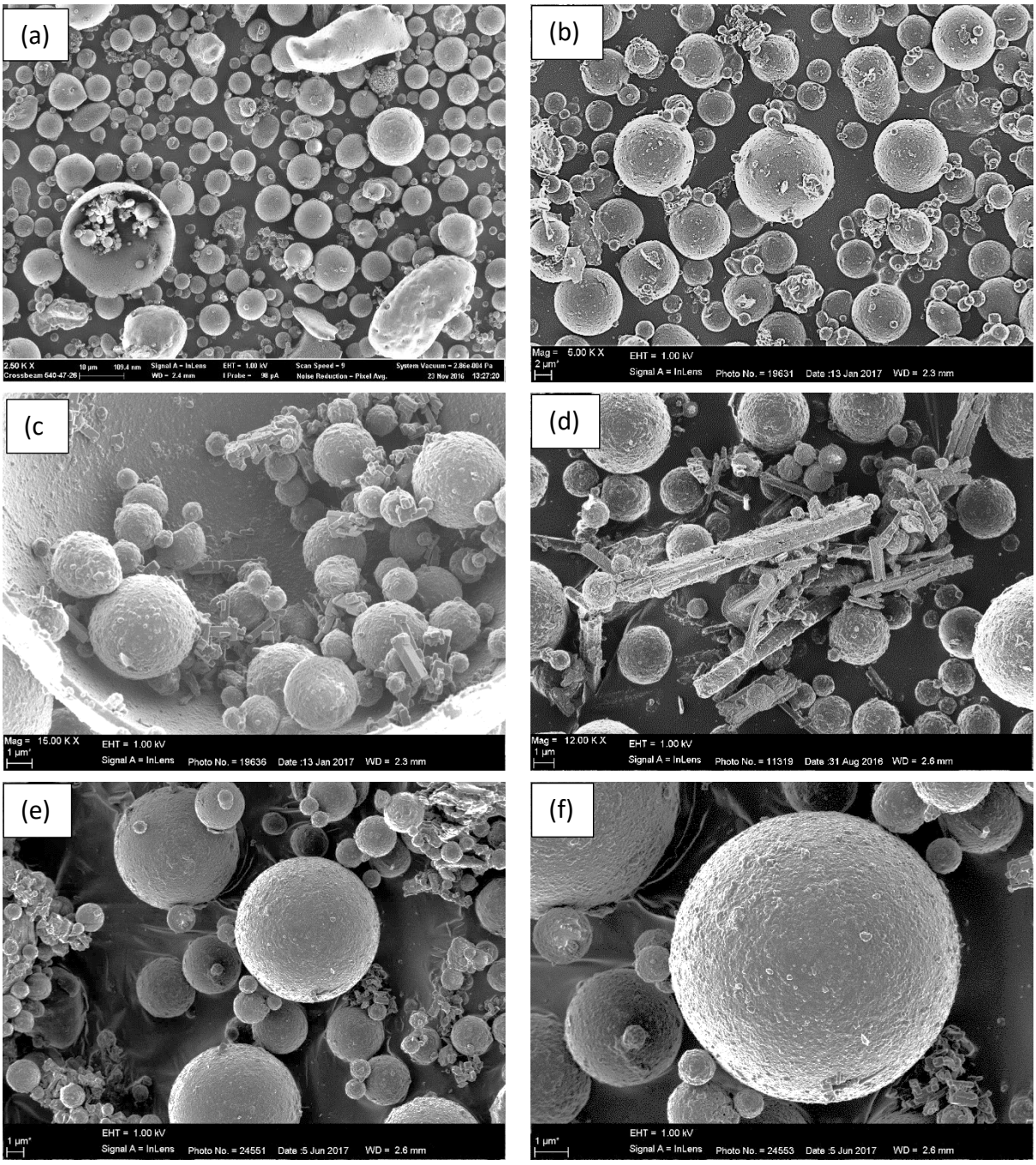

Figure 6.2.6: FE-SEM images of sulphuric acid treated (SAL) coal fly ash.

Figure 6.2.6 shows the FE-SEM images of sulphuric acid treated coal fly ash particles. After treatment, the sample still exhibited spherical, “ball bearing” particles of varying sizes similar to the untreated coal fly ash (Figure 5.4). The acid treated particles, however, had far less particle-particle agglomeration (Figures 6.2.6(a) and (b)) when compared to the untreated coal fly ash sample. The spherical particles were surrounded by tabular/ needle-like structures of various lengths and sizes (Figure 6.2.6(c) and (d)). These tabular structures are taken to be anhydrite ($CaSO_4$) as identified by XRD, since calcium sulphate crystals are known to be needle-like type crystals (Rashad *et al.*, 2004). Figure 6.2.6(e) and (f) show that the surface roughness of the fly ash particles did not change after acid treatment, meaning the increase in specific surface area recorded by BET measurements might have been to an increase in porosity in the fly ash particles.

6.3. Characterization of physico-chemically modified and silane treated coal fly ashes.

Silane treatment of the fly ash samples was carried out as discussed in section 4.3.3. Grafting of a coupling agent was carried out at room temperature using 2% v/v Si-69: ethanol solution. Untreated fly ash (UFA) ash was added to the solution and stirred for 15 minutes at 1000 rpm to ensure uniform distribution of the coupling agent. The resulting slurry was oven-dried for 12 hours at 120 °C to ensure completion of the dehydration and bond formation steps. The product was milled in a laboratory ball mill to ensure homogenisation.

In summary, the samples characterised and compared in Chapter 6.3 and their corresponding sample codes are

- Untreated coal fly ash : UFA
- Silane treated UFA: UFA-Si69
- Coal fly ash thermochemically treated with $(NH_4)_2SO_4$ followed by aqueous dissolution to remove water-soluble phases (TCT-L) and then treated with a silane coupling agent: TCT-Si69
- Coal fly ash leached in sulphuric acid (SAL) and then treated with silane coupling agent: SAL-Si69

6.3.1: Chemical and mineralogical characterization of physico-chemically modified and silane treated coal fly ashes.

The chemical composition of the minor and major elements found in UFA-Si69, SAL-Si69 and TCT-Si69 is presented in Table 6.3.1. The samples were prepared as pressed powders. Blank and certified reference materials are analysed with each batch of samples. The analysis was performed in duplicate and the values were not normalised as no LOI was done. The composition of the silane treated samples was essentially the same as that of the corresponding untreated samples; no significant change occurred during silane treatment.

Table 6.3.1: Elemental composition of untreated and silane treated coal fly ashes as determined by XRF analysis.

	Concentration (wt. %)[a]									
	SiO_2	Al_2O_3	CaO	Fe_2O_3	TiO_2	MgO	K_2O	P_2O_5	SO_3	Total
UFA-Si69	51.8	35.8	4.3	2.8	1.6	1.2	0.8	0.9	1.5	100.7
SAL-Si69	54.8	28.9	3.5	1.9	1.3	0.7	0.7	0.2	4.3	96.4
TCT-Si69	62.6	19.1	3.7	2.7	1.9	1.1	0.4	1.0	4.7	96.8

[a] Other elements present in small amounts (<0.1%): ZrO_2, MnO, V_2O_5, Cr_2O_3, NiO, Na_2O, CuO.

Figure 6.3.1 and Table 6.3.2 present the X-ray diffraction pattern and quantitative results of the silane treated samples respectively. The silane treated samples exhibited the same XRD patterns and quantitative data as the respective untreated samples. No significant changes to the mineralogical composition occurred during the silane treatment.

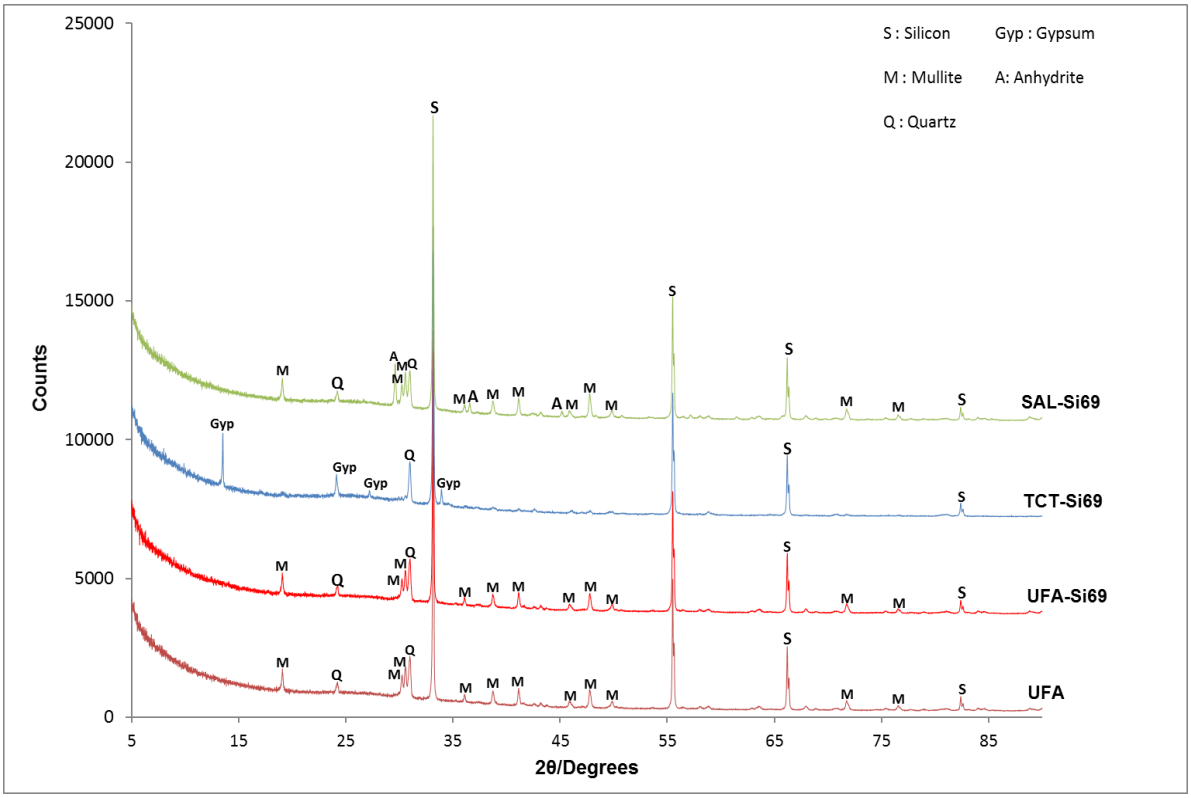

Figure 6.3.1: Background-corrected X-Ray Diffraction pattern of silane treated UFA. SAL and TCT.

Table 6.3.2: Quantitative XRD results of untreated and silane treated coal fly ashes *(n = 2)*.

Mineral phase	UFA wt.%	UFA-Si69 wt.%	SAL-Si69 wt.%	TCT-Si69 wt.%
Amorphous	69.1	67.1	58.4	87.5
Mullite	29.1	25.3	28.4	3.6
Quartz	5.8	7.0	6.8	6.3
Gypsum	n.d.	n.d.	n.d.	2.7
Anhydrite	n.d.	n.d.	6.2	n.d.
Hematite	0.7	0.7	n.d.	n.d.

n.d.: not detected.

6.3.2: Spectroscopic analysis

The infrared spectra of the silane coupling agent Si-69 is shown in Figure 6.3.2 and the band assignments are shown in Table 6.3.3.

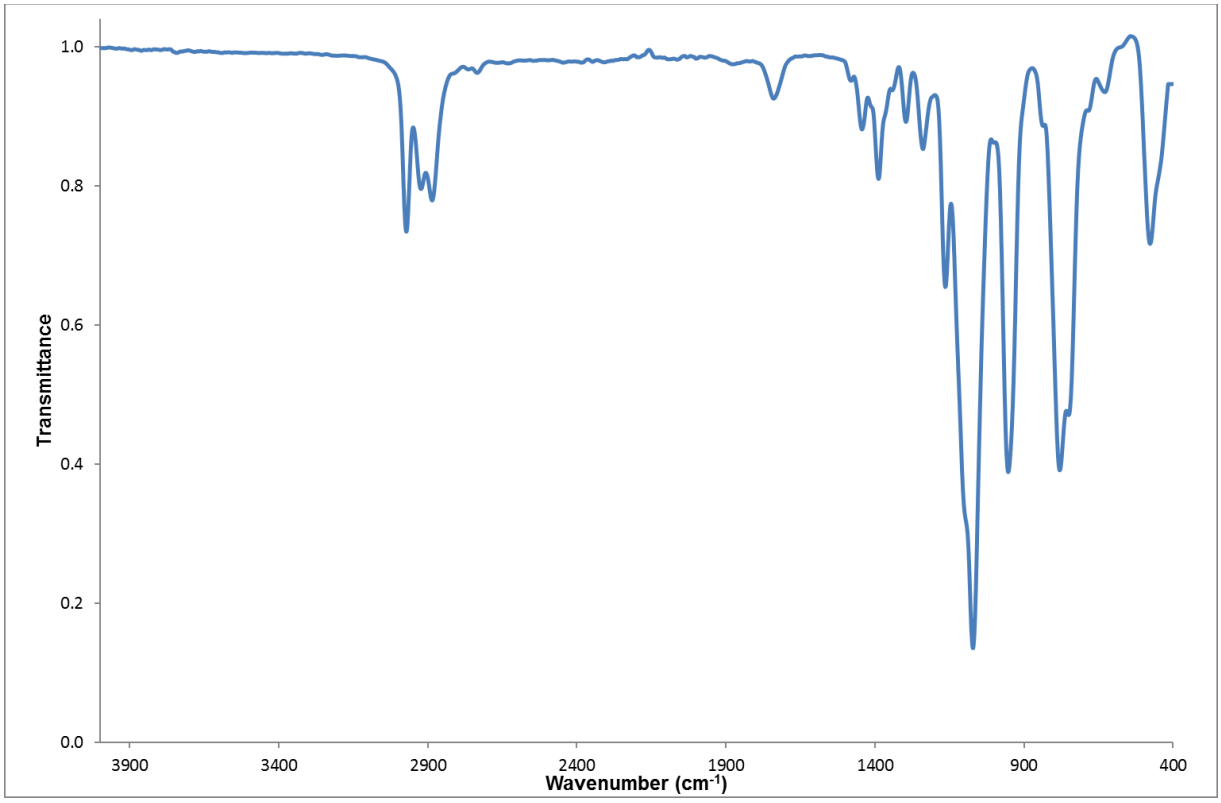

Figure 6.3.2: FTIR spectrum of Bis(triethoxysilylpropyl)tetrasulfide (Si-69).

Table 6.3.3: IR band assignments (Zhu and van Ooij, 2002) for the Bis(triethoxysilylpropyl)tetrasulfide (Si-69).

Band position	Band assignment
2940	Si–O–CH_2CH_3 (CH_3 asymmetric stretch)
1391	Si–O–CH_2CH_3 (CH_3 asymmetric stretch)
1298	Si–O–CH_2CH_3 (CH_2 wag)
1246	CH_2 wagging in –CH_2–S
1166	CH_2CH_3 rock of Si–O–CH_2CH_3
1122	Si–O–Si (Si–O asymmetric stretching)
1107	Si–O–CH_2CH_3 (Si–O asymmetric stretching)
1031	Si–O–Si (Si–O asymmetric stretching)
1078	Si–O–CH_2CH_3 (Si–O asymmetric stretching)
960	Si–O–CH_2CH_3 (Si–O asymmetric stretching)
886	Hydrogen-bonded Si–OH
789	Si–C stretching
480	Si–(O–CH_2CH_3)$_3$ symmetric deformation

Figure 6.3.3 shows the FTIR spectra of UFA-Si69, the untreated coal fly ash sample after treatment with 2% of the silane coupling agent at room temperature. A comparison with the spectrum of the untreated coal fly ash (UFA) shows the presence of Si-69 which is observable by the appearance of symmetric deformation and asymmetric stretching bands of the methyl groups of the ethoxy species in the 1500 – 1300 cm^{-1} and 3000 – 2800 cm^{-1} regions, respectively (Marrone *et al.*, 2004; Vilmin *et al.*, 2014). The bands in the region around 1100 cm^{-1} which are due to Si–O–Si become broader and more intense in the silane treated sample. These differences show that the Si-69 undergoes extensive crosslinking to form a dense siloxane network during the treatment (Zhu and van Ooij, 2002).

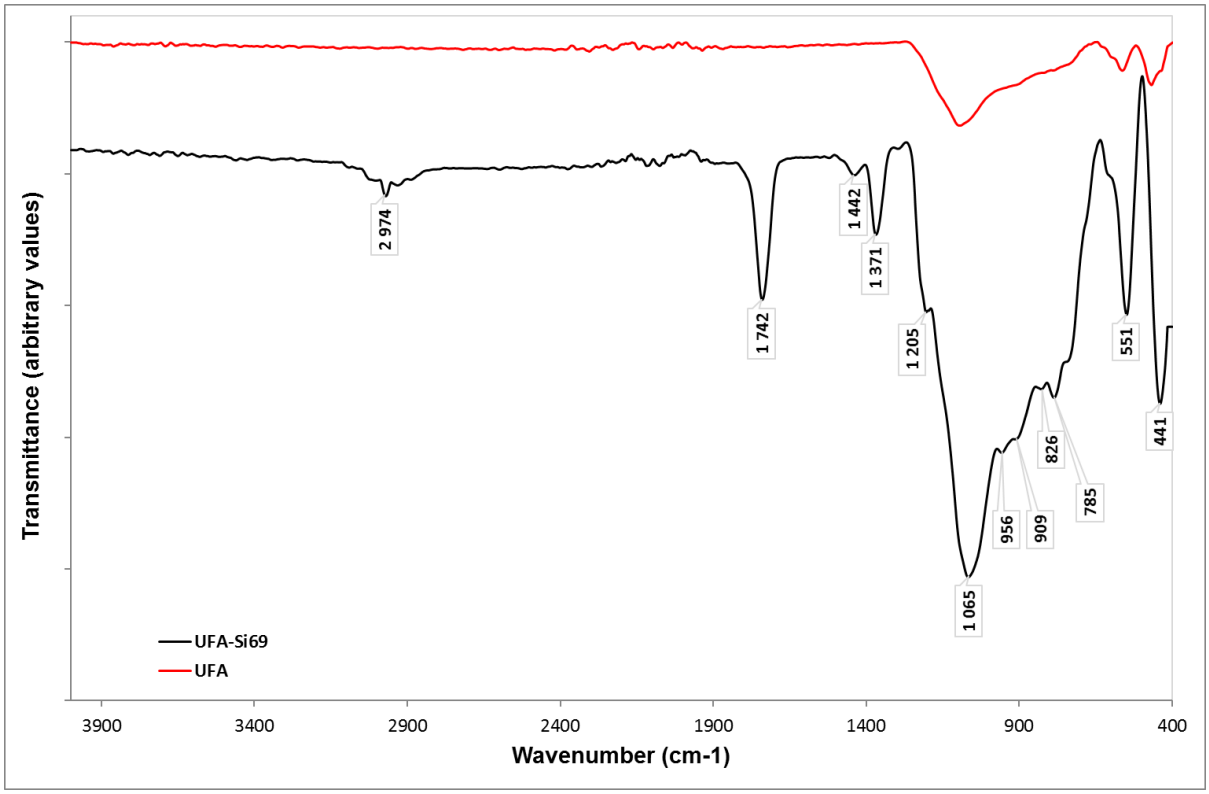

Figure 6.3.3: FTIR spectrum of untreated coal fly ash (UFA) and silane-treated coal fly ash (UFA-Si69).

Figures 6.3.4 and 6.3.5 represent the spectra of TCT-L and SAL modified with Si-69 (TCT-Si69 and SAL-Si69 respectively). Similar to the UFA-Si69 sample, the presence of the silane coupling agent is evident from the presence of symmetric deformation and asymmetric stretching bands of the methyl groups of the ethoxy species in the 1500 – 1300 cm^{-1} and 3000 – 2800 cm^{-1} regions, respectively.

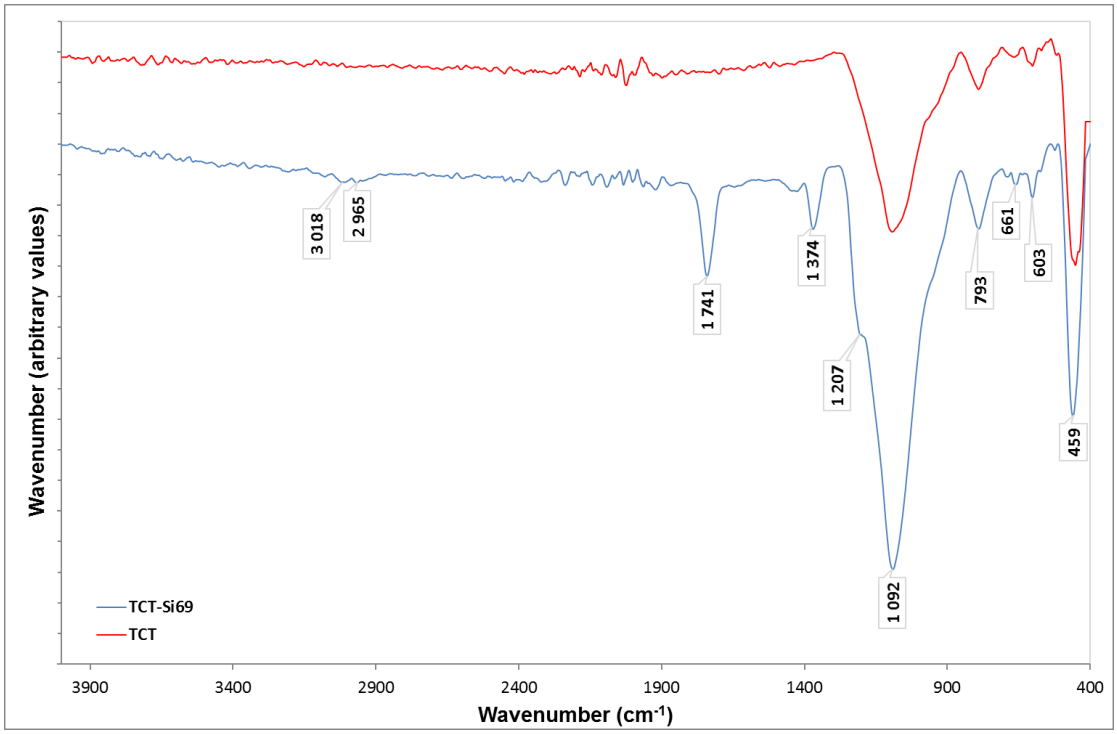

Figure 6.3.4: FTIR spectrum of TCT and silane treated TCT (TCT-Si69) coal fly ashes.

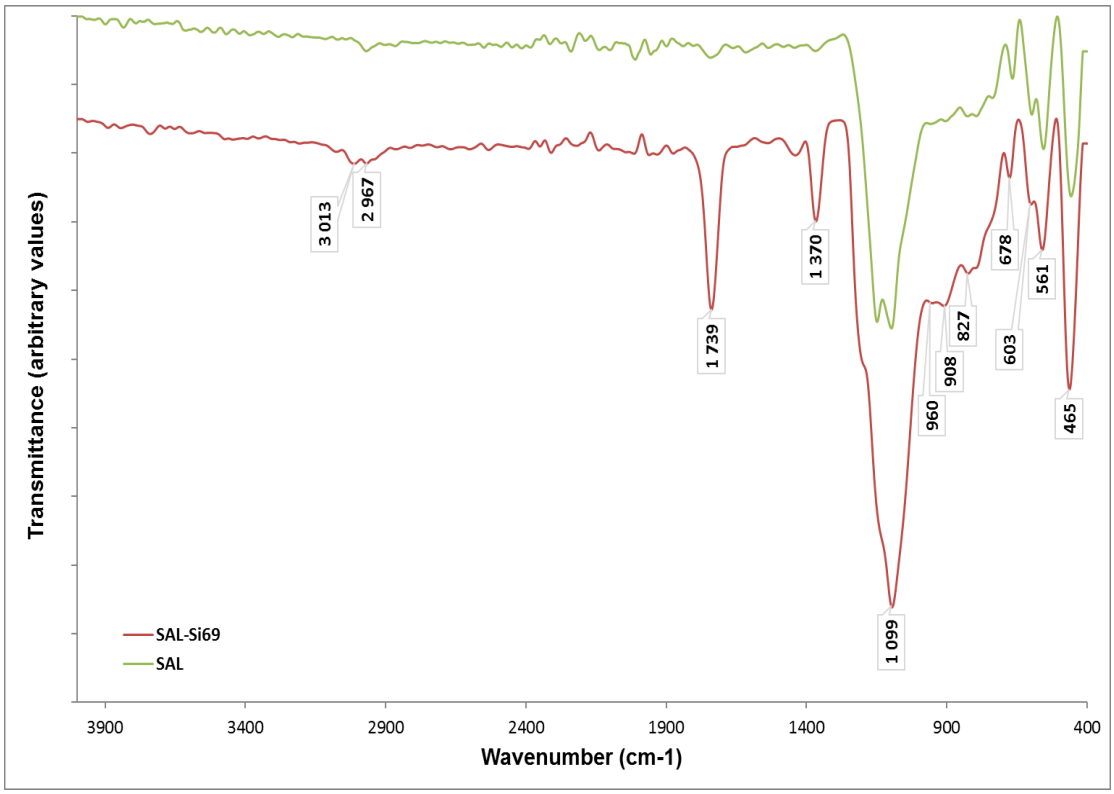

Figure 6.3.5: FTIR spectrum of SAL and SAL-Si69 coal fly ashes.

6.3.3: Thermal analysis

TGA measurements were performed to evaluate the thermal properties of the surface modified coal fly ash samples.

Figure 6.3.6 presents the TG and DTG curves of the silane coupling agent used for surface treatment of all the samples. Bis[3-(triethoxysilyl)propyl]tetrasulfide decomposed in one step between 125°C and 400°C showing a maximum rate of mass loss at 282°C.

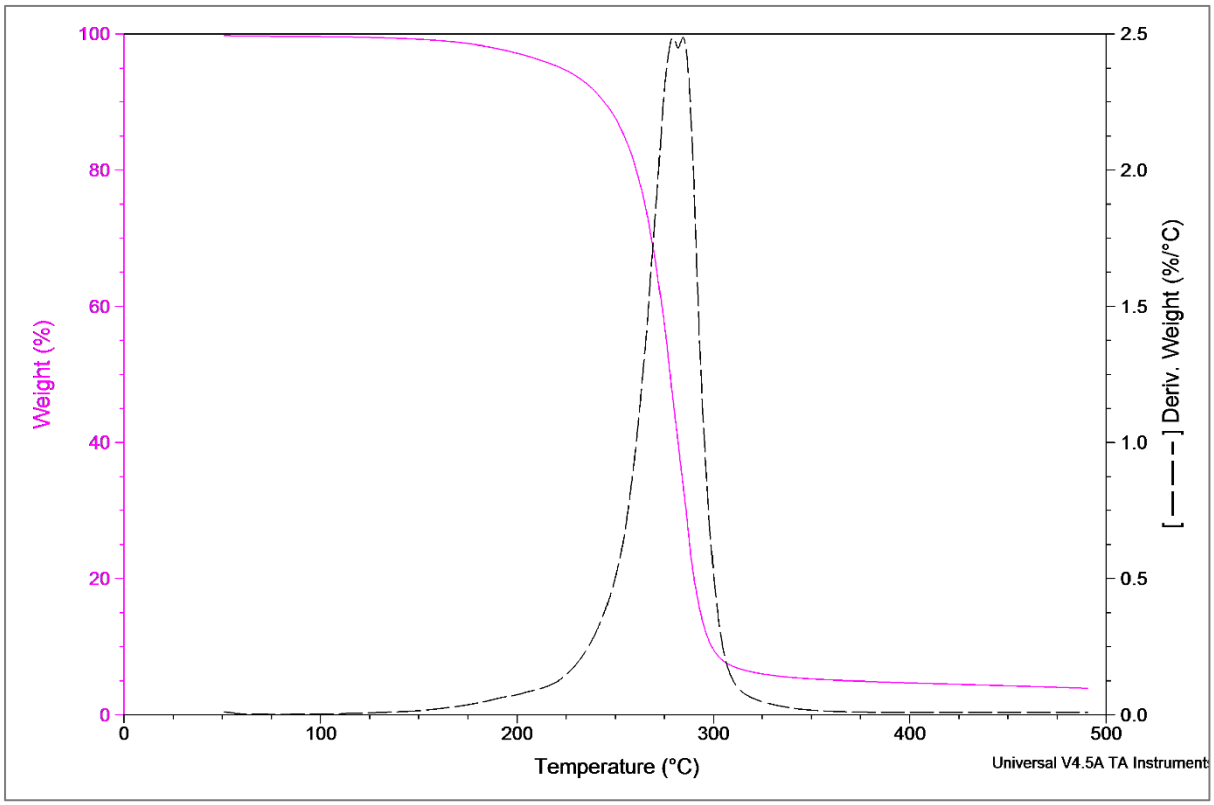

Figure 6.3.6 Thermal analysis of Bis[3-(triethoxysilyl)propyl]tetrasulfide (Si-69).

Figure 6.3.7 shows the TGA and DTG curves of untreated (UFA) and silane treated fly ash (UFA –Si69). The TGA and DTA curves of UFA-Si69 differ from that of UFA in the temperature range between 150°C and 400°C, which is attributed to the decomposition of Si69 bound to the coal fly ash. The decomposition step of Si-69 is evident in the DTG curve of UFA-Si69. The mass loss in UFA-Si69 at 150°C (~0.38%), the temperature applied during rubber vulcanization, was essentially the same as the mass loss observed for UFA (~0.39%).

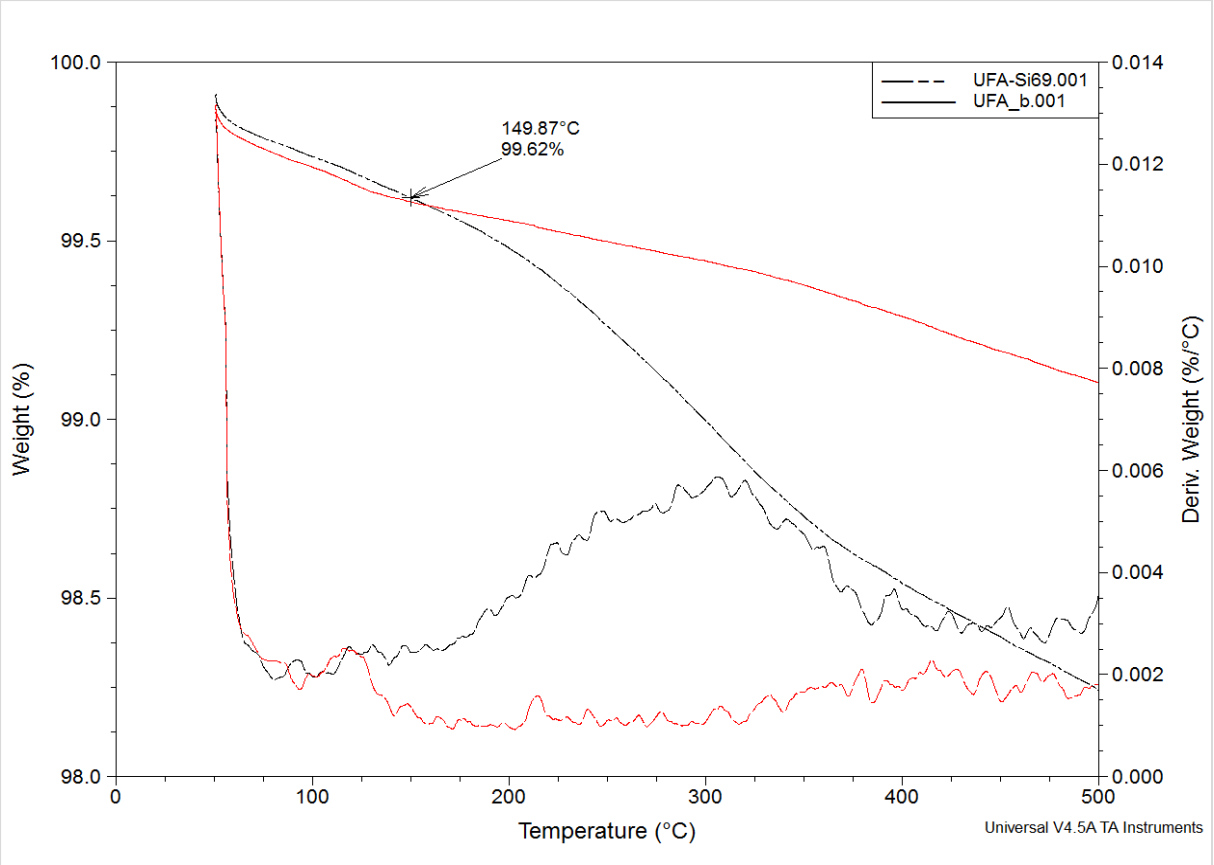

Figure 6.3.7: Thermal analysis of UFA (solid red line) and UFA-Si69 (dashed black line).

The TGA and DTG curves of silane treated-thermochemically treated (TCT-Si69) and thermochemically treated and leached fly ash (TCT-L) are presented in Figure 6.3.8. The TGA curve for TCT-Si69 deviated from that of the TCT-L in the region between 150°C and 400°C, and a small hump is observed over the same temperature range in the DTG curve of TCT-Si69. These effects are also attributed to the loss of the silane coupling agent. There was a slight difference in mass loss recorded at 150°C in the TCT-Si69 (~2.6%) compared to the mass loss in TCT-L (~2.18%).

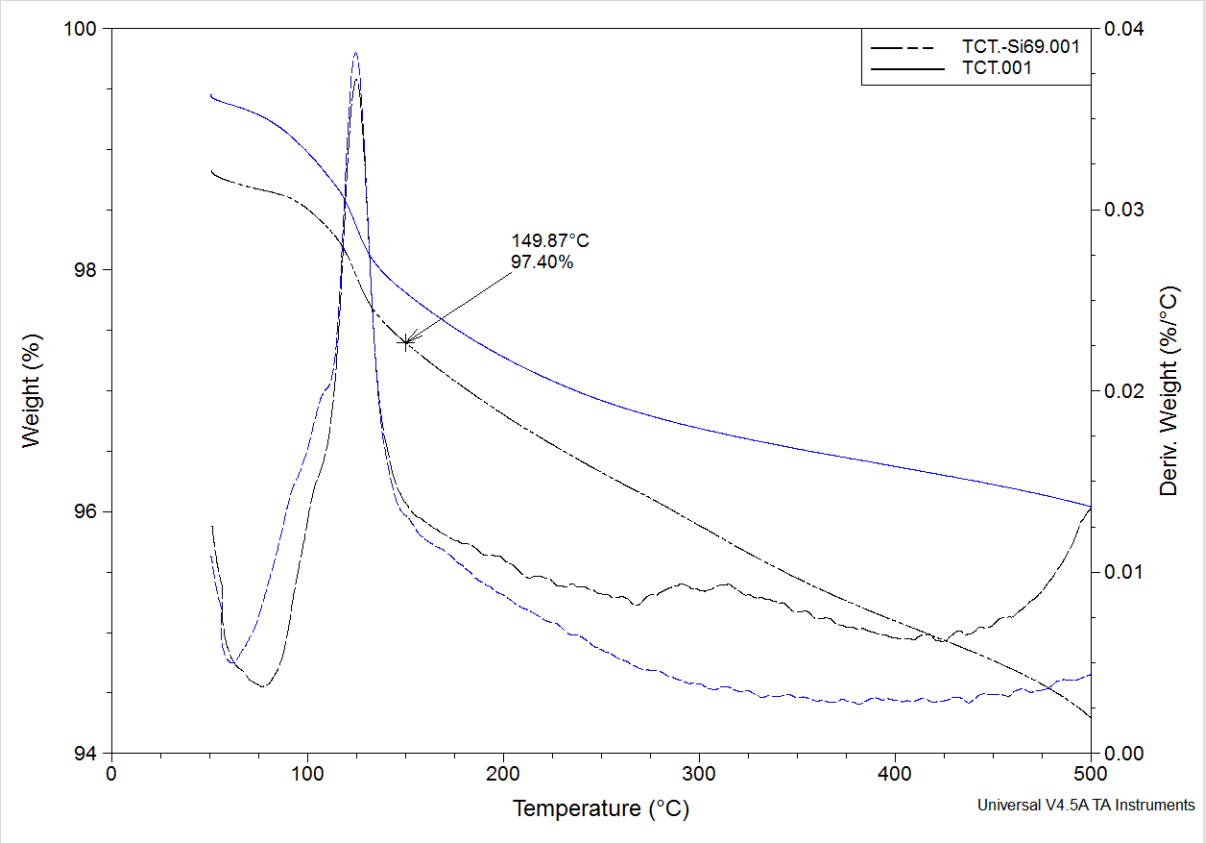

Figure 6.3.8: Thermal analysis of silane treated-thermochemically treated fly ash (TCT-Si69).

Figure 6.3.9 represents the TGA and DTG curves of silane treated-sulphuric acid leached (SAL-Si69) and sulphuric acid treated (SAL) fly ash. The curve for SAL-Si69 also indicated a loss of silane in the region between 150 and 400°C but to a lesser extent compared to UFA-Si69. The mass loss at 150°C in SAL-Si69 (~1.9%) was similar to that of SAL (~2.2%).

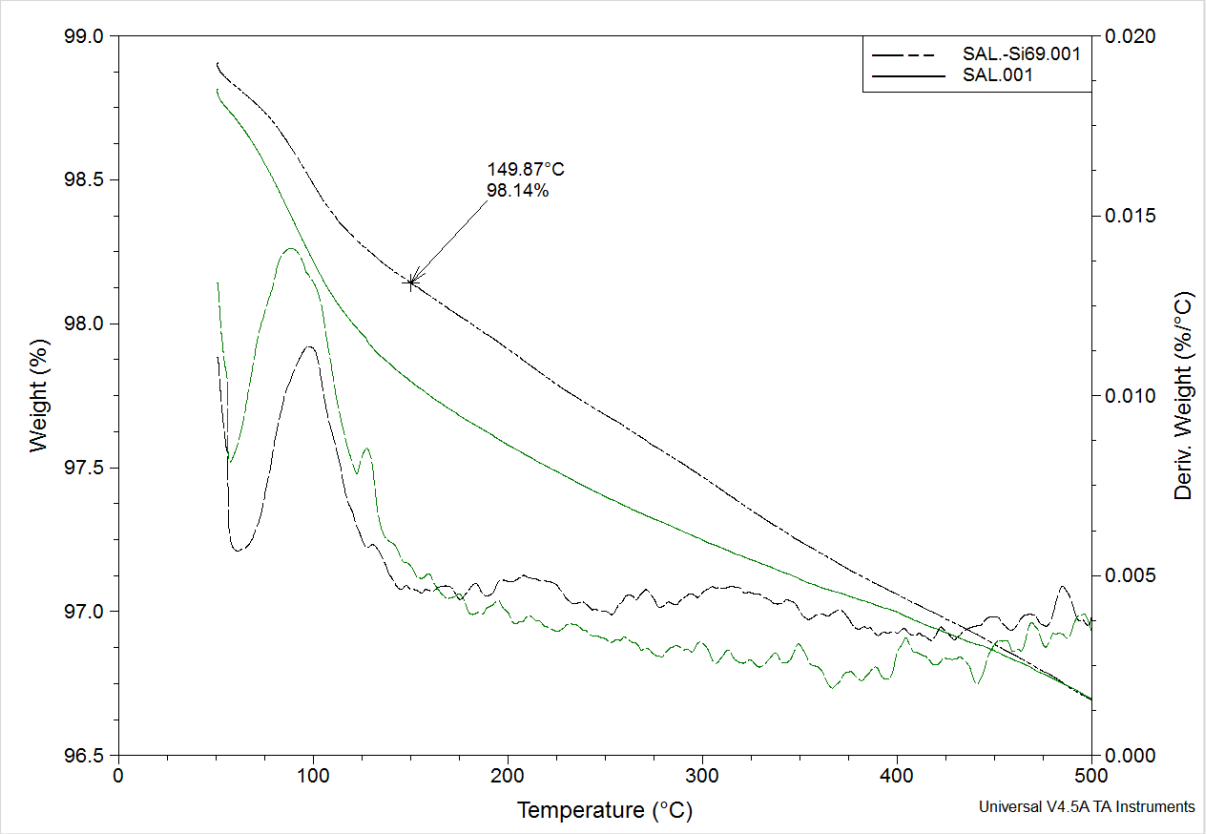

Figure 6.3.9: Thermal analysis of silane treated-sulphuric acid leached coal fly ash (SAL-Si69).

6.3.4 Particle size distribution

The silane treated UFA (UFA-Si69) was completely hydrophobic and would not disperse in the water therefore the particle size distribution for UFA-Si69 could not be obtained. Particle size distribution for TCT-Si69 and SAL-Si69 could be measured, indicating that the two samples contained particles that had not been coated by the silane coupling agent and therefore had hydrophilic properties that allowed them to disperse in solution. The particle size distribution of the silane treated SAL (SAL-Si69) and TCT-L (TCT-Si69) are shown in Figure 6.3.10. For comparison, the particle size distribution of the untreated coal fly ash is also included.

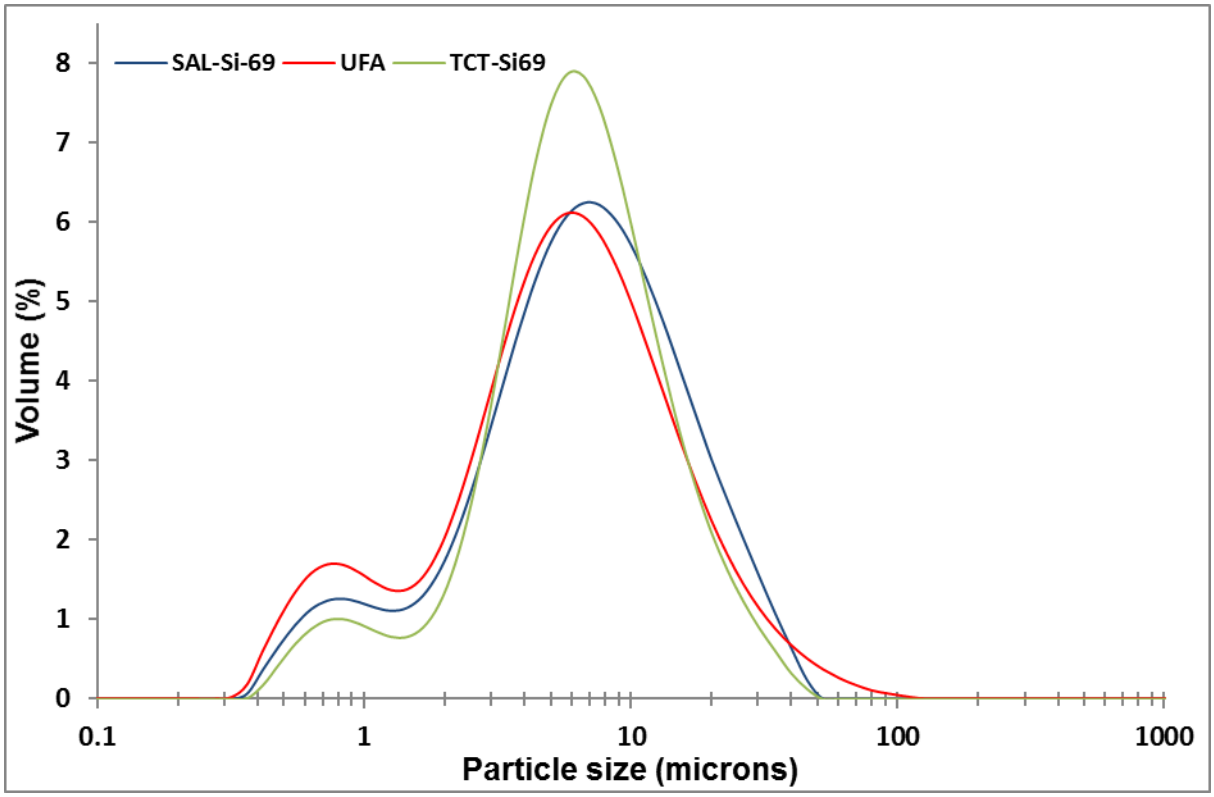

Figure 6.3.10: Particle size distribution of untreated and silane treated coal fly ashes.

There were marginal changes in the d_{50} and d_{90} values of both the silane treated SAL and TCT samples when compared to the untreated coal fly ash sample. The d_{50} value for the SAL increased from 5.49 to 5.79 and d_{90} decreased from 16.40 to 14.88 after silane treatment. The d_{50} and d_{90} of the TCT sample, on the other hand, decreased after silane treatment from 9.36 to 6.16 and from 19.55 to 18.19 respectively.

Table 6.3.4: Particle size distribution of the treated and untreated coal fly ash samples (n=2).

Sample	d_{10}(µm)	d_{50}(µm)	d_{90}(µm)
UFA	0.99 ± 0.01	5.19 ± 0.18	16.04 ± 1.53
UFA Si-69	-	-	-
SAL Si-69	1.96 ± 0.12	5.79 ± 0.19	14.88 ± 0.38
TCT Si-69	1.39 ± 0.42	6.16 ± 0.45	18.19 ± 0.17

6.3.5 Contact angle measurement

Wettability studies can be used to explain the degree to which solid surfaces are modified and become water repellent (Feyyisa *et al.*, 2017). It involves the determination of contact angles, which illustrates the extent of wetting when a solid and a liquid interact (Bracco and Holst, 2013). Ranjbar *et al.* (2015) defined the water contact angle as "a parameter that determines the hydrophilicity/hydrophobicity of the material. The angle is related to the value of the contact angle between the water droplet and the solid". Small contact angles (<<90°) correspond to high wettability, while large contact angles (>>90°) correspond to low wettability (Feyyisa *et al.*, 2017). Surface modification of a similar coal fly ash sample treated with sodium lauryl sulphate was previously confirmed via wettability measurements (van der Merwe *et al.*, 2014). In that study, contact angle measurements were used to prove that the hydrophilic surface of untreated fly ash was rendered hydrophobic after surface treatment.

The contact angles of untreated fly ash (UFA) and silane treated UFA (UFA-Si69) were measured using water and diodomethane as wetting liquids. Figure 6.3.11(a) shows the contact angle image of diodomethane on a glass plate covered with untreated fly ash (UFA). As shown, the contact angle of diodomethane on the surface of the untreated fly ash powder is between 38.8° and 46.0° indicating high wettability of the UFA sample. The contact angle of pure water on the UFA could not be determined because the drop was absorbed too quickly. Figures 6.3.11(a) and (b) show the angles of diodomethane and water on the surfaces of silane treated coal fly ash (UFA-Si69). The contact angles of the diodomethane and water on the UFA-Si69 powder were 147° and 145° respectively. The increasing contact angle indicates low wettability of the sample and high hydrophobicity of the silane treated fly ash samples. Contact angle images for SAL-Si69 and TCT-Si69 could not be obtained because the water and diodomethane drops were absorbed too quickly by the samples.

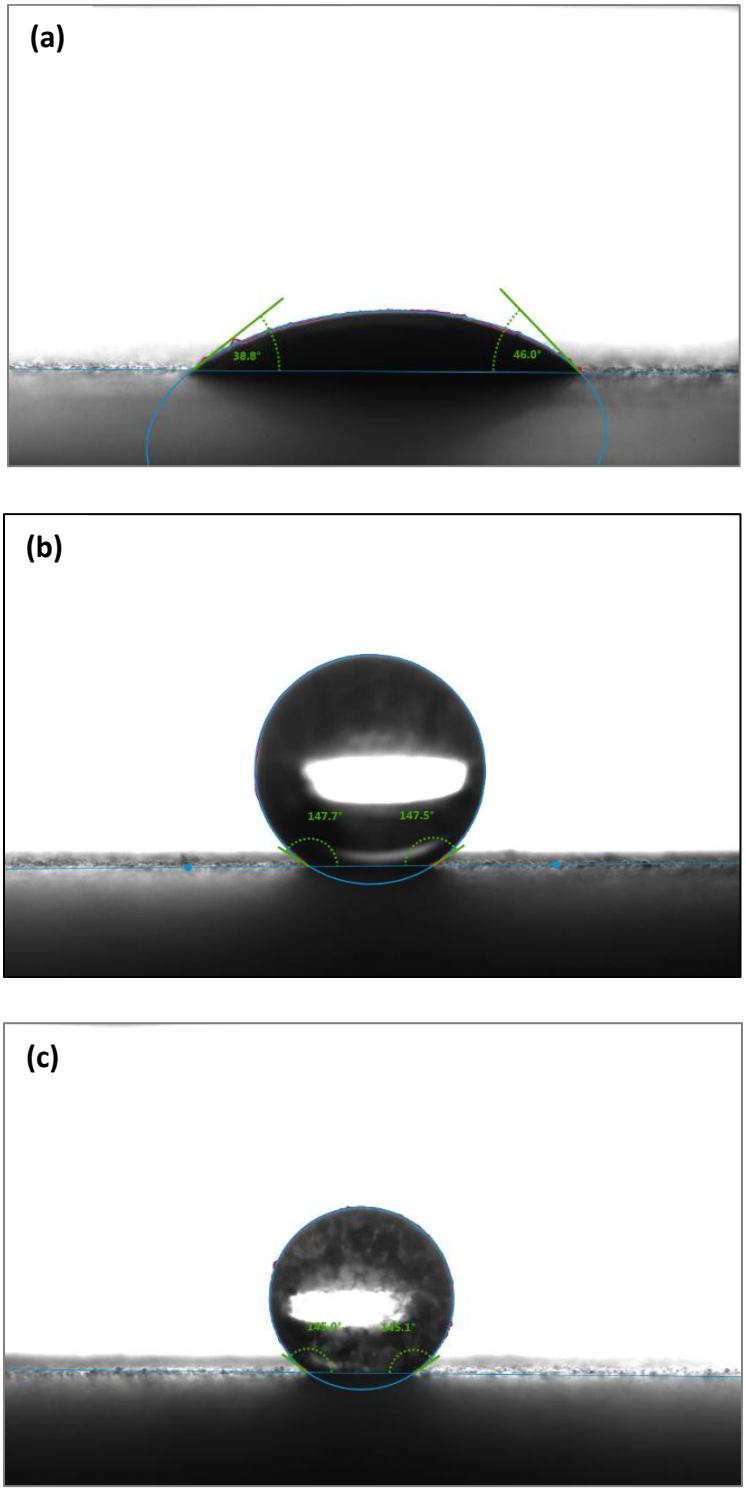

Figure 6.3.11: Sessile drops of (a) diodomethane on UFA, (b) diodomethane on UFA-Si69 and (c) pure water on UFA-Si69 to illustrate integrity of silane coating on UFA.

The contact angle results are essential in proving the success of silane treatment on UFA but not on TCT-L and SAL. Although the presence of Si-69 in all 3 samples was confirmed by TGA

and FTIR measurements (Sections 6.3.2 and 6.3.3), wettability tests indicate that surface modification was achieved only for the UFA sample. It therefore seems that coupling of Si69 with the fly ash surface only took place for the UFA sample and not for TCT-L and SAL.

6.4. Summary

This section summarises the findings of this chapter and compares the results obtained from thermochemical-, sulphuric acid- and silane treatments applied so as to put things into perspective for the reader.

6.4.1 Chemical and mineralogical composition

The elemental composition of untreated (UFA), thermochemically treated (TCT), sulphuric acid treated (SAL) and the respective silane (Si-69) treated fly ash samples are compared in Table 6.4.1.

Table 6.4.1: The elemental composition of UFA, TCT-L, SAL, UFA-Si69, SAL-Si69 and TCT-Si69 fly ash samples.

	Concentration (wt. %)[a]									
	SiO_2	Al_2O_3	CaO	Fe_2O_3	TiO_2	MgO	K_2O	P_2O_5	SO_3	Total
UFA	51.7	33.8	5.2	3.4	1.8	1.1	0.9	0.7	0.2	102.7
TCT-L	61.8	20.0	4.6	3.3	2.2	0.8	0.5	0.6	3.1	96.3
SAL	55.3	28.8	4.0	2.0	1.4	0.5	0.9	0.1	4.4	97.1
UFA-Si69	53.6	33.0	4.2	3.2	1.7	1.2	0.7	0.7	1.5	102.7
TCT-Si69	63.9	18.8	3.5	2.9	1.9	0.9	0.3	0.8	4.7	96.4
SAL-Si69	58.4	28.0	3.4	1.9	1.4	0.5	0.6	0.1	4.3	96.8

[a] Other elements present in small amounts (<0.1%): ZrO_2, MnO, V_2O_5, Cr_2O_3, NiO, Na_2O, CuO.

The results show that there was a decrease in the alumina content of the fly ash samples after application of thermochemical and sulphuric acid treatment processes. The alumina content decreased from 33.8% by weight in untreated fly ash (UFA) to 20.0 wt. %, in thermochemically treated and leached (TCT-L) fly ash, and 28.8 wt. % in sulphuric acid leached (SAL) fly ash. There was a negligible change in alumina content in UFA and SAL after silane treatment. The change in CaO content after silane treatment was also negligible in all three samples. Sulphur analysis showed that the SO_3 content increased from 0.2 wt. % in UFA to 3.1 wt. % in TCT-L and 4.4 wt. % after the thermochemical and sulphuric acid treatments. There was a negligible change in sulphur content in the silane treated SAL sample. The changes in the content of the oxides of other elements (e.g. Fe, Ti, K and P) were negligible after all treatments.

Table 6.4.2 presents a summary of the quantitative XRD results for untreated (UFA), thermochemically treated (TCT), sulphuric acid treated (SAL) and the respective silane (Si-69) treated fly ash samples.

Table 6.4.2: Quantitative XRD results of UFA, TCT-L, SAL, UFA-Si69, SAL-Si69 and TCT-Si69 fly ash samples.

Mineral phase	UFA wt.%	TCT-FA wt.%	TCT-L wt.%	SAL wt.%	UFA-Si69 wt.%	SAL-Si69 wt.%	TCT-Si69 wt.%
Amorphous	69.1	39.5	86.6	57.1	67.1	58.4	87.5
Mullite	29.1	1.6	3.5	29.6	25.3	28.4	3.6
Quartz	5.8	3.8	6.9	7.0	7.0	6.8	6.3
Gypsum	-	-	3.0	-	-	-	2.7
Anhydrite	-	3.8	-	6.4	-	6.2	-
Hematite	0.7	-	-	-	0.7	-	-
Alunogen	-	16.0	-	-	-	-	-
Godovikovite	-	9.8	-	-	-	-	-
Millosevichite	-	25.6	-	-	-	-	-

The quantitative XRD results show an increase in amorphous content from 69.1% to 86.6% after thermochemical treatment and aqueous dissolution while the amorphous content decreased to 57.1 following acid treatment. Compared to the untreated sample the amorphous content of the respective silane treated samples remained relatively constant before and after silanization. The mullite content decreased after thermochemical treatment and dissolution and remained the same after acid treatment. Gypsum formed in TCT-L and was also present in TCT-Si69 but was not detected in the SAL samples. Anhydrite was formed in TCT-FA but was not detected after the dissolution. SAL and SAL-Si69 both contained anhydrite.

6.4.2 Physical properties

The d_{50} values obtained from particle size analysis and the surface area for untreated (UFA), thermochemically treated (TCT), sulphuric acid treated (SAL) and the respective silane (Si-69) treated fly ash samples are summarised in Table 6.4.3.

Table 6.4.3: Particle size distribution (d_{50}) and BET surface area of UFA, TCT-L, SAL, UFA-Si69, SAL-Si69 and TCT-Si69 fly ash samples.

Sample	UFA	TCT-L	SAL	UFA-Si69	TCT-Si69	SAL-Si69
d_{50}(μm)	5.19	6.47	5.42	-	6.16	5.79
Surface Area (m^2/g)	0.99	7.97	11.02	0.62	9.37	10.26

The results show a slight increase the d_{50} values from 5.19 μm for UFA to 6.47 μm for TCT-L following thermochemical treatment and 5.42 μm for SAL following sulphuric acid treatment. The d_{50} value for UFA-Si69 could not be determined because the sample was completely hydrophobic and would not disperse in the Hydro 2000G dispersion unit. The d_{50} values for TCT and SAL samples after silane treatment were 6.16 μm and 5.79 μm respectively.

Surface area analysis results showed a significant increase in the fly ash sample after thermochemical and sulphuric acid treatment. The surface area increased from 0.99 m^2/g

(UFA) to 7.97 m^2/g (TCT-L) and 11.02 m^2/g (SAL). There was negligible change in the surface area of the respective silane treated samples.

Table 6.4.4 presents a summary of the results obtained from zeta potential measurements for untreated (UFA), thermochemically treated (TCT), sulphuric acid treated (SAL) fly ash samples.

Table 6.4.4: Initial pH, zeta potential and isoelectric points of UFA, TCT-L and SAL aqueous suspensions.

Sample	UFA	TCT-L	SAL
Initial pH	8.78	4.00	4.27
Zeta potential at initial pH (mV)	-27.6	+16.3	-0.5
pH at Isoelectric point	3.72	7.75 - 8.4	4.27

The pH of an aqueous solution of the fly ash sample change from 8.78 to 4.00 after thermochemical treatment and to 4.27 after sulphuric acid treatment. The zeta potential at the initial pH was -27.6 mV for UFA, +16.3 mV for TCT and -0.5 mV for SAL. The pH at the isoelectric point was 3.72 for UFA, between 7.75 and 8.4 for TCT-L and 4.27 for SAL.

Chapter Seven

Properties of the vulcanized composites

This chapter presents and discusses the results obtained from the evaluation of the mechanical properties of the fly ash-rubber composites.

7.1. Cure characteristics of carbon black and fly ash filled cis-1,4-polysisoprene compounds

Curing is a heat treatment via various methods in order to cross-link polymer chains in rubber, and in doing so, increasing the stiffness and elasticity of the rubber. When a system uses sulphur for curing, the process is called vulcanization (Karahan and Atiş, 2011; Karaağaç *et al.*, 2012). Due to the high energy and time demands, rubber curing is an expensive and complex process, therefore optimizing the cure cycles is very important. The cure or vulcanization kinetics are of interest largely due to the need to (1) produce uniform cures in rubber profiles, (2) obtain duplicate cures and (3) attain sufficient cures in thick rubber sections (He *et al.*, 2005; Karaağaç *et al.*, 2012). Moving die rheometers (e.g. Alpha Technologies, Montech, Scarabeus and Göttfert) are used to assess the cure characteristics of a test sample during vulcanization. The cure curves are obtained by oscillating die at a constant angular displacement while monitoring the torque required as a function of time at a constant temperature. They can be used to estimate values like the minimum (M_L) and maximum (M_H) torque and to evaluate parameters such as scorch time (t_s: time for the onset of cure) and optimum curing time (t_{90}: time for the completion of cure) (Ansarifar *et al.*, 2004).

Figure 7.1.1 presents the cure curve for cis-1,4-polyisoprene rubber filled with TCT-L (NR/TCT-L) illustrating the vulcanizate maximal and minimal torque.

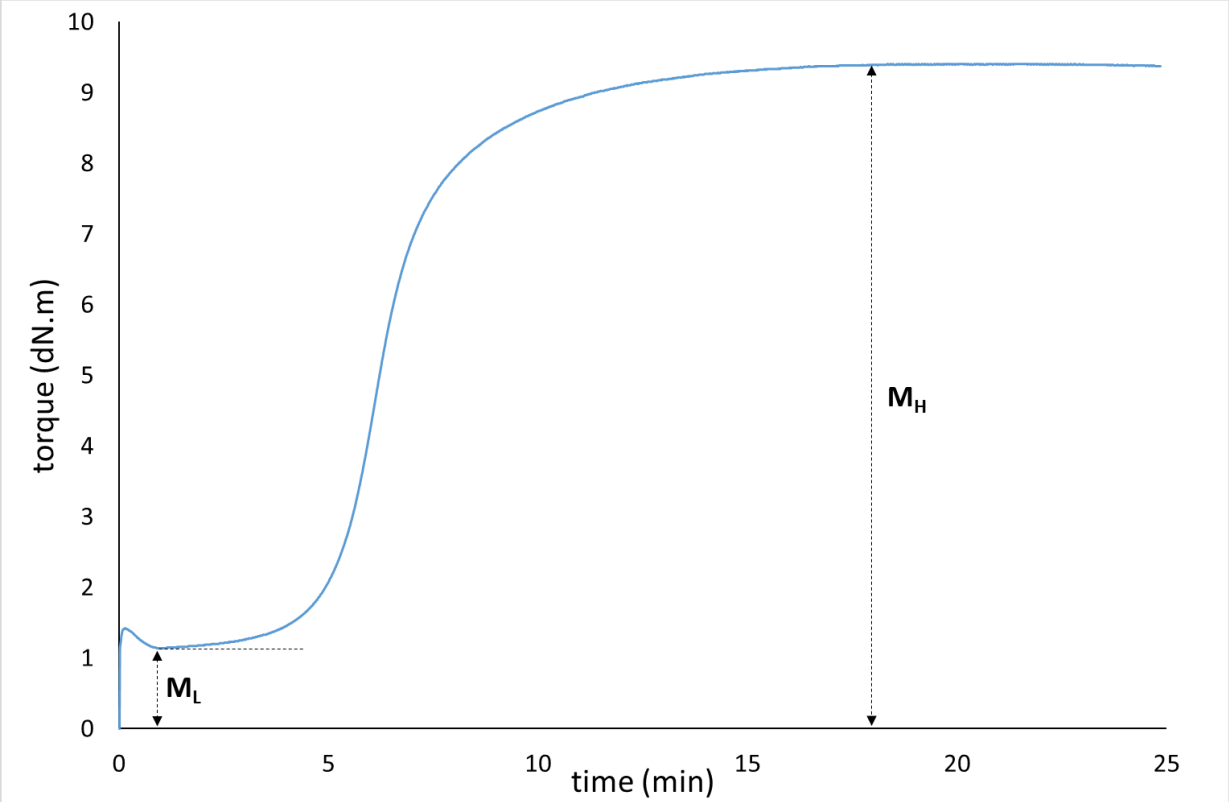

Figure 7.1.1: Cure curve obtained at 150°C obtained for TCT-L filled cis-1,4-polysisoprene rubber.

The results obtained from cure curves can be summarized in table format, where table 7.1.1 gives cure results for carbon black filled isoprene rubber while table 7.1.2 gives a summary of the fly ash filled isoprene rubber compounds.

Table 7.1.1: Cure characteristics of carbon black- and hybrid (FA-CB)-filled cis-1,4-polyisoprene rubber.

Sample	M_L (dNm)	M_H (dNm)	Cure rate (dNm)	T_{90} (min)	Scorch time (t_s,min)
Neat	1.0	8.0	7.0	9.5	6.8
N330	1.6	12.9	11.3	3.8	-
N660	1.4	12.1	10.7	5.9	3.1
N774	1.5	11.2	9.7	5.2	3.2
N990	1.35	9.7	8.4	6.5	4.9
UFA-N330	1.3	11.0	9.6	7.0	4.0
UFA-N660	1.3	10.5	9.2	6.6	3.9
UFA-N774	1.0	10.7	9.7	7.1	4.3
UFA-N990	1.1	10.0	8.9	12.1	8.3
TCT-N330	1.3	11.2	9.9	9.1	5.5
TCT-N660	1.2	11.4	10.2	8.7	5.1
TCT-N774	1.1	11.7	10.7	9.3	5.6
TCT-N990	1.1	9.6	8.5	8.5	5.3
SAL-N330	1.3	11.4	10.1	8.4	4.8
SAL-N660	1.2	10.2	9.0	9.3	5.6
SAL-N774	1.3	10.5	9.2	9.5	5.8
SAL-N990	0.9	10.4	9.5	10.7	7.6

Table 7.1.2: Cure characteristics of fly ash-filled cis-1,4-polyisoprene rubber.

Sample	M_L (dNm)	M_H (dNm)	Cure rate (dNm)	T_{90} (min)	Scorch time (t_s,min)
Neat	1.0	8.0	7.0	9.5	6.8
UFA	0.9	8.8	8.0	11.2	8.4
TCT	1.1	9.4	8.3	9.4	6.6
SAL	1.0	9.3	8.3	10.6	7.5
UFA-Si69	0.9	9.9	9.0	11.2	8.4
TCT-Si69	1.1	8.8	7.7	11.7	9.3
SAL-Si69	1.2	9.4	8.2	11.4	8.4
UFA-Si69 insitu	0.6	10.4	9.8	13.4	8.0
TCT-Si69 insitu	0.6	10.6	9.9	11.5	8.1
SAL-Si69 insitu	0.7	10.1	9.4	13.2	10.0

Each vulcanizate exhibits differing cure characteristics owing to differences in the filler properties. The carbon black-filled vulcanizates (Table 7.1.1) exhibited the lowest scorch time (t_s) and cure time (t_{90}), which may be attributed to carbon black having the highest specified surface area with which the curatives and rubber may interact. In addition, carbon blacks have a high surface reactivity as result of a range of oxygen-containing groups (McGill and Shelver, 1995). The t_{90} of the carbon blacks ranged from 3.8 (N330) to 6.5 mins (N990). Filler associated parameters such as surface area, particle size, moisture content (polarity), metal ions and surface reactivity affect the cure characteristics (Ooi *et al.*, 2013). Generally, fillers that have high metal oxide content and high moisture content impart a faster cure rate (Da Costa, L. L Y Visconte, *et al.*, 2002). Past work by Sombatsompop *et al.* (2007) proposed that the presence of excessive metal oxides (e.g., Al_2O_3, CaO, MgO) in lignite fly ash accelerated the curing process by acting as activators (facilitating formation of a zinc-accelerator complex with sulphur) and thus decreasing the cure time of natural rubber compounds. However, this was not the case for the fly ash samples used in this study. This was due to the differences in the metal oxide content of lignite fly ash and the bituminous fly ash used in our study; with

lignite fly ash having a higher metal oxide content (Kanking *et al.*, 2012). For cis-1,4-polyisoprene vulcanizates filled with hybrid FA-CB filler, there was a marked increase in scorch and cure times but no definite trend was observed. Total replacement of the carbon black (25 phr FA, Table 7.1.2) yielded even longer scorch and cure times. UFA-filled vulcanizates had a longer cure time than the neat cis-1,4-polyisoprene rubber, meaning the filler slowed the cure properties of the neat rubber. When compared to carbon black, this behaviour can be attributed to the lower specific surface area, larger average particle size and lower interaction between fly ash and rubber (Da Costa, L. L Y Visconte, *et al.*, 2002; Arayapranee *et al.*, 2005). Following physicochemical treatment, TCT-L and SAL exhibited improved cure characteristics when compared to UFA. This may be explained by the increase in specific surface area of the two samples after treatment. However, the cure characteristics of SAL-filled vulcanizates were still inferior to those of neat rubber while TCT neither worsened nor improved the cure characteristics of the rubber.

Silane treatment was expected to enhance the cure characteristics (i.e. impart short cure times (t_{90}) and scorch times (t_s)) by forming filler-silane-rubber matrix linkages as supported by the results of Ismail *et al.* (2001), Da Costa *et al.* (2002) and Pongdong *et al.* (2015). Silanization was successful on the UFA sample (UFA-Si69). There was, however, no indication that the treatment had any actual influence on the cure and scorch times. The scorch and cure times of rubber filled with UFA were 8.4 and 11.2 min, respectively. When UFA-Si69 was used, the scorch and cure times were 8.4 and 11.2 mins, respectively. Similar observations were made by Thongsang and Sombatsompop (2007) who investigated the effect of silane treated fly ash silica on viscosity, cure and viscoelastic properties of natural rubber. According to Poh and Ng (1998), and Thongsang and Sombatsompop (2007) the slight increase in cure time following addition of Si69 indicates an interference effect on the formation of crosslinking between rubber molecules produced by the presence of Si69. Figure 7.1.2 shows chemical reactions between being-vulcanised rubber and Si69-treated fly ash particles that can be used to explain this observation. The bulky triethoxysilylpropyl groups on both ends of the Si69 chains increase steric hindrance for cross-linking of rubber molecules.

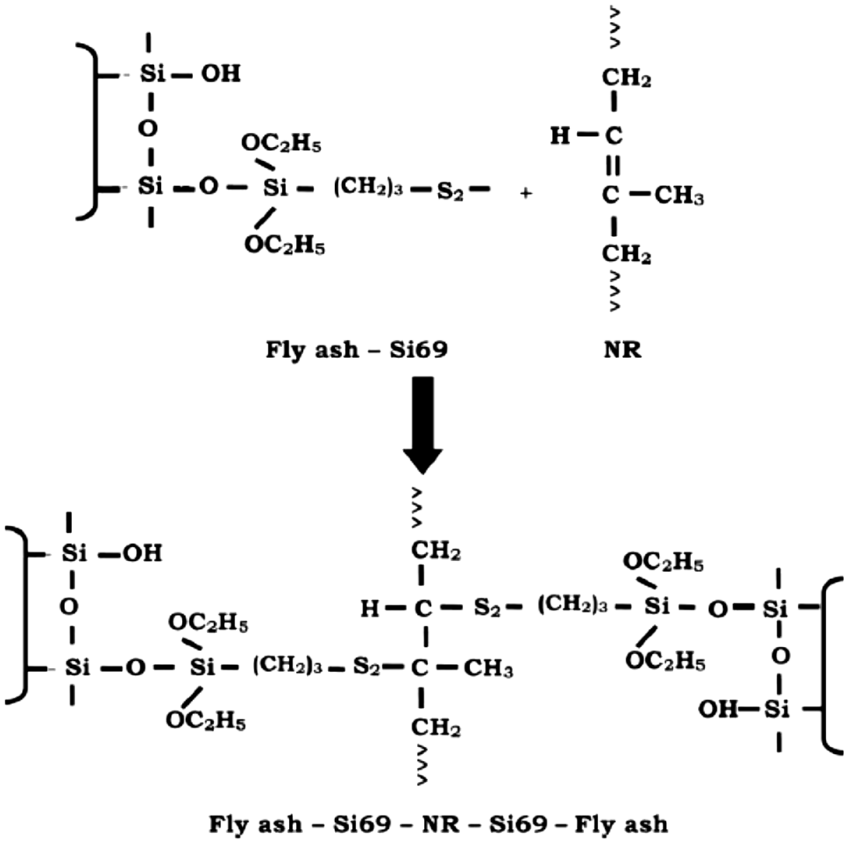

Figure 7.1.2: A chemical reaction between Si69-treated FA particles and NR molecules (Guo *et al.*, 2013).

The minimum torque (M_L) and maximum (M_H) are related to the stiffness of the compound. M_L is proportioned to the viscosity and processability of the uncured compound while M_H reveals the ultimate crosslink density resulting from the vulcanization process (Dick, 2003). For both fly ash and carbon black, the addition of filler was accompanied by a marked increase in the maximum torque (M_H), indicating that the presence of the fillers in the rubber matrix reduces the mobility of the rubber's macromolecular chains. As expected for the 25 phr CB's, NR/N330 exhibited the highest M_H (11.3 dNm) followed by NR/ N660 (10.7 dNm), NR/N774 9.7 (dNm) and NR/N990 (8.5 dNm), respectively. The high M_H values for carbon black composites point towards the higher restriction to the molecular motion of the macromolecules, possibly a result of greater interaction between carbon black and rubber. Composites with hybrid FA:CB fillers resulted in lower M_H values indicating lesser restriction to the molecular motion of the macromolecules, probably caused by reduced interaction between the fly ash and the rubber matrix (Da Costa, L L Y Visconte, *et al.*, 2002).

7.2. Mechanical properties of carbon black and fly ash filled cis-1,4-polysisoprene compounds

The initial aim of the study was to compare the mechanical properties of rubber composites filled with fly ash (NR/FA) to those filled with N330 carbon black (NR/N330), a high reinforcing and low modulus carbon black that is applied in industrial goods. Preliminary experiments were carried out and the results are presented in Figures 7.2.1.

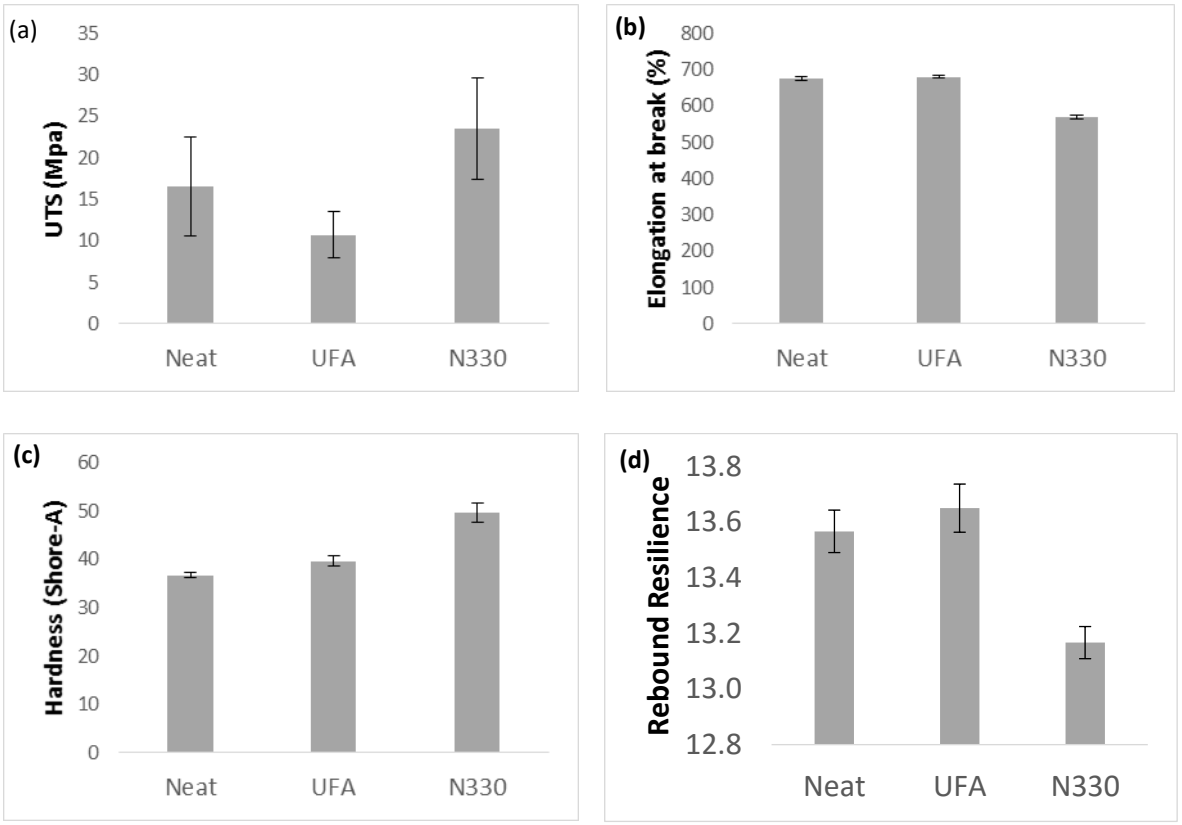

Figure 7.2.1:Plots of (a) ultimate tensile strength (UTS) measurements, (b) elongation at break, (c) hardness and (d) rebound resilience of cis-1,4-polyisoprene vulcanizates with no filler (Neat) and filled with UFA and N330 *(n = 3)*.

The preliminary tests demonstrated that the mechanical properties of NR/N330 vulcanizates were far superior to the NR/UFA vulcanizates and therefore UFA could not possibly be used as a replacement for N330 CB. In light of these results, no further tests using N330 CB (25 phr) in comparison to the fly ash samples were conducted. Only partially replaced (12.5 phr FA: 12.5 N330 CB) N330 CB was tested. The study then focused on comparing fly ash samples to the medium to low reinforcing carbon blacks (N660, N774 and N990).

Table 7.1.2 represents the tensile properties (modulus at 600% elongation ($M_{600\%}$), elongation at break (E_b), ultimate tensile strength (UTS)), hardness and rebound of neat, carbon black- and fly ash- filled cis-1,4-polyisoprene rubber vulcanizates.

Table 7.2.1: Mechanical properties of neat, carbon black- and fly ash-filled cis-1,4-polyisoprene rubber vulcanizates.

Sample		$M_{600\%}$ (MPa)	E_b (%)	UTS (MPa)	Hardness (Shore-A)	Rebound (%)
Neat		4.66	714	19.0	35.7	35.7
N660		22.1	618	25.5	43.3	12.8
N774		20.4	642	30.4	44.0	13.78
N990		12.4	678	28.5	41.7	12.18
UFA	UFA	6.1	698	18.5	38.7	38.7
	UFA-N330	17.0*	615	19.9	42.7	42.7
	UFA-N660	14.4*	652	24.9	43.0	43.0
	UFA-N774	14.0*	642	22.2	41.3	41.3
	UFA-N990	10.5	670	24.9	39.7	39.7
	UFA-Si69	9.3	665	22.5	40.7	38.0
	UFA-Si69 in-situ	11.2	628	16.3	-	-
TCT-L	TCT-L	8.2	662	19.6	40.7	40.7
	TCT-N330	19.5*	612	22.1	43.0	43.0
	TCT-N660	19.4*	637	27.6	43.7	43.7
	TCT-N774	18.2*	647	29.3	42.3	42.3
	TCT-N990	10.2	671	24.8	41.3	41.3
	TCT-Si69	7.5	665	18.1	39.3	41.6
	TCT-Si69 in-situ	9.5	633	14.9	-	-
SAL	SAL	6.4	683	21.7	39.1	39.1
	SAL-N330	17.0*	640	25.5	42.7	42.7
	SAL-N660	16.3*	650	27.5	42.0	42.0
	SAL-N774	16.1*	644	25.8	41.3	41.3
	SAL-N990	10.8	656	21.5	40.7	40.7
	SAL-Si69	9.0	669	23.1	40.0	30.3
	SAL-Si69 in-situ	11.5	606	12.2	-	-

*samples with $M_{600\%}$ matching or better than the lowest reinforcing carbon black (N990).

As expected, neat rubber exhibited the lowest $M_{600\%}$ (4.7 MPa) while vulcanizates containing 25 phr N660 CB exhibited the highest $M_{600\%}$ (22.1 MPa) followed by N770- and N990-filled vulcanizates with tensile moduli of 20.4 and 12.4 MPa respectively. This can be explained by the differences in the surface area of the carbon blacks. N660 and N774 CB's have specific surface area values of 35 m^2/g and 30 m^2/g respectively, and are described as medium reinforcement and modulus fillers. N990 has a low specific surface area (9 m^2/g) and exhibits low reinforcement and low modulus in vulcanizates (IARC Working Group on the Evaluation of Carcinogenic Risks to Humans, 2010a). It was observed that the hybrid filler samples had lower moduli than their respective carbon black-filled samples therefore they were less reinforcing, however, the hybrid fillers were better than the neat sample. This suggests that none of the fly ash samples tested improved the mechanical properties of carbon black-filled composites. The observation may be ascribed to the fundamental properties of FA that are associated with the interaction between filler and rubber, such as surface reactivity, shape, particle size, degree of dispersion and structure (Ooi *et al.*, 2013). Generally, easy slippage of the polymer matrix over the smooth surface of the spherical fly ash particles reduces the mechanical strength of the composites (Srinivasan and Bandyopadhyay, 2017). In spite of the decrease in moduli, the order of increasing tensile moduli amongst the carbon black composites remained the same with UFA-N330 hybrid vulcanizate exhibiting the highest modulus (16.98 MPa) followed by UFA-N660 (14.44 MPa), UFA-N774 (13.99 MPa) and lastly UFA-N990 (10.50 MPa).

When the UFA loading was increased to 25 phr with no CB applied, the $M_{600\%}$ of the rubber vulcanizates worsened, as also observed by Sombatsompop *et al.* (2004), Kanking *et al.* (2012), and Ismail et al. (1999). Kanking *et al.* (2012) explained the results using SEM micrographs which revealed poor dispersion of fly ash in the rubber matrix due to particle aggregation. According to Ismail *et al.* (1999), the decrease in strength may be a result of agglomeration of fly ash particles due to hydrophilic particle-particle interactions. These undispersed agglomerates serve as failure-initiating flaws and result in poor mechanical properties. Sombatsompop *et al.* (2004) observed that interaction between fly ash and the rubber matrix was poor, noted by voids present between the rubber phase and the fly ash particles. The $M_{600\%}$ amongst the UFA-filled vulcanizates increased in the order UFA<UFA-Si69<UFA-Si69 in-situ. NR/UFA vulcanizates had the lowest $M_{600\%}$ (6.07 MPa) amongst the

UFA samples. These three samples showed an improvement in reinforcement when compared to the neat rubber (4.66 MPa). However, this was still lower than the least reinforcing carbon black (NR/N990).

Silane treatment results in improved dispersion and wetting of UFA in the rubber matrix and therefore the increase in $M_{600\%}$ was expected (Ismail *et al.*, 1999). According to Thongsang *et al.* (2012a) and Ansarifar *et al.* (2005), the reaction of Si69 ethoxy groups and silanol groups on the surfaces of fly ash reduces the number of silanol groups thus weakening the filler-filler interactions and preventing formation of aggregates. These changes help improve the mechanical properties of the vulcanizates. Following silane treatment, the $M_{600\%}$ of the UFA filled-sample increased, with the NR/ UFA-Si69 in-situ vulcanizates exhibiting a better modulus (11.19 MPa) than the pre-treated UFA-Si69/NR vulcanizates (9.33 MPa). The tensile moduli were, however, less than that of CB-N990.

Thermochemically treated and leached (TCT-L) samples exhibited improved $M_{600\%}$. The order of increasing $M_{600\%}$ amongst the TCT-L filled vulcanizates was TCT-Si69<TCT-L<TCT-Si69 in-situ. Unlike with the UFA samples, the silane treated TCT-L had the lowest $M_{600\%}$ amongst the TCT-L samples. Silane grafting onto TCT-L was unsuccessful, as evident in the contact angle measurements (Section 6.3.5), and this therefore explains why TCT-Si69 did not show an improved $M_{600\%}$. Hybrid fillers of TCT-L and CB yielded the same trend as that of UFA samples, TCT-N990<TCT-N774<TCT-N660<TCT-N330. All the $M_{600\%}$ values for TCT-L samples were higher than for the corresponding UFA samples. This might be attributed to the higher surface area of the TCT-L sample (7.97 m^2/g) compared to the UFA sample (0.99 m^2/g).

Sulphuric acid treated samples essentially exhibited similar trends and $M_{600\%}$ values as the UFA samples with the 25 phr samples increasing in the order SAL<SAL-Si69<SAL-Si69 in-situ and the partial replacement having the order SAL-N990<SAL-N774<SAL-N660<SAL-N330. The SAL sample had the highest surface area (11.02 m^2/g) and was expected to exhibit the highest $M_{600\%}$, however the sample exhibited inferior properties in the compounds. The NR/SAL vulcanizates did not cure evenly, some parts of the pressed rubber was observed to be under-cured. This could be explained by the acidity of the SAL sample which might have been responsible for retarding the curing of the rubber. Acidic components are traditionally applied as retarders in curing systems and interfere with the activity of basic accelerators, causing a

delay in the vulcanization reaction. Acids slow down the curing rate, retard scorch time and reduce the ultimate state of cure (Barlow, 1993).

The trends observed for elongation at break (E_b), hardness and rebound corresponded with that of the $M_{600\%}$ for similar reasons. However, the ultimate tensile strength (UTS) of the partially replaced vulcanizates show unexpected results. FA-N990 vulcanizates exhibited better UTS followed by FA-N660, FA-N774 and FA-N330 respectively. Investigation of filler dispersion in these compounds is necessary in order to give an explanation.

In general, the fly ash (UFA, TCT-L and SAL) filled vulcanizates have lower $M_{600\%}$, E_b, UTS, hardness and rebound when compared to the compounds with carbon black (N330, N660, N774 and N990). It is evident that, even in the presence of coupling agent, the fly ash samples do not act as significantly reinforcing fillers. The NR/FA vulcanizates improved the mechanical properties of the neat rubber but imparted properties far inferior to the least reinforcing carbon black (N990). The inferior properties of the fly ash filled or partially replaced vulcanizates may be explained by several factors. Firstly, fly ash has larger particles than carbon blacks and therefore smaller surface areas. Secondly, the fly ash particles show a greater tendency towards aggregation therefore the dispersion of the FA is not uniform when compared to the carbon blacks (Da Costa, L L Y Visconte, *et al.*, 2002). Furthermore, the increased acidity of the fly ash surfaces after treatment (TCT-L and SAL) interferes with the activity of the basic accelerators during vulcanization, resulting in under-cured rubber.

Chapter Eight

Conclusions and recommendations for future developments

Final conclusions and recommendations for further study are presented.

8.1. Overview

The aim of this study was to evaluate the capabilities of ultrafine fly ash (untreated and physico-chemically modified) when it is applied as filler in natural rubber. Physico-chemical modification of the ultrafine coal fly ash was achieved using two techniques originally intended for aluminium extraction from coal fly ash. These entailed thermochemical treatment using ammonium sulphate (TCT-FA), followed by controlled aqueous dissolution (TCT-L) as well as acid leaching by a sulphuric acid reflux method (SAL). In addition, chemical modification of ultrafine fly ash and physico-chemically modified (TCT-L and SAL) ultrafine fly ash using a silane coupling agent (Si-69) was investigated. The chemical and physical properties of the untreated and modified fly ash were characterized in order to effectively track the changes brought about by the chemical and physical modifications applied. Rubber composites containing fly ash, carbon black and fly ash-carbon black hybrids were prepared and the mechanical properties of the rubber composites analysed in order to assess the viability of untreated and modified fly ash as filler in rubber. Several analytical techniques such as XRD, XRF, SEM, TGA, FTIR, BET, zeta potential and PSD analysis were utilised to characterise the fly ash samples and ICP-MS was used to determine the extraction efficiencies of the elements from fly ash during the modification process. The results of the physico-chemical treatments and characterisation are summarised below.

8.2. Characterization of untreated and physico-chemically modified fly ash

8.2.1 Characterization of untreated fly ash (UFA)

Characterization of the untreated Lethabo coal fly ash (UFA) sample was necessary in order to effectively track changes brought about by the chemical (Si-69 treatment) and physico-chemical (thermochemical and sulphuric acid treatment) modifications applied; as well as to better understand the interaction between fly ash samples and cis-1,4-polyisoprene rubber. UFA was composed mostly of SiO_2 (52.6%), Al_2O_3 (37.1%), CaO (4.3%), Fe_2O_3 (2.9%), MgO (1.4%) and TiO_2 (1.6%) with trace amounts of elements such as ZrO_2, MnO, V_2O_5, Cr_2O_3, NiO, Na_2O and CuO (< 0.1%). Quantitative XRD results of UFA indicated that the sample consisted of an amorphous alumino-silicate glass phase (69.1 wt. %) and two crystalline phases; mullite (29.1 wt. %) and quartz (5.8 wt. %). Thermal analysis by TGA in an inert nitrogen environment at temperatures ranging from 0 to 1400°C yielded a total mass loss of 4%, an LOI of approximately 2.4% and no $CaSO_4$ mass loss was observed. The BET surface area of UFA was determined to be 0.99 m^2/g and the particle size distribution (PSD) analysis yielded a bimodal peak ranging widely in particle size (0.5 – 100.0 µm). The mean particle size of the ash was 5.2 µm with 90% of the volume distribution having particle sizes smaller than 16.0 µm. Zeta potential studies revealed that UFA, when dispersed in deionised water, had a pH of approximately 9 and a negative zeta potential (-27 mV). The isoelectric point (IEP) of UFA was measured at pH 3.72. Morphological characterization by FE-SEM revealed predominantly spherical ash particles with a highly diversified particle size that was consistent with the PSD results. Considerable agglomeration of fly ash particles was evident in the micrographs.

8.2.2 Characterization of thermochemically treated and leached fly ash (TCT-L)

The thermochemical treatment of UFA with ammonium sulphate $(NH_4)_2SO_4$ followed by aqueous dissolution of the resulting water soluble sulphates accomplished the desired physical modifications to the fly ash particles. Three water soluble phases resulting from extraction of aluminium from the ash were identified by XRD to be alunogen $Al_2(SO_4)_3.17H_2O$, godovikovite $NH_4Al(SO_4)_2$, and millosevichite $Al_2(SO_4)_3$. A fourth crystalline phase, calcium sulphate/anhydrite, was formed from extraction of calcium. These four phases were removed during the aqueous leaching process. BET surface area of the fly ash sample increased from 0.99 m^2/g in UFA to 7.97 m^2/g in TCT-L. Following thermochemical treatment, there were

marginal changes in the d_{10} and d_{50} values, however, the particle size distribution remained largely unchanged. Morphological characterization by FE-SEM revealed that the fly ash particles remained predominantly spherical in shape, however, surface roughness of the particles increased. There was far less particle-particle agglomeration evident in the TCT-L sample as compared to UFA. Zeta potential measurements revealed that the TCT-L sample, when dispersed in deionized water, had an acidic pH (approx. 4) and a positive zeta potential (+16.3 mV). The isoelectric point (IEP) of TCT-L was measured between pH 7.75 and 8.4. The major chemical constituents of TCT-L were SiO_2 (63.0%), Al_2O_3 (19.1%), CaO (3.7%), Fe_2O_3 (2.7%), TiO_2 (1.9%) and MgO (1.1%). The SiO_2 content was enriched in the sample after extraction of aluminium and co-extraction of calcium, iron and magnesium. Thermal analysis by TGA in an inert nitrogen environment at temperatures ranging from 0 to 1400°C yielded a total mass loss of approximately 10%.

8.2.3 Characterization of sulphuric acid treated coal fly ash (SAL)

Following sulphuric acid treatment, the BET surface are of the fly ash sample increased from 0.99 m^2/g to 11.02 m^2/g. Unlike thermochemical treatment, the treatment did not alter the particle size distribution. The particles remained predominantly spherical in shape and there was a noticeable decrease in particle-particle agglomeration in the FE-SEM micrographs. The SAL sample, when dispersed in deionised water, yielded an acidic pH (approx. 4.27) and a negative zeta potential (-0.5 mV). The isoelectric point (IEP) of SAL was measured at pH 4.27. The major constituents of the SAL coal fly ash were SiO_2 (55.5%), Al_2O_3 (28.5%), CaO (4.0%), Fe_2O_3 (1.7%), TiO_2 (1.3%) and MgO (0.7%). Similar to the result obtained for TCT-L, the increase in SiO_2 content can be explained by the extraction of Al with minimal co-extraction of Si from UFA. Quantitative XRD analysis indicated no change in the mullite content, a decrease in the amorphous content (69.1% - 57.1%) and an enrichment of quartz/SiO_2 (5.8% - 7.0%) consistent with the XRF data. Thermal analysis by TGA in an inert nitrogen environment at temperatures ranging from 0 to 1400°C yielded a total mass loss of approximately 10% resulting from loss of water of hydration and decomposition of anhydrite.

8.3. Key Findings on application of fly ash filler in rubber vulcanizates.

The cure characteristics and the mechanical properties of cis-1,4-polyisoprene rubber filled with carbon black or fly ash (UFA, TCT and SAL) either treated with silane coupling agent (Si69) or used untreated were studied. From this work, it is concluded that:

- Carbon black filled-vulcanizates had the lowest scorch (t_s) and optimum cure (t_{90}) times which translates to a higher cure rate.
- Partial replacement of carbon black with fly ash (12.5 phr FA: 12.5 phr CB) resulted in a decrease in the scorch and cure times, meaning a decrease in cure rate.
- Increasing the fly ash loading to 25 phr (no carbon black) further increased the scorch and cure times. The scorch and cure times of the UFA- and SAL-filled vulcanizates were longer than those of the neat cis-1,4-polyisoprene rubber, meaning they deteriorated the cure properties of the rubber. TCT-filled vulcanizates had similar cure characteristics to the neat rubber therefore it neither improved no worsened the cure properties.
- The deterioration in cure properties after incorporation of fly ash was attributed to the lower specific surface area, larger average particle size and lower interaction between fly ash and rubber
- There was no indication that Si69 treatment had any influence on the cure properties of the vulcanizates.
- 25 phr carbon black composites exhibited superior mechanical properties (modulus, ultimate tensile strength, hardness and rebound) compared to the hybrid fillers and the fly ash fillers.
- Incorporation of fly ash to form the hybrid FA-CB fillers deteriorated the mechanical properties of the vulcanizates when compared to 25 phr carbon black-filled composites. Hybrids of UFA, TCT-L and SAL with N330, N600 and N774 had superior mechanical properties to the least reinforcing carbon black (N990). The reduction in mechanical properties is attributed to poor fly ash dispersion and poor FA-NR matrix interaction.
- SAL-filled samples did not cure well, sometimes appearing under-cured. This was attributed to the acidity of SAL samples which may have caused cure retardation.

- When compared to UFA-filled composites, Si69 grafting onto UFA produced composites with improved $M_{600\%}$, UTS, elongation at break, hardness and rebound. In-situ Si69 treatment produced even better results. This is attributed to the reduction in filler-filler interactions which causes agglomeration and subsequent improvement in fly ash distribution in the rubber matrix.

In summary, the thermochemical treatment and aqueous dissolution was successful in increasing the surface area and surface roughness, and decreasing the particle-particle agglomeration. Sulphuric acid treatment decreased the particle-particle agglomeration but there was no increase in surface roughness and the increase in specific surface recorded by BET might have been a result of increase in particle porosity instead. Silane treatment was only successful on the UFA and not on the TCT and SAL sample.

Incorporation of fly ash in cis-1,4-polyisoprene vulcanizates resulted in marginal improvement in the cure and mechanical properties when compared to the neat rubber, however, the fly ash samples were not reinforcing and the properties they imparted were inferior to the least reinforcing carbon black. Silane treatment of the fly ash further improved the mechanical properties of the vulcanizates. TCT-filled vulcanizates performed better than the UFA- and SAL- filled vulcanizates.

8.4. Recommendations and future work.

The following recommendations are made for future studies in order to better understand the properties of the carbon black-, hybrid FA-CB-, and fly ash-filled composites.

This study was carried out at a filler loading (25 phr) and mixing conditions that are optimum for carbon composites, not taking into consideration the difference in properties between the fly ash and carbon black. It is therefore recommended that further studies be carried out using varying fly ash content and FA: CB blend ratios in order to determine the effect of filler loading on the cure and mechanical properties.

The N660 data was closer to the N330 than expected and may have been a result of poor mixing and the structure of the N330 not being broken down completely. Therefore, it is recommended that the effect of mixing time be investigated and SEM imaging be used on fractured rubber compounds in order to study filler dispersion in the rubber matrix.

Furthermore, it is recommended that a Die C (ASTM D412) dumbbell cutter be used to cut the samples for mechanical properties testing. For this study, a special cutter was used which produced smaller dumbbells with no raised ends that would have made them fit better in the grips. This gave slippage problems on the extensometer.

NMR and IR of rubber vulcanizates to try and explain the chemistry side of observations.

Crosslink density to determine if the chemical treatment interferes with crosslinking, which in turn affects mechanical properties.

Widen the replacement range: e.g. 3:22 phr, 5:20 phr, 8:17 phr etc. This is to determine if the effect of CB is linear or not.

References

Ahmaruzzaman, M. (2010) 'A review on the utilization of fly ash', *Progress in Energy and Combustion Science*. Elsevier Ltd, 36(3), pp. 327–363. doi: 10.1016/j.pecs.2009.11.003.

Al-Hartomy, O. A. *et al.* (2011) 'Influence of carbon black structure and specific surface area on the mechanical and dielectric properties of filled rubber composites', *International Journal of Polymer Science*, 2011. doi: 10.1155/2011/521985.

Alkadasi, N., Hundiwale, D. . and Kapadi, U. . (2004) 'Effect of Coupling Agent on the Mechanical Properties of Fly Ash-Filled Polybutadiene Rubber', *Journal of Applied Polymer Science*, 91(2), pp. 1322–1328. doi: 10.1002/app.13280.

Allen, T. (1996) 'Particle Size Measurement', 208(5010), p. 483. doi: 10.1038/208529b0.

American Coal Ash Association (2013) 'Fly Ash Facts for Highway Engineers', *Journal of Chemical Information and Modeling*, 53(9), pp. 1689–1699. doi: 10.1017/CBO9781107415324.004.

Ansarifar, A. *et al.* (2005) 'The use of a silanised silica filler to reinforce and crosslink natural rubber', *International Journal of Adhesion and Adhesives*, 25(1), pp. 77–86. doi: 10.1016/j.ijadhadh.2004.04.002.

Ansarifar, A., Lim, H. P. and Nijhawan, R. (2004) 'Assessment of the effect of a bifunctional organosilane on the bound rubber and properties of some natural rubber compounds', *International Journal of Adhesion and Adhesives*, 24(1), pp. 9–22. doi: 10.1016/S0143-7496(03)00095-2.

Arayapranee, W., Naranong, N. and Rempel, G. L. (2005) 'Application of rice husk ash as fillers in the natural rubber industry', *Journal of Applied Polymer Science*, 98(1), pp. 34–41. doi: 10.1002/app.21004.

Arkles, B. (2006) 'Silane Coupling Agents: Connecting Acros Boundaries', *Gelest Inc*, pp. 1–56. doi: 10.1002/pol.1983.130210618.

ASTM International (2010) 'Standard Specification for Coal Fly Ash and Raw or Calcined Natural Pozzolan for Use', *Annual Book of ASTM Standards*, (C), pp. 3–6. doi: 10.1520/C0618.

Atkins, P. and De Paula, J. (2010) *Atkins' Physical Chemistry*. Ninth. Oxford: Oxford University Press.

Babel, S. and Kurniawan, T. A. (2003) 'Low-cost adsorbents for heavy metals uptake from contaminated water: a review.', *Journal of hazardous materials*, 97(1–3), pp. 219–243. doi:

10.1016/S0304-3894(02)00263-7.

Bailey, S. E. *et al.* (1999) 'A review of potentially low-cost sorbents for heavy metals', *Water Research*, 33(11), pp. 2469–2479. doi: 10.1016/S0043-1354(98)00475-8.

Al Bakri Abdullah, M. M. *et al.* (2012) 'Fly ash-based geopolymer lightweight concrete using foaming agent', *International Journal of Molecular Sciences*, 13(6), pp. 7186–7198. doi: 10.3390/ijms13067186.

Barlow, F. (1993) *Rubber Compounding: Principles: Materials, and Techniques, Second Edition*. Second. New York, Basel and Hong Kong: Marcel Dekker, Inc.

Barshick, C., Duckworth, D. and Smith, D. (2000) *Inorganic Mass Spectrometry*. New York: Marcel Dekker, Inc.

Bates, J. B. (1976) 'Fourier Transform Infrared Spectroscopy Published by : American Association for the Advancement of Science', *Science*, 191(4222), pp. 31–37.

Belver, C., Bañares Muñoz, M. A. and Vicente, M. A. (2002) 'Chemical activation of a kaolinite under acid and alkaline conditions', *Chemistry of Materials*, 14(5), pp. 2033–2043. doi: 10.1021/cm0111736.

Bracco, G. and Holst, B. (2013) *Surface science techniques*, *Springer Series in Surface Sciences*. doi: 10.1007/978-3-642-34243-1.

Brouwer, P. (2010) *Theory of XRF*, *Almelo: PANalytical BV*. PANalytical B.V.

Bustanafruz, F. and Fazli, M. (2013) 'Studies on Thermal Decomposition of Aluminium Sulfate to Produce Alumina Nano Structure', 2, pp. 463–468.

Cao, D., Selic, E. and Herbell, J.-D. (2008) 'Utilization of fly ash from coal-fired power plants in China', *Journal of Zhejiang University-Science A*, 9(5), pp. 681–687. doi: 10.1631/jzus.A072163.

Central Intelligence Agency (2014) *The World Fact Book*. Available at: http://www.indexmundi.com/g/r.aspx?t=100&v=82&l=en (Accessed: 2 August 2017).

Chamber of Mines of South Africa (2017) *Coal*. Available at: http://www.chamberofmines.org.za/sa-mining/coal (Accessed: 9 January 2017).

Chaowasakoo, T. and Sombatsompop, N. (2007) 'Mechanical and morphological properties of fly ash/epoxy composites using conventional thermal and microwave curing methods', *Composites Science and Technology*, 67(11–12), pp. 2282–2291. doi: 10.1016/j.compscitech.2007.01.016.

Choi, S. S. (2002) 'Properties of silica-filled styrene-butadiene rubber compounds containing acrylonitrile-butadiene rubber: The influence of the acrylonitrile-butadiene rubber type', *Journal of*

Applied Polymer Science, 85(2), pp. 385–393. doi: 10.1002/app.10614.

ÇIlgI, G. K. and Cetişli, H. (2009) 'Thermal decomposition kinetics of aluminum sulfate hydrate', *Journal of Thermal Analysis and Calorimetry*, 98(3), pp. 855–861. doi: 10.1007/s10973-009-0389-5.

Clifton, J. R. (1972) 'Thermal analysis of calcium sulfate dihydrate and supposed a and forms of calcium sulfate hemihydrate from 25 to 500 C', *Journal of Research of the National Bureau of Standards Section A: Physics and Chemistry*, 76A(1), p. 41. doi: 10.6028/jres.076A.005.

Clogston, J. D. and Patri, A. K. (2011) 'Zeta Potential Measurement', in McNeil, S. E. (ed.) *Characterization of Nanoparticles Intended for Drug Delivery*. Totowa, NJ: Humana Press, pp. 63–70. doi: 10.1007/978-1-60327-198-1_6.

Da Costa, H. M., Visconte, L. L. Y., *et al.* (2002) 'Mechanical and dynamic mechanical properties of rice husk ash-filled natural rubber compounds', *Journal of Applied Polymer Science*, 83(11), pp. 2331–2346. doi: 10.1002/app.10125.

Da Costa, H. M., Visconte, L. L. Y., *et al.* (2002) 'Mechanical and dynamic mechanical properties of rice husk ash-filled natural rubber compounds', *Journal of Applied Polymer Science*, 83(11), pp. 2331–2346. doi: 10.1002/app.10125.

Dick, J. S. (2003) *Basic Rubber Testing*. First. West Conshohoken: ASTM International.

Dizge, N. *et al.* (2008) 'Adsorption of reactive dyes from aqueous solutions by fly ash: Kinetic and equilibrium studies', *Journal of Hazardous Materials*, 150(3), pp. 737–746. doi: 10.1016/j.jhazmat.2007.05.027.

Dodd, J. and Tonge, K. (1987) *Analytical Chemistry By Open Learning: Thermal Methods*. New York: John Wiley & Sons.

Donnet, J.-B., Bansal, R. C. and Wang, M.-J. (1993) *Carbon Black*. Second. New York: Marcel Dekker, Inc.

Donnet, J.-B. and Voet, A. (1976) *Carbon Black*. First. New York and Basel: Marcel Dekker,.

Doucet, F. J. *et al.* (2015) 'Extraction of Aluminum and other Strategic Metals from Coal Fly Ash using a Novel Process and Low-cost Recoverable Reagent', in *2015 World of Coal Ash (WOCA) Conference in Nasvhille, TN*. Nashville, pp. 1–10.

Doucet, F. J. *et al.* (2016) 'Thermochemical processing of a South African ultrafine coal fly ash using ammonium sulphate as extracting agent for aluminium extraction', *Hydrometallurgy*. Elsevier B.V., 166, pp. 174–184. doi: 10.1016/j.hydromet.2016.07.017.

Dow Corning (2009) 'Silane Coupling Agents The Concept of Coupling with'.

Earle, R. and Scheetz, B. E. (1998) 'Utilization of fly ash Barry E Scheetz * and Russell Earle t', *Current Opinion in Solid State & Material Science*, 3, pp. 510–520.

Electrical4u (2011) *Thermal Power Generation Plant or Thermal Power Station | Electrical4u*. Available at: http://www.electrical4u.com/thermal-power-generation-plant-or-thermal-power-station/.

Eshel, G. *et al.* (2004) 'Critical Evaluation of the Use of Laser Diffraction for Particle-Size Distribution Analysis', *Soil Science Society of America Journal*, 68(3), p. 736. doi: 10.2136/sssaj2004.0736.

Eskom (2017) *Coal Power*. Available at: http://www.eskom.co.za/AboutElectricity/ElectricityTechnologies/Pages/Coal_Power.aspx (Accessed: 9 January 2017).

Feyyisa, J. L. *et al.* (2017) 'Contact Angle Measurements for Use in Specifying Organosilane-Modified Coal Combustion Fly Ash', 29(2), pp. 1–14. doi: 10.1061/(ASCE)MT.1943-5533.0001943.

Fraay, A. L. ., Bijen, J. . and de Haan, Y. . (1989) 'The Reaction of Fly Ash in Concrete . A critical Examination', *Cement and Concrete*, 19, pp. 235–246.

Frickel, N. *et al.* (2010) 'Functional silanes as surface modifying primers for the preparation of highly stable and well-defined magnetic polymer hybrids', *Langmuir*, 26(4), pp. 2839–2846. doi: 10.1021/la902904f.

Gangarao, H. V. ., Taly, N. and Vijay, P. . (2007) *Reinforced Concrete Design With FRP Composites*. London: CRC Press.

Garde, K., McGill, W. J. and Woolard, C. D. (1999) 'Surface modification of fly ash–characterisation and evaluation as reinforcing filler in polyisoprene', *Plastic, rubber and composites*, 28(1), pp. 1–10.

Goldstein, J. *et al.* (2012) *Scanning Electron Microscopy and X-Ray Microanalysis: A Text for Biologists, Materials Scientists, and Geologists*. 2nd edn. Springer Science& Business Media, LLc.

Gören, R. *et al.* (2012) 'Colloidal stability-slip casting behavior relationship in slurry of mullite synthesized by the USP method', *Ceramics International*, 38(1), pp. 679–685. doi: 10.1016/j.ceramint.2011.07.056.

Gunasekara, C. *et al.* (2015) 'Zeta potential, gel formation and compressive strength of low calcium fly ash geopolymers', *Construction and Building Materials*. Elsevier Ltd, 95, pp. 592–599. doi: 10.1016/j.conbuildmat.2015.07.175.

Guo, C., Zhou, L. and Lv, J. (2013) 'Effects of expandable graphite and modified ammonium polyphosphate on the flame-retardant and mechanical properties of wood flour-polypropylene composites', *Polymers and Polymer Composites*, 21(7), pp. 449–456. doi: 10.1002/app.

Guo, R. Q., Rohatgi, P. K. and Nath, D. (1997) 'Preparation of aluminium – fly ash particulate composite by powder metallurgy technique', *Journal of Manufacturing Science*, 32(15), pp. 3971–3974. doi: 10.1023/A:1018625118090.

Gupta, V. K. *et al.* (2003) 'Removal of cadmium and nickel from wastewater using bagasse fly ash - A sugar industry waste', *Water Research*, 37(16), pp. 4038–4044. doi: 10.1016/S0043-1354(03)00292-6.

Gupta, V. K. and Ali, I. (2004) 'Removal of lead and chromium from wastewater using bagasse fly ash - A sugar industry waste', *Journal of Colloid and Interface Science*, 271(2), pp. 321–328. doi: 10.1016/j.jcis.2003.11.007.

Haines, P. (1995) *Thermal Methods of Analysis*. London: Blackie Academic and Professional.

Hawkes, P. W. and Spence, J. C. H. (2007) *Science of Microscopy*, *Journal of Chemical Information and Modeling*. doi: 10.1017/CBO9781107415324.004.

He, H. *et al.* (2005) 'Grafting of swelling clay materials with 3-aminopropyltriethoxysilane', *Journal of Colloid and Interface Science*, 288(1), pp. 171–176. doi: 10.1016/j.jcis.2005.02.092.

Hundiwale, D. G. *et al.* (2002) 'Mechanical properties of natural rubber filled with flyash', *Journal of Applied Polymer Science*, 85(5), pp. 995–1001. doi: 10.1002/app.10465.

Hunter, R. (2013) *Zeta Potential In Colloid Science: Principles and Applications*. London: Academic Press.

Hwang, N. and Barron, A. (2011) 'BET Surface Area Analysis of Nanoparticles'.

IARC Working Group on the Evaluation of Carcinogenic Risks to Humans (2010a) 'Carbon black, titanium dioxide, and talc.', *IARC monographs on the evaluation of carcinogenic risks to humans / World Health Organization, International Agency for Research on Cancer*, 93, pp. 1–413.

IARC Working Group on the Evaluation of Carcinogenic Risks to Humans (2010b) 'Carbon Black', *IARC Monographs on the Evaluation of Carcinogenic Risks to Humans*, 93, pp. 1–190. doi: 21449489.

Ismail, H. and Kheong, O. . (2008) 'The Effect of Bis-(3-Triethoxysilylpropyl)– Tetrasulfide, Si69 on Properties of Recycled Poly (Vinyl chloride)/Acrylonitrile–Butadiene Rubber/Fly Ash (PVCr/NBR/FA) Composites', *Journal of Reinforced Plastics and Composites*, 27(15), pp. 1649–1661. doi: 10.1177/0731684407086612.

Ismail, H., Mega, L. and Abdul Khalil, H. P. S. (2001) 'Effect of a silane coupling agent on the properties of white rice husk ash-polypropylene/natural rubber composites', *Polymer International*, 50(5), pp. 606–611. doi: 10.1002/pi.673.

Ismail, H., Nasaruddin, M. . and Rozman, H. . (1999) 'The effect of multifunctional additive in white rice husk ash filled natural rubber compounds', *European Polymer Journal*, 35(8), pp. 1429–1437. doi: 10.1016/S0014-3057(98)00223-7.

Iyer, R. (2002) 'The surface chemistry of leaching coal fly ash', 93, pp. 321–329.

Iyer, R. S. and Scott, J. A. (2001) 'Power station fly ash - A review of value-added utilization outside of the construction industry', *Resources, Conservation and Recycling*, 31(3), pp. 217–228. doi: 10.1016/S0921-3449(00)00084-7.

Jaggi, N. and Vij, D. R. (2006) *Handbook of Applied Solid State Spectroscopy*, *Fourier Tranform Infrared Spectroscopy*. Edited by D. R. Vij. New York: Springer Science+Business Media, LLc. doi: 10.1007/0-387-37590-2.

Janos, P., Buchtova, H. and Ryznarova, M. (2003) 'Sorption of dyes from aqueous solutions onto fly ash', *Water Research*, 37(20), pp. 4938–4944. doi: 10.1016/j.watres.2003.08.011.

Jariwala, M., Crawford, J. and LeCaptain, D. J. (2007) 'In situ raman spectroscopic analysis of the regeneration of ammonium hydrogen sulfate from ammonium sulfate.', *Ind. Eng. Chem. Res.*, 46, pp. 4900–4905.

Jariwala, M., Crawford, J. and LeCaptain, D. J. (2007) 'In situ raman spectroscopic analysis of the regeneration of ammonium hydrogen sulfate from ammonium sulfate', *Industrial and Engineering Chemistry Research*, 46(14), pp. 4900–4905. doi: 10.1021/ie070350v.

Jeyageetha, C. and Kumar, S. P. (2016) 'Study of SEM / EDXS and FTIR for Fly Ash to Determine the Chemical Changes of Ash in Marine Environment', 5(7), pp. 1688–1693.

Júnior, J. A. A. and Baldo, J. B. (2014) 'The Behavior of Zeta Potential of Silica Suspensions', *New Journal of Glass and Ceramics*, 04(02), pp. 29–37. doi: 10.4236/njgc.2014.42004.

Kalyoncu, R. (1996) 'Coal Combustion Byproducts', *Minerals Yearbook*, 1(Metals and Minerals).

Kanking, S. *et al.* (2012) 'Use of bagasse fiber ash as secondary filler in silica or carbon black filled natural rubber compound', *Materials and Design*. Elsevier Ltd, 41, pp. 74–82. doi: 10.1016/j.matdes.2012.04.042.

Karaaĝaç, B., Inal, M. and Deniz, V. (2012) 'Predicting optimum cure time of rubber compounds by

means of ANFIS', *Materials and Design*, 35, pp. 833–838. doi: 10.1016/j.matdes.2011.03.062.

Karahan, O. and Atiş, C. D. (2011) 'The Durability Properties of Polypropylene Fiber Reinforced Fly Ash Concrete', *Materials & Design*, 32(2), pp. 1044–1049. doi: 10.1016/j.matdes.2010.07.011.

Kiyoura, R. and Urano, K. (1970) 'Mechanism, Kinetics, and Equilibrium of Thermal Decomposition of Ammonium Sulfate', *Industrial & Engineering Chemistry Process Design and Development*, 9(4), pp. 489–494. doi: 10.1021/i260036a001.

Kiyoura, R. and Urano, K. (1970) 'Mechanism, kinetics and equilibrium of thermal decomposition of ammonium sulphate.', *Ind. Eng. Chem. Process Des. Develop.*, 9(489–494).

Kruger, R. A., Hovy, M. and Wardle, D. (1999) 'The Use of Fly Ash Fillers in Rubber'.

Kruger, R. A. and Krueger, J. E. (2005) 'Historical development of coal ash utilisation in South Africa', *World of Coal Ash*, pp. 1–8.

Kruse, K. *et al.* (2012) *Characterizing Class C Fly Ashes for Alkali Silica reaction Mitigation Effectiveness*.

Kutchko, B. G. and Kim, A. G. (2006) 'Fly ash characterization by SEM-EDS', *Fuel*, 85(17–18), pp. 2537–2544. doi: 10.1016/j.fuel.2006.05.016.

Kuusik, R., Salkkonen, P. and Niinistö, L. (1985) 'Thermal decomposition of calcium sulphate in carbon monoxide', *Journal of Thermal Analysis*, 30(1), pp. 187–193. doi: 10.1007/BF02128129.

Kuwahara, Y. *et al.* (2010) 'A novel conversion process for waste slag: synthesis of a hydrotalcite-like compound and zeolite from blast furnace slag and evaluation of adsorption capacities', *Journal of Materials Chemistry*, 20(24), p. 5052. doi: 10.1039/c0jm00518e.

Landman, A. A. (2003) *LITERATURE REVIEW OF FLY ASH IN Aspects of solid-state chemistry of fly ash and ultramarine pigments*. University of Pretoria. Available at: http://upetd.up.ac.za/thesis/available/etd-06042004-062900/unrestricted/02chapter1.pdf.

Leblanc, J. (2010) *Filled Polymer: Science and Industrial Applications*. New York: CRC Press.

Li, S. *et al.* (2017) 'An efficient approach for lithium and aluminum recovery from coal fly ash by pre-desilication and intensified acid leaching processes', *Metals*, 7(7). doi: 10.3390/met7070272.

Lin, W. and Barron, A. (2014) 'An Introduction to X-ray Diffraction', pp. 1–10.

Lowell, S. *et al.* (2012) *Characterization of Porous Solids and Powders: Surface Area, Pore Size and Density*. New York: Springer Science & Business Media, LLc.

Lu, S. G. *et al.* (2009) 'Removal mechanism of phosphate from aqueous solution by fly ash', *Journal of*

Hazardous Materials, 161(1), pp. 95–101. doi: 10.1016/j.jhazmat.2008.02.123.

Luo, F. *et al.* (2013) 'Utilization of fly ash acid residue as a reinforcing filler in ethylene propylene diene monomer rubber', *Journal of Applied Polymer Science*, 129(3), pp. 1053–1059. doi: 10.1002/app.38783.

Mark, J., Erman, B. and Roland, M. (2013) *The science and technology of rubber*. 4th edn. Academic Press.

Marrone, M. *et al.* (2004) 'A Fourier Transform Infrared (FTIR) Study of the Reaction of Triethoxysilane (TES) and Bis[3-triethoxysilylpropyl]tetrasulfane (TESPT) with the Surface of Amorphous Silica', *The Journal of Physical Chemistry B*, 108(11), pp. 3563–3572. doi: 10.1021/jp036148x.

Matador Rubber s.r.o (2007) *Rubber Chemistry*.

Matjie, R. H., Bunt, J. R. and Van Heerden, J. H. P. (2005) 'Extraction of alumina from coal fly ash generated from a selected low rank bituminous South African coal', *Minerals Engineering*, 18(3), pp. 299–310. doi: 10.1016/j.mineng.2004.06.013.

Matsunaga, T. *et al.* (2002) 'Crystallinity and selected properties of fly ash particles', *Materials Science and Engineering A*, 325(1–2), pp. 333–343. doi: 10.1016/S0921-5093(01)01466-6.

McGill, W. . and Shelver, S. . (1995) 'The Effect of Carbon Black on Tetramethylthiuram Disulfide Accelerator Sulfur Vulcanization of Polyisoprene', *Journal of Applied Polymer Science*, 58(9), pp. 1433–1440.

van der Merwe, E. M. *et al.* (2011) 'Characterization of Coal Fly Ash Modified by Sodium Lauryl Sulphate', in *World of Coal Ash (WOCA) Conference*. Denver, CO, USA.

van der Merwe, E. M., Prinsloo, L. C., *et al.* (2014) 'Surface and bulk characterization of an ultrafine South African coal fly ash with reference to polymer applications', *Applied Surface Science*. Elsevier B.V., 317, pp. 73–83. doi: 10.1016/j.apsusc.2014.08.080.

van der Merwe, E. M., Mathebula, C. L. and Prinsloo, L. C. (2014) 'Characterization of the surface and physical properties of South African coal fly ash modified by sodium lauryl sulphate (SLS) for applications in PVC composites', *Powder Technology*. Elsevier B.V., 266, pp. 70–78. doi: 10.1016/j.powtec.2014.06.008.

Mohamed, S. *et al.* (2016) 'Process development for elemental recovery from PGM tailings by thermochemical treatment: Preliminary major element extraction studies using ammonium sulphate as extracting agent', *Waste Management*. Elsevier Ltd, 50, pp. 334–345. doi:

10.1016/j.wasman.2017.04.009.

Mohan, S. and Gandhimathi, R. (2009) 'Removal of heavy metal ions from municipal solid waste leachate using coal fly ash as an adsorbent', *Journal of Hazardous Materials*, 169(1–3), pp. 351–359. doi: 10.1016/j.jhazmat.2009.03.104.

Molina, A. and Poole, C. (2004) 'A comparative study using two methods to produce zeolites from fly ash', *Minerals Engineering*, 17(2), pp. 167–173. doi: 10.1016/j.mineng.2003.10.025.

Montaser, A. (1998) *Inductively Coupled Plasma Mass Spectrometry*. Washington D: Wiley-VCH.

MonTech Werkstoffprufmaschinen (no date) 'MDR 3000 Basic', pp. 1–49.

Murayama, N., Yamamoto, H. and Shibata, J. (2002) 'Mechanism of zeolite synthesis from coal fly ash by alkali hydrothermal reaction', *International Journal of Mineral Processing*, 64(1), pp. 1–17. doi: 10.1016/S0301-7516(01)00046-1.

Muriithi, G. N. *et al.* (2017) 'Synthesis and characterization of hydrotalcite from South African Coal fly ash', *Powder Technology*. Elsevier B.V., 312, pp. 299–309. doi: 10.1016/j.powtec.2017.02.018.

Nagaishi, T. *et al.* (1982) 'REACTION OF AMMONIUM SULPHATE WITH ALUMINIUM OXIDE', *Journal of Thermal Analysis*, 23, pp. 201–207.

Nath, D. C. D. *et al.* (2009) 'Structure-property interface correlation of fly Ash-isotactic polypropylene composites', *Journal of Materials Science*, 44(22), pp. 6078–6089. doi: 10.1007/s10853-009-3839-3.

Nayak, N. and Panda, C. R. (2010) 'Aluminium extraction and leaching characteristics of Talcher Thermal Power Station fly ash with sulphuric acid', *Fuel*, 89(1), pp. 53–58. doi: 10.1016/j.fuel.2009.07.019.

Nollet, H. *et al.* (2003) 'Removal of PCBs from wastewater using fly ash', *Chemosphere*, 53(6), pp. 655–665. doi: 10.1016/S0045-6535(03)00517-4.

Nookala, R. (2006) *Mechanistic Study of Silane assisted Rubber to Brass Bonding*. University of Cincinnati.

Numluk, P. and Chaisena, A. (2012) 'Sulfuric acid and ammonium sulfate leaching of alumina from Lampang clay', *E-Journal of Chemistry*, 9(3), pp. 1364–1372. doi: 10.1155/2012/758296.

Ohm, R. F. (1990) *The Vanderbilt Rubber Handbook*. 13th edn. R.T. Vanderbilt Company.

Ooi, Z. X., Ismail, H. and Bakar, A. A. (2013) 'Optimisation of oil palm ash as reinforcement in natural rubber vulcanisation: A comparison between silica and carbon black fillers', *Polymer Testing*, 32(4),

pp. 625–630. doi: 10.1016/j.polymertesting.2013.02.007.

Openshaw, S. C. (1992) *Utilization of Coal Fly Ash*. University of Florida.

Öztürk, N. and Kavak, D. (2005) 'Adsorption of boron from aqueous solutions using fly ash: Batch and column studies', *Journal of Hazardous Materials*, 127(1–3), pp. 81–88. doi: 10.1016/j.jhazmat.2005.06.026.

Pardo, S. . *et al.* (2010) 'Rheological, Thermal, and Mechanical Characteristics of Fly Ash-Thermoplastic Composites With Different Coupling Agents', *Polymers and Polymer Composites*, 31(10), pp. 1722–1730. doi: 10.1002/pc.

Payá, J. *et al.* (1998) 'Thermogravimetric methods for determining carbon content in fly ashes', *Cement and Concrete Research*, 28(5), pp. 675–686. doi: 10.1016/S0008-8846(98)00030-1.

Pelovski, Y. *et al.* (1992) 'The thermal decomposition of aluminum sulfate in different gas phase environments', *Thermochimica Acta*, 205(C), pp. 219–224. doi: 10.1016/0040-6031(92)85263-U.

Poh, B. T. and Ng, C. C. (1998) 'EFFECT OF SILANE COUPLING AGENTS ON THE MOONEY SCORCH TIME OF SILICA-FILLED NATURAL RUBBER COMPOUND', 34(7), pp. 975–979.

Pongdong, W. *et al.* (2015) 'Influence of Filler from a Renewable Resource and Silane Coupling Agent on the Properties of Epoxidized Natural Rubber Vulcanizates', 2015. doi: 10.1155/2015/796459.

Querol, X. *et al.* (2002) 'Synthesis of zeolites from coal fly ash: an overview', *International Journal of Coal Geology*, 50(1–4), pp. 413–423. doi: 10.1016/S0166-5162(02)00124-6.

Ranjbar, N. *et al.* (2015) 'Cement and Concrete Research Graphene nanoplatelet- fl y ash based geopolymer composites', *Cement and Concrete Research*, 76, pp. 222–231. doi: 10.1016/j.cemconres.2015.06.003.

Rashad, M. M. *et al.* (2004) 'Crystallization of calcium sulfate dihydrate under simulated conditions of phosphoric acid production in the presence of aluminum and magnesium ions', *Journal of Crystal Growth*, 267(1–2), pp. 372–379. doi: 10.1016/j.jcrysgro.2004.03.060.

Rattanasom, N., Prasertsri, S. and Ruangritnumchai, T. (2009) 'Comparison of the mechanical properties at similar hardness level of natural rubber filled with various reinforcing-fillers', *Polymer Testing*, 28(1), pp. 8–12. doi: 10.1016/j.polymertesting.2008.08.004.

Rees, C. A. *et al.* (2007) 'In situ ATR-FTIR study of the early stages of fly ash geopolymer gel formation', *Langmuir*, 23(17), pp. 9076–9082. doi: 10.1021/la701185g.

Reynolds-Clausen, K. and Singh, N. (2016) *Eskom's revised Coal Ash Strategy and Implementation Progress*.

Rohatgi, P. K. *et al.* (1998) 'Pressure infiltration technique for synthesis of aluminum - Fly ash particulate composite', *Materials Science and Engineering A*, 244(1), pp. 22–30. doi: 10.1016/S0921-5093(97)00822-8.

Rohatgi, P. K. (2006) 'Applications of Fly Ash in Synthesizing Low Cost Metal Matrix Composites for Automotive and other Engineering Applications', *Manufacturing Engineering*, 58(11), pp. 71–76.

Rosyadah Ahmad, N. N. *et al.* (2016) 'Surface modification in inorganic filler of mixed matrix membrane for enhancing the gas separation performance', *Reviews in Chemical Engineering*, 32(2), pp. 181–200. doi: 10.1515/revce-2015-0031.

Rothon, R. N. (2002) *Particulate Fillers for Polymers*.

Sanchez, D. (2014) *Which Countries Produce And Consume Most Electricity In Africa?* Available at: http://afkinsider.com/76584/producing-consuming-electricity-africa/.

Sciences, A. (2013) 'Surface modification of Coal Fly Ash by Sodium Lauryl Sulphate', (February).

Sedres, G. (2016) *Recovery of SiO2 and Al2O3 from coal fly ash*.

Semakina, O. K. *et al.* (2015) 'Research of Surface Properties of Fillers for Polymers', *Procedia Chemistry*, 15, pp. 79–83. doi: 10.1016/j.proche.2015.10.012.

Shemi, A. *et al.* (2012) 'Alternative techniques for extracting alumina from coal fly ash', *Minerals Engineering*, 34, pp. 30–37. doi: 10.1016/j.mineng.2012.04.007.

Shemi, A. *et al.* (2015) 'Extraction of alumina from coal fly ash using an acid leach-sinter-acid leach technique', *Hydrometallurgy*. Elsevier B.V., 157, pp. 348–355. doi: 10.1016/j.hydromet.2015.08.023.

Sibanda, V. *et al.* (2016) 'Towards the Utilization of Fly Ash as a Feedstock for Smelter Grade Alumina Production: A Review of the Developments', *Journal of Sustainable Metallurgy*. Springer International Publishing, 2(2), pp. 167–184. doi: 10.1007/s40831-016-0048-6.

Siesler, H. W. *et al.* (2008) *Near-Infrared Spectroscopy: Principles, Instruments, Applications*. Weinheim: John Wiley & Sons.

Sim, K. S. *et al.* (2010) 'Reducing scanning electron microscope charging by using exponential contrast stretching technique on post-processing images', *Journal of Microscopy*, 238(1), pp. 44–56. doi: 10.1111/j.1365-2818.2009.03328.x.

Singla, M. and Chawla, V. (2010) 'Mechanical properties of epoxy resin–fly ash composite', *Journal of Minerals & Materials Characterization & Engineering*, 9(3), pp. 199–210.

Sombatsompop, N. *et al.* (2004) 'Fly ash particles and precipitated silica as fillers in rubbers. I. Untreated fillers in natural rubber and styrene-butadiene rubber compounds', *Journal of Applied Polymer Science*, 93(5), pp. 2119–2130. doi: 10.1002/app.20693.

Sombatsompop, N., Wimolmala, E. and Markpin, T. (2007) 'Fly-Ash Particles and Precipitated Silica as Fillers in Rubbers. II. Effects of Silica Content and Si69-Treatment in Natural Rubber/Styrene–Butadiene Rubber Vulcanizates', *Polymers and Polymer Composites*.

Srinivasan, A. and Bandyopadhyay, S. (2017) *Advances in Polymer Materials and Technology*. First. Croydon: CRC Press.

Srivastava, V. K., Shembekar, P. S. and Prakash, R. (1988) 'Fracture behaviour of fly-ash filled FRP composites', *Composite Structures*, 10(4), pp. 271–279. doi: 10.1016/0263-8223(88)90006-2.

Sun, L. *et al.* (2017) 'Experimental study of extracting alumina from coal fly ash using fluidized beds at high temperature', *Fuel*. Elsevier Ltd, 199, pp. 22–27. doi: 10.1016/j.fuel.2017.02.073.

Swanepoel, J. . and Strydom, C. . (2002) 'Utilisation of fly ash in a geopolymeric material.pdf', *Apllied Geochemistry*, 17(17), pp. 1143–1148.

Tarun R. Naik, S. S. S. (1993) 'Fly Ash Generation and Utilization - An Overview', *Recent Trend in Fly Ash Utilization*, (June).

Thomas, M. D. A. (2007) 'Optimizing the Use of Fly Ash in Concrete', *Portland Cement Association*, p. 24.

Thomas, S. *et al.* (2017) *Polyurethane Polymers: Composites and Nanocomposites*. First. Amsterdam: Elsevier.

Thongsang, S. *et al.* (2012a) 'Dynamic mechanical analysis and tribological properties of NR vulcanizates with fly ash/precipitated silica hybrid filler', *Tribology International*. Elsevier, 53, pp. 134–141. doi: 10.1016/j.triboint.2012.04.006.

Thongsang, S. *et al.* (2012b) 'Dynamic mechanical analysis and tribological properties of NR vulcanizates with fly ash/precipitated silica hybrid filler', *Tribology International*. Elsevier, 53, pp. 134–141. doi: 10.1016/j.triboint.2012.04.006.

Thongsang, S. and Sombatsompop, N. (2007) 'Dynamic rebound behavior of Silica/Natural rubber composites: Fly ash particles and precipitated silica', *Journal of Macromolecular Science Part B-*

Physics, 46(4), pp. 825–840. doi: Doi 10.1080/00222340701389308.

Thongsang, S., Sombatsompop, N. and Ansarifar, A. (2008) 'Effect of fly ash silica and precipitated silica fillers on the viscosity, cure, and viscoelastic properties of natural rubber', *Polym. Adv. Technol.*, 19(April), pp. 1296–1304. doi: 10.1002/pat.

Tiwari, M. K., Bajpai, S. and Dewangan, U. K. (2016) 'Fly Ash Utilization : A Brief Review in Indian Context', pp. 949–956.

Truex, T. J., Hammerle, R. H. and Armstrong, R. . (1977) 'The Thermal Decomposition of Aluminium Sulfate', *Thermochimica Acta*, 19, pp. 301–34.

Valentim, B. *et al.* (2009) 'Variations in fly ash composition with sampling location: Case study from a Portuguese power plant', *Coal Combustion and Gasification Products*, 1(1), pp. 14–24. doi: 10.4177/CCGP-D-09-00017.1.

Vandenberghe, R. E. *et al.* (2010) 'Study of loss-on-ignition anomalies found in ashes from combustion of iron-rich coal', *Fuel*. Elsevier Ltd, 89(9), pp. 2405–2410. doi: 10.1016/j.fuel.2010.01.022.

Vassilev, S. V. and Vassileva, C. G. (2007) 'A new approach for the classification of coal fly ashes based on their origin, composition, properties, and behaviour', *Fuel*, 86(10–11), pp. 1490–1512. doi: 10.1016/j.fuel.2006.11.020.

Vilmin, F. *et al.* (2014) 'Reactivity of bis[3-(triethoxysilyl)propyl] tetrasulfide (TESPT) silane coupling agent over hydrated silica: Operando IR spectroscopy and chemometrics study', *Journal of Physical Chemistry C*, 118(8), pp. 4056–4071. doi: 10.1021/jp408600h.

Volli, V. and Purkait, M. K. (2016) 'Preparation and characterization of hydrotalcite-like materials from flyash for transesterification', *Clean Technologies and Environmental Policy*. Springer Berlin Heidelberg, 18(2), pp. 529–540. doi: 10.1007/s10098-015-1036-4.

Wahoud, A., Alouche, A. and Abdulbake, M. (2011) 'Sulfuric acid baking and leaching of spent sulfuric acid catalyst', *Periodica Polytechnica Chemical Engineering*, 55(1), pp. 31–34. doi: 10.3311/pp.ch.2011-1.06.

Wang, S. *et al.* (2005) 'Removal of dyes from aqueous solution using fly ash and red mud', *Water Research*, 39(1), pp. 129–138. doi: 10.1016/j.watres.2004.09.011.

Wang, W. *et al.* (2012) 'Synthesis of fly ash cenosphere/polyaniline and mullite/polyaniline core-shell composites', *Materials Chemistry and Physics*. Elsevier B.V, 135(2–3), pp. 1077–1083. doi: 10.1016/j.matchemphys.2012.06.020.

Weng, B. C. H. (1995) 'Treatment of Metal Industrial Wastewater', 120(6), pp. 1470–1487.

Weng, C.-H. and Huang, C. P. (2004) 'Adsorption characteristics of Zn(II) from dilute aqueous solution by fly ash', *Colloids and Surfaces A: Physicochemical and Engineering Aspects*, 247(1), pp. 137–143. doi: 10.1016/j.colsurfa.2004.08.050.

West, R. R. and Sutton, W. J. (1954) 'Thermography of Gypsum', *Journal of The American Ceramic Society-West and Sutton*, 37(5), pp. 221–224.

West, R. R. and Sutton, W. J. (2005) 'Thermography of Gypsum', *Journal of The American Ceramic Society-West and Sutton*, 37(5), pp. 1–4. Available at: papers2://publication/uuid/C8DF3217-3C09-4426-BF6D-F2E34FB44EB9.

Willard, H., Merritt, L. and Dean, J. (1974) *Instrumental Methods of Analysis*. New York: D. Van Nostrand Company.

Wypych, G. (2010) *Handbook of Fillers*. ChemTec Publishing. doi: 978-1-61583-171-5.

Xanthos, M. (2010) *Functional Fillers for Plastics*, *Functional Fillers for Plastics*. doi: 10.1002/9783527629848.

Xanthos, M. (2016) 'Part One Polymers and Fillers Functional', *Functional Fillers for Plastics: Second, updated and enlarged edition*, 3(2), pp. 1–15. doi: 978-3-527-32361-6.

Xie, Y. *et al.* (2010) 'Silane coupling agents used for natural fiber/polymer composites: A review', *Composites Part A: Applied Science and Manufacturing*. Elsevier Ltd, pp. 806–819. doi: 10.1016/j.compositesa.2010.03.005.

Xu, D. *et al.* (2016) 'A new process of extracting alumina from high-alumina coal fly ash in NH4HSO4 + H2SO4mixed solution', *Hydrometallurgy*. Elsevier B.V., 165, pp. 336–344. doi: 10.1016/j.hydromet.2015.12.010.

Xu, X. *et al.* (2011) 'Adsorption of fluoride from aqueous solution on magnesia-loaded fly ash cenospheres', *Desalination*. Elsevier B.V., 272(1–3), pp. 233–239. doi: 10.1016/j.desal.2011.01.028.

Yang, C. *et al.* (2016) 'and characterization of Mn intercalated Mg-Al hydrotalcite', *Journal of Colloid and Interface Science Synthesis*, 479, pp. 115–120.

Yao, Z. T. *et al.* (2014) 'A review of the alumina recovery from coal fly ash, with a focus in China', *Fuel*, 120, pp. 74–85. doi: 10.1016/j.fuel.2013.12.003.

Yao, Z. T. *et al.* (2015) 'A comprehensive review on the applications of coal fly ash', *Earth Science*

Reviews, 141, pp. 105–121. doi: 10.1016/j.earscirev.2014.11.016.

Zhu, D. and van Ooij, W. J. (2002) 'Structural characterization of bis-[triethoxysilylpropyl]tetrasulfide and bis-[trimethoxysilylpropyl]amine silanes by Fourier-transform infrared spectroscopy and electrochemical impedance spectroscopy', *Journal of Adhesion Science and Technology*, 16(9), pp. 1235–1260. doi: 10.1163/156856102320256873.

Appendices

Appendix A: Physico-chemical modification of coal fly ash – preliminary study

A1. Thermochemical treatment of coal fly ash using ammonium sulphate, $(NH_4)_2SO_4$

A1.1 Methodology

Three samples of ultrafine coal fly ash thoroughly mixed with ammonium sulphate at a constant solid-solid mass ratio of 2:3 (m/m) were prepared as indicated in Table A1. The resulting mixture was placed in fused quartz crucibles, heat-treated in a static muffle furnace at 500°C, and weighed at regular intervals until a constant mass was reached.

Table A1: Mass of coal fly ash (UFA) and $(NH_4)_2SO_4$ used in thermochemical treatment experiments, and time required to reach constant mass.

	Mass of reagents		Time to reach constant mass (hrs)
	UFA (g)	$(NH_4)_2SO_4$ (g)	
Small	2.0	3.0	5
Medium	24.0	36.0	12
Large	80.0	120.0	10

The resulting sintered solids were crushed using a mortar and pestle. 3 g of each sample was placed in 300 mL of deionised water and was continuously stirred for 24 hours to maintain the treated coal fly ash particles in suspension throughout the aqueous dissolution process. pH, temperature and conductivity readings were recorded at 30 s intervals using a HI9828/10–01 Hanna Multi-parameter Water Quality Reader. The aqueous dissolution process was stopped when the conductivity of the reaction remained unchanged for 30 minutes. After dissolution, the leachants were filtered under reduced pressure through 0.4 µm membrane filters (Whatman Nucleopore® Track-Etched polycarbonate, Whatman UK

Ltd) in closed polycarbonate filtration vessels (Sterifill, 47 mm Millipore). The filtrate was acidified to a pH below 2 using 55% nitric acid (HNO_3; Promark Chemicals South Africa) and stored in a refrigerator awaiting ICP-MS analysis at an accredited laboratory (Waterlab Pty Ltd., Pretoria, South Africa). The solid product was dried in an oven at 50°C before being characterised by FE-SEM and FTIR.

A1.2 Results and Discussion

Figure A1 presents low and high magnification FE-SEM micrographs of untreated and thermochemically treated fly ash. The untreated fly ash (a. and b) exhibited predominantly spherical, coarse-surfaced particles with a broad size distribution. Irregularly shaped particles were also present in the sample. Agglomeration is evident in the micrographs and may be a result of rapid cooling or inter-particle contact. The thermochemically treated fly ash samples retained the desired sphericity and there is a noticeable increase in particle surface roughness which translates to increase in surface area (Figures c-g). Particle-particle agglomeration appeared to have decreased after thermochemical treatment and leaching of the sample.

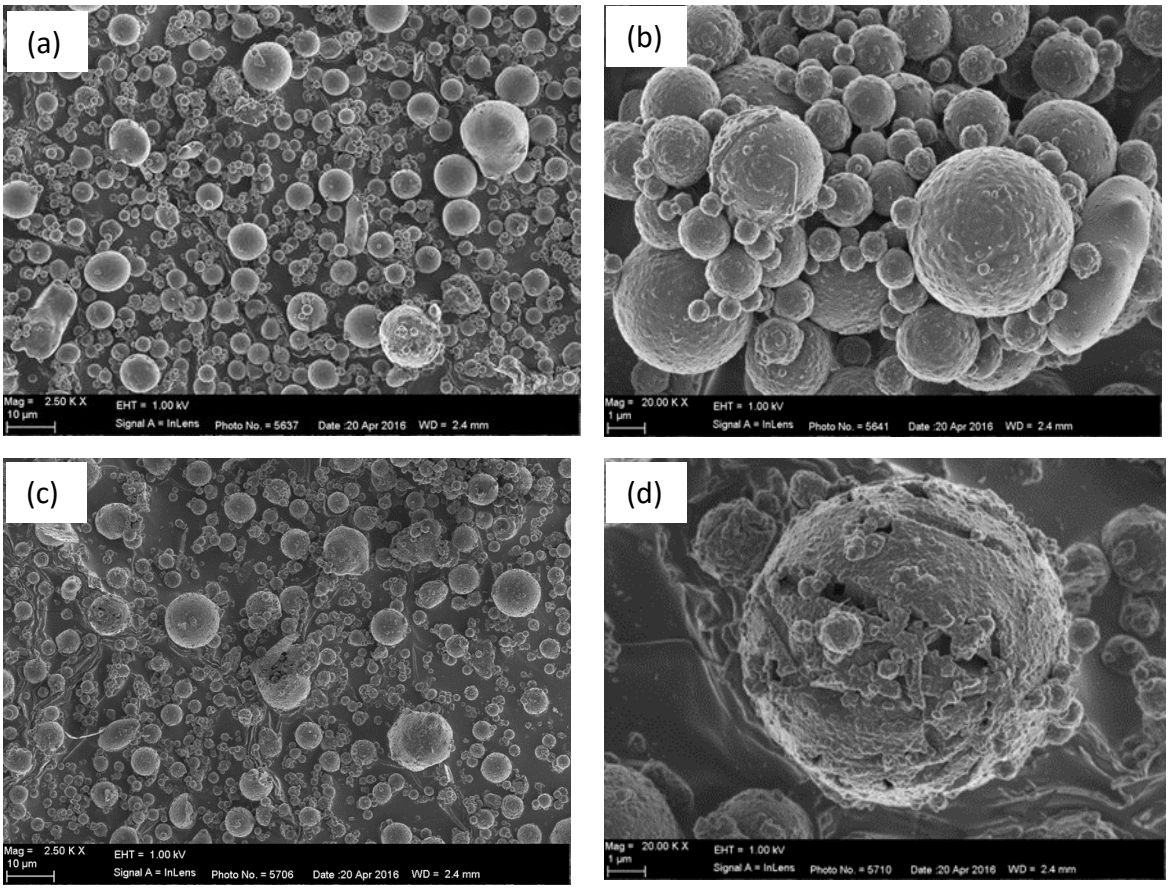

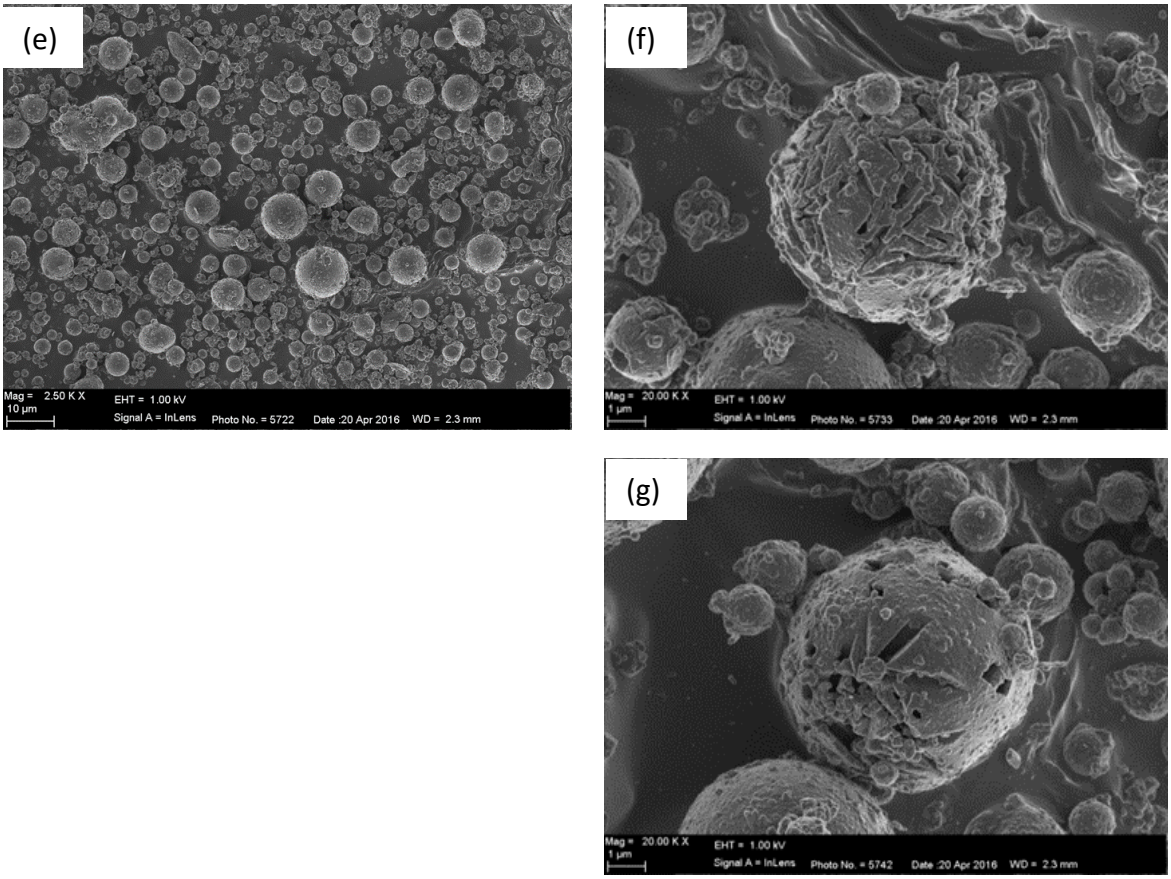

Figure A1: Scanning electron micrographs of untreated (a. and b.) thermochemically treated small (c. and d.), medium (e. and f.) and large (g.) fly ash samples.

A2. Sulphuric acid treatment of coal fly ash

A2.1 Methodology

Two acid leaching experiments were carried out, one with a 1:4 solid: liquid ratio and the other 1:10. 2 × 200 mL of 5 M sulphuric acid solutions were left to reflux in 500 mL round bottomed flasks until the temperature of the solution stabilised at 95 ± 3°C. 20 g (1:10 solid: liquid ratio) or 50 g (1:4 solid: liquid ratio) of coal fly ash were added to the solutions and left to reflux for 6 hours with stirring. The suspensions were left to cool for 12 hours and then centrifuged for 60 s at 4000 rpm. The supernatants were collected and stored at 4°C, while the remaining solids were washed 3 times with 100 mL deionised water before being dried at 50°C. The solid residue was analysed by FE-SEM, FTIR, and the supernatant was analysed using ICP-MS.

A2.2 Results and Discussion

Figure A2 presents the SEM micrographs of untreated and sulphuric acid treated coal fly ash samples.

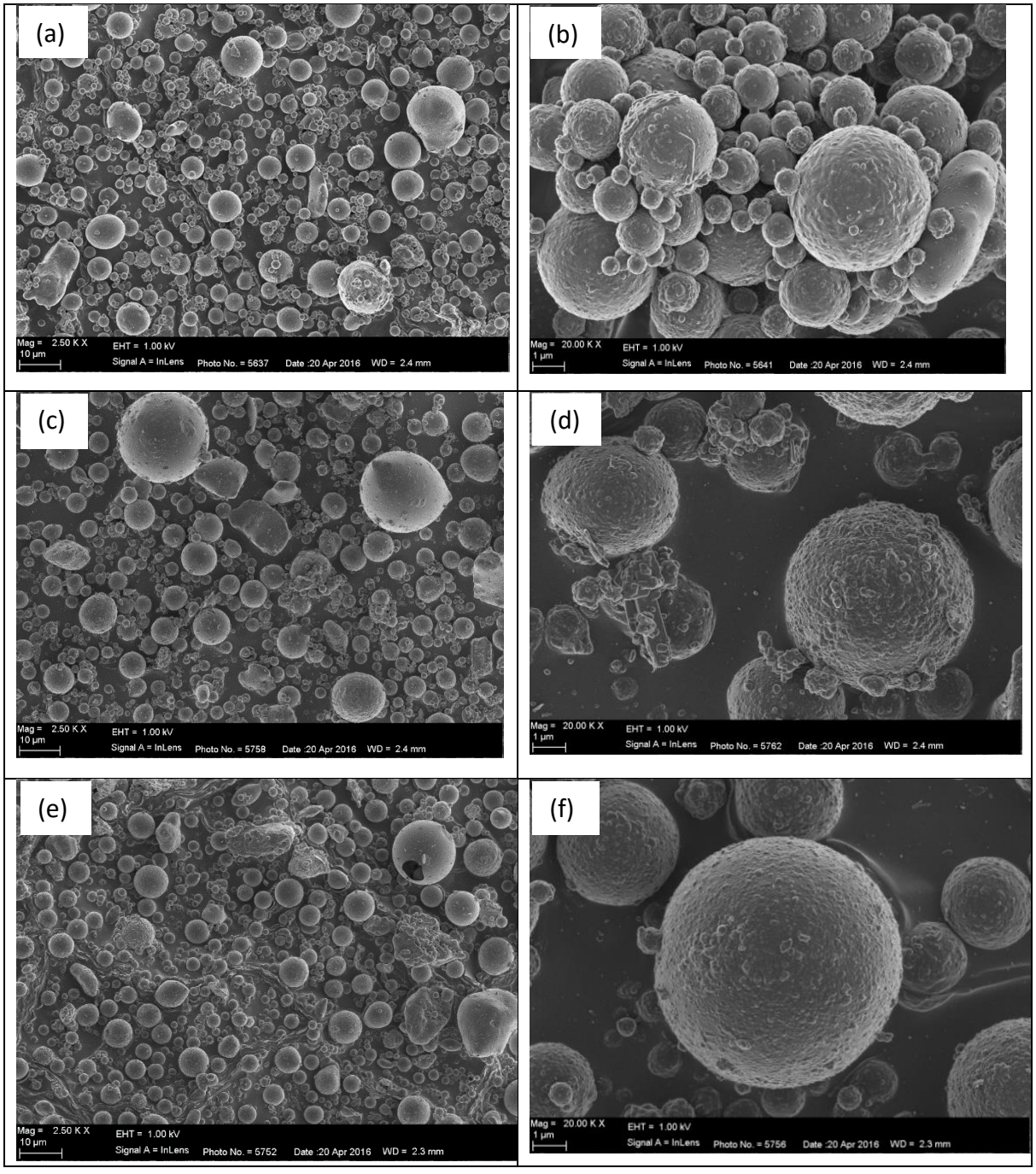

Figure A2: Scanning electron micrographs of untreated fly ash (a. and b.), sulphuric acid treated 1:4 (c. and d.) and 1:20 (e. and f.) fly ashes.

SAL samples retained the desired sphericity after treatment and show very little particle-particle agglomeration. The particle surfaces appear to be smoother than in the untreated fly ash.

A2.3 Thermochemical-activation and aluminium extraction.

Figures A3 to A6 show the profiles of two solution parameter; pH and conductivity. These were monitored when thermochemically activated CFA was dispersed in ultra-pure water to extract Aluminium. On addition to the ultra-pure water, all the treated CFA samples caused an immediate rapid decrease in solution pH to below 4. Doucet et al. (2015) investigated the effect of thermochemical-activation of South African CFA on efficiency Aluminium extraction. In their study they found that when untreated CFA was added to ultra-pure water, the pH of the solution rapidly increased before steadily plateauing and stabilizing at 9.61. This was followed by a slight increase in solution conductivity to approximately 290 μS/cm. Compared to this, the results obtained in this experiment suggest that there was a significant structural change in CFA.

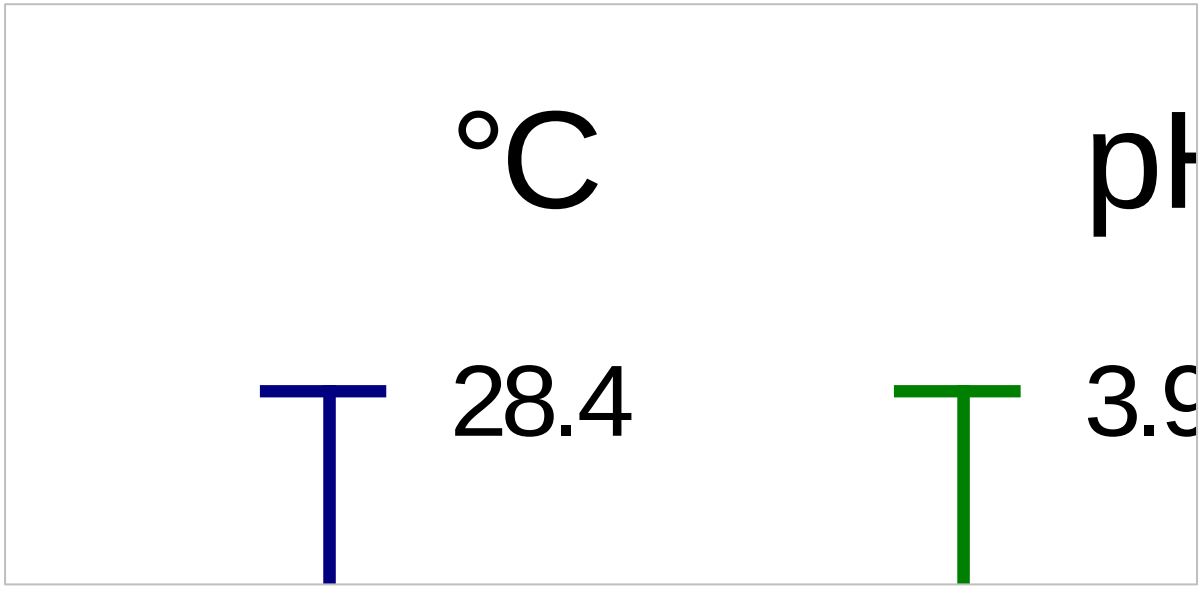

Figure A3: Solution pH and conductivity profiles for the leaching of thermochemically treated coal fly ash (small).

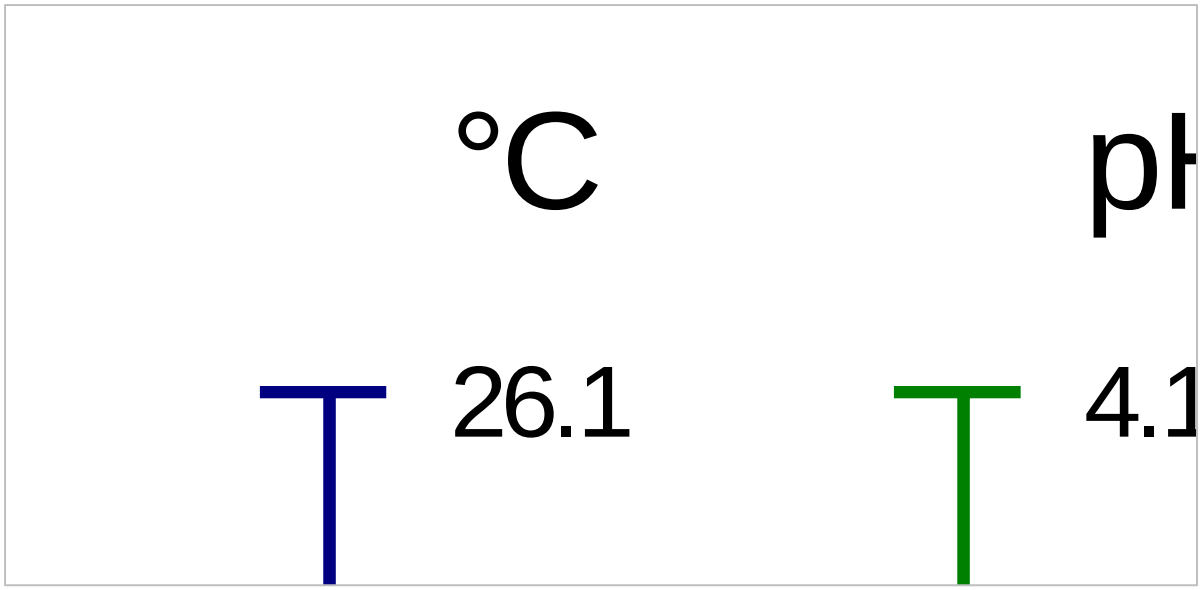

Figure A4: Solution pH and conductivity profiles for the leaching of thermochemically treated coal fly ash (medium).

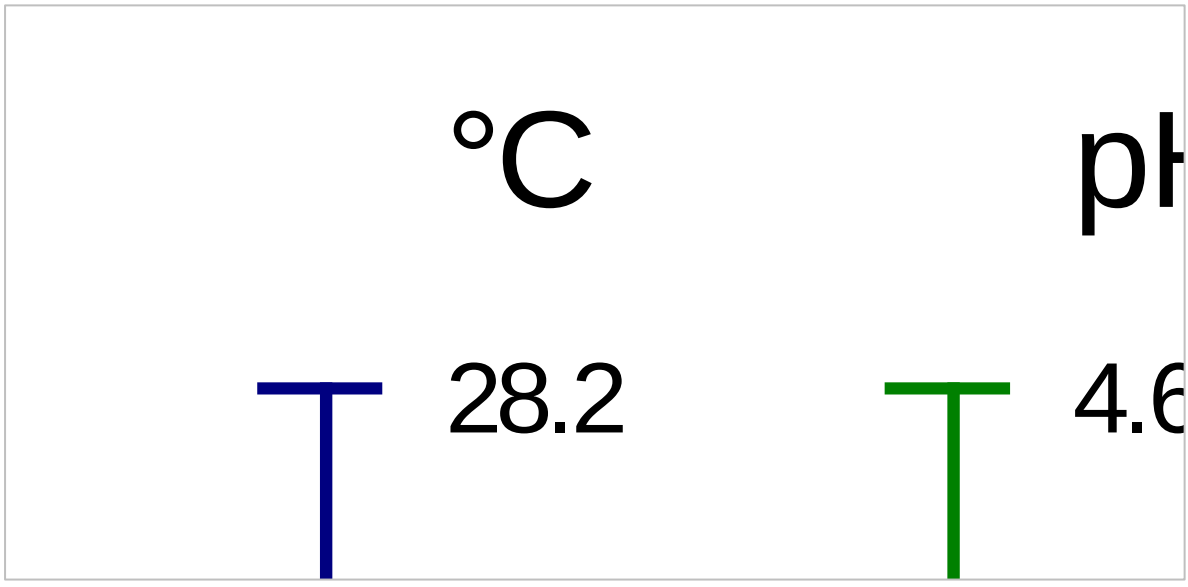

Figure A5: Solution pH and conductivity profiles for the leaching of thermochemically treated coal fly ash (large).

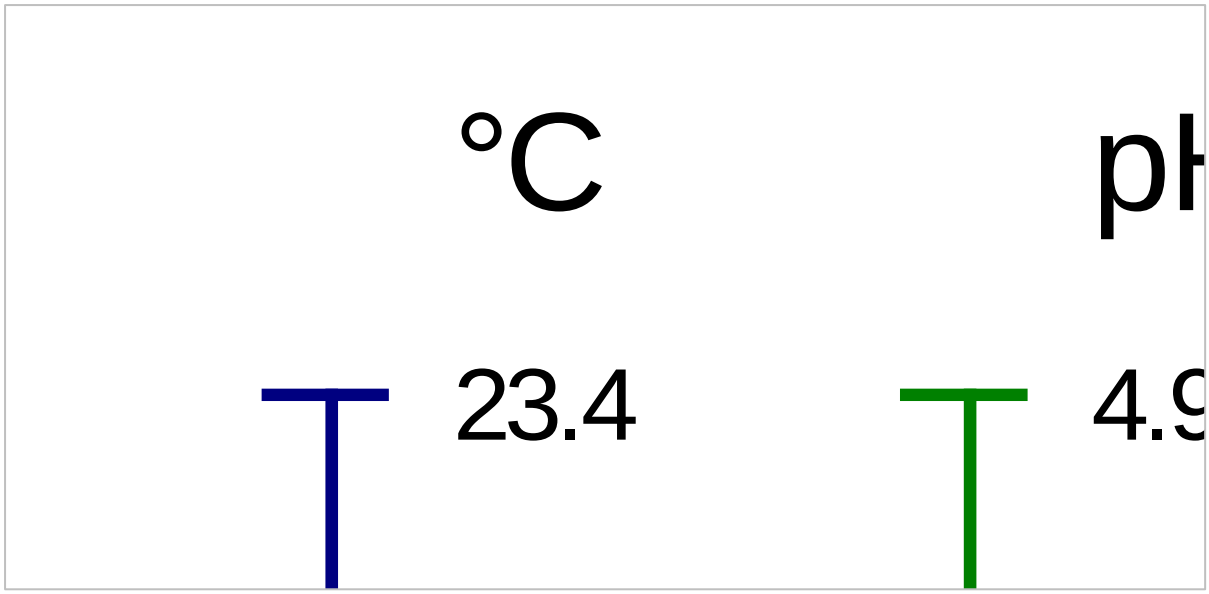

Figure A6: Solution pH and conductivity profiles for the leaching of thermochemically-activated South African ultrafine coal fly ash (large with mixing).

Up-scaling the CFA-$(NH_4)_2SO_4$ mixture mass had no significant effect on the solution pH as all the sample sizes levelled off at approximately pH 3. However, up-scaling resulted in a considerable increase in the conductivity of the solution. After 24 hours the small sample conductivity had a plateau at ≈ 2600 μS/cm, the medium at ≈ 2900 μS/cm, while the large sample conductivity was approximately 3200 μS/cm and still increasing. The thermochemical-activation of the large sample size with mixing demonstrated that the higher conductivity and lower pH of the large sample was not due to un-reacted $(NH_4)_2SO_4$.